BIOGEOCHEMISTRY OF ARCHAEAL MEMBRANE LIPIDS: TOWARD A BETTER UNDERSTANDING OF THE BIAS OF TEX_{86} IN THE TRANSITIONAL ZONE BETWEEN PEARL RIVER ESTUARY AND COASTAL SOUTH CHINA SEA

by

JINXIANG WANG

(Under the Direction of Chuanlun L. Zhang)

ABSTRACT

TEX_{86} has been increasingly applied for sea surface temperature reconstruction. This proxy is derived from the relative distribution of glycerol dialkyl glycerol tetraethers (GDGTs). Recently, however, increasing evidence showed that TEX_{86} could be affected by multiple variables (e.g. seasonal or terrestrial input, methanotroph input). In this study, GDGTs and TEX_{86} were studied in water column and sediments of the Pearl River estuary and coastal South China Sea. The results exhibited 1) unusually low TEX_{86}-derived temperatures in the transitional area, and 2) strong correlation between Ring Index (weighted average number of cyclopentane rings in GDGTs) and Marine Group II (MG II) *Euryarchaeota*. Lipid and molecular DNA both indicate that 1) archaeal community composition is the crucial factor to bias TEX_{86}, and 2) MG II synthesize ringed GDGTs, which may alter TEX_{86} in the transitional area. Our study warns against using TEX_{86} for interpretation of the (coastal) sediment record.

INDEX WORDS: TEX_{86}; Isoprenoid GDGTs; Marine Group II Euryarchaeota; The lower Pearl River; Estuary; Coastal South China Sea

BIOGEOCHEMISTRY OF ARCHAEAL MEMBRANE LIPIDS: TOWARD A BETTER UNDERSTANDING OF THE BIAS OF TEX_{86} IN THE TRANSITIONAL ZONE BETWEEN PEARL RIVER ESTUARY AND COASTAL SOUTH CHINA SEA

by

JINXIANG WANG

B.S., China University of Geosciences (Wuhan), China, 2011

A Thesis Submitted to the Graduate Faculty of The University of Georgia in Partial Fulfillment of the Requirements for the Degree

MASTER OF SCIENCE

ATHENS, GEORGIA

2015

© 2015

Jinxiang Wang

All Rights Reserved

BIOGEOCHEMISTRY OF ARCHAEAL MEMBRANE LIPIDS: TOWARD A BETTER UNDERSTANDING OF THE BIAS OF TEX_{86} IN THE TRANSITIONAL ZONE BETWEEN PEARL RIVER ESTUARY AND COASTAL SOUTH CHINA SEA

by

JINXIANG WANG

Major Professor:	Chuanlun L. Zhang
Committee:	Patricia L. Yager (Chair)
	Ming-Yi Sun

Electronic Version Approved:

Suzanne Barbour
Dean of the Graduate School
The University of Georgia
August 2015

ACKNOWLEDGEMENTS

First and foremost I would like to thank my friends and family for continuous support during the past several years. I would especially like to thank Rebekah Wang, who has provided endless support and encouragement.

I am extremely grateful to my supervisor Prof. Chuanlun Zhang for the collaboration along the way to understand Organic Geochemistry and unravel new insights. I appreciate very much all the time he spent with me in the lab, that he was always available when I needed help, his support encouragement and patience during the last three exciting and instructive years and I very much enjoyed working with him.

My deepest gratitude goes to the thesis committee chair, Prof. Patricia Yager, and the committee member, Prof. Ming-Yi Sun, for their tireless support, endless discussions, and incredible patience in explaining me any kind of scientific issues.

Many thanks go to the faculty and staff, Dr. Brian Binder, Dr. Adrian Burd, Dr. Daniela Di Iorio, Dr. James Hollibaugh, Dr. Christof Meile, Sharon Barnhart, Jackie Fortson and Cat Mills, for their support and help during I'm studying in the Department of Marine Sciences, UGA.

I want to thank all co-authors of the individual papers and chapters. Particularly, I'm grateful to Dr. Wei Xie and Dr. Peng Wang for giving me the molecular DNA data to support the idea in the papers. My work would not been possible without the help of captain Jianping Huang and colleagues in Tongji University.

Special Thanks to Leslie.

TABLE OF CONTENTS

Page

ACKNOWLEDGEMENTS iv

LIST OF TABLES vii

LIST OF FIGURES viii

CHAPTER

1 INTRODUCTION AND LITERATURE REVIEW 1

1.1 Sea Surface temperature (SST) and paleothermometry 1

1.2 TEX_{86} and archaeal membrane lipids 2

1.3 The Pearl River and its estuary 5

1.4 Objective and outline of this thesis 7

1.5 References 8

2 UNUSUALLY LOW TEX_{86} VALUES IN THE TRANSITIONAL ZONE BETWEEN PEARL RIVER ESTUARY AND COASTAL SOUTH CHINA SEA: IMPACT OF CHANGING ARCHAEAL COMMUNITY COMPOSITION 16

2.1 Introduction 18

2.2 Material and methods 20

2.3 Results and discussion 25

2.4 Conclusions 35

2.5 References 36

3 CONTRIBUTION OF MARINE GROUP II EURYARCHAEOTA TO CYCLOPENTYL TETRAETHERLIPIDS IN THE PEARL RIVER ESTUARY AND COASTAL SOUTH CHINA SEA: IMPACT ON TEX_{86} PALEOTHERMOMETER57

3.1 Introduction....61

3.2 Material and methods....64

3.3 Results and discussion....69

3.4 Conclusions....75

3.5 References....76

4 SUMMARY....93

APPENDICES

A SUPPLEMENTAL TABLES IN CHAPTER TWO....95

B SUPPLEMENTAL FIGURES IN CHAPTER THREE....96

LIST OF TABLES

Chapter 2 Page

Table 2.1: Sampling information for samples in this study 56

Table 2.2: Environmental parameters and the abundance of GDGTs 57

Table 2.3: Linear regression analysis between GDGT-2/-3 and crenarchaeol 58

Chapter 3

Table 3.1: Sampling information, abundance of GDGTs and qPCR of Marine Group II and total Archaea for samples in this study 91

Table 3.2: Regression analysis between [MG II]/[Archaea] ratio and %GDGTs, Ring Index and the ratio of GDGT-2 to GDGT-3 92

LIST OF FIGURES

Chapter 1 Page

Figure 1.1: GDGT structures 14

Figure 1.2: Empirical correlation between TEX_{86} and annual mean SST 15

Chapter 2

Figure 2.1: GDGT structures 46

Figure 2.2: Map of sampling locations in the lower Pearl River and the PR estuary 47

Figure 2.3: TEX_{86} profiles in the lower Pearl River and the PR estuary 48

Figure 2.4: TEX_{86}-derived temperature from SPM, sediments and soil 50

Figure 2.5: The discrepancy of TEX_{86}-temperature in the transitional zone 51

Figure 2.6: Correlation between GDGT-2/-3 and their derived TEX_{86} 53

Figure 2.7: Cluster analysis of the relative distribution of GDGTs in the sediments 54

Figure 2.8: Archaeal community composition in the surface water 55

Chapter 3

Figure 3.1: Map of sampling locations 85

Figure 3.2: Archaeal community composition along the salinity gradient 86

Figure 3.3: Mean values of TEX_{86}-derived temperatures in SPM and sediments 87

Figure 3.4: TEX_{86} of the SPM and sediments plotted against Ring Index (RI_1) 88

Figure 3.5: Distribution of Ring Index (RI), abundance of MG II and [MG II]/[Archaea] ratio ..89

Figure 3.6: Fractional abundance of GDGTs, RI, and ratio of GDGT-2 to GDGT-3 vs. the ratio of [MG II]/[Archaea] 90

CHAPTER 1

INTRODUCTION AND LITERATURE REVIEW

1.1 Sea Surface temperature (SST) and paleothermometry

Global warming is changing natural environments and human societies in diverse ways. The global average surface temperature increased by 0.6±0.2 ºC over the 20th century and accelerated warming trend in the past two decades (IPCC, 2013, http://www.ipcc.ch). As the atmosphere CO_2 concentrations have increased by over 100 ppm in comparison to its preindustrial levels (IPCC, 2013, http://www.ipcc.ch), most of the global warming is attributed to the increasing greenhouse gases caused by human activities. To have a better understanding of the anthropogenic impact on climate change, scientists should provide more accurate climate records to build and test models that are employed to predict future climate trends.

Sea surface temperature (SST) has an important role in the global climate system and may influence a number of climatic processes. Our capability of foreseeing future climate change benefits from what we can learn from the past climate patterns. Thus, determination of the paleo-SST is of primary importance for the reconstruction of the natural climatic changes, modeling of climate and reconstruction of ocean circulation. This can be achieved by modeling or assessed with temperature proxies.

Several geochemical proxies for SST reconstruction have been proposed since the 1950s, and they can generally be divided between proxies based on inorganic (calcite and opal shells

and sheletons) and organic remains (lipid biomarkers) (see Table 1 of Huguet, 2007). Since chemical and/or physical factors may have significant impact on inorganic proxies, the organic remains are proposed as a proxy to reconstruct the paleo-SST (Huguet, 2007). The first proxy, $U^{k'}_{37}$, is built on the basis of the ratio of long-chain unsaturated ketones that are synthesized by haptophyte algea (Brassell et al., 1986). However, the $U^{k'}_{37}$ can be affected by a series of environmental factors, e.g. seasonality, depth habitat changes of the haptophytes, species composition, signal accumulation through time, etc. (Herbert, 2003). In 2002, a second proxy, TEX_{86}, based on archaeal organic remains was proposed by Schouten et al. (2002).

1.2. TEX_{86} and archaeal membrane lipids

TEX_{86} (TetraEther Index of tetraethers consisting of 86 carbons) is a sea surface temperature proxy based on the relative distribution of the cyclic moieties of glycerol dislkyl glycerol tetraethers (GDGTs, Fig. 1.1), membrane lipids of the Thaumarchaeota (Schouten et al., 2002), a group of microorganisms belonging to the domain of Archaea and occurring ubiquitously in the ocean.

1.2.1 Biological sources of GDGTs

Archaeal membrane lipids include a monolayer of glycerol dialkyl glycerol tetraethers (GDGTs) containing 0-8 cyclopentane rings in their two biphytane moieties. One particular GDGT, crenarchaeol (and its isomer), is only found in Group I Thaumarchaeota, which contains 4 cyclopentane moieties and 1 cyclohexane moiety (Sinninghe Damste et al., 2002). These

archaeal membrane lipids, ubiquitously present in natural environments, were firstly detected as intact core lipids in 2000 (Hopmans et al., 2000).

The Thaumarchaeota contain tetraethers, which have been commonly recognized as the predominant source of GDGTs in the ocean. Over the last two decades, Archaea have been increasingly shown to play important roles in global carbon and nitrogen cycles and paleoclimate reconstruction (Schouten et al., 2013). Planktonic marine Archaea are comprised of two dominant groups – the Thaumarchaeota and Euryarchaeota. Thaumarchaeota, formerly classified as Group I Crenarchaeota (Brochier-Armanet et al., 2008; Spang et al., 2010), have been recognized as the main driver in ammonia oxidation in the marine (Konneke et al., 2005) and terrestrial (de la Torre et al., 2008; Sinninghe Damste et al., 2012) environments. Recently, Lincoln et al. (2014) show that planktonic Euryarchaeota (MG II) produce the same types of archaeal tetraether lipids as do Thaumarchaeota. Their results have important implications for environmental surveys of marine Archaea, and the use of their lipids for interpretation of the sedimentary record.

1.2.2. GDGTs as a new temperature proxy

Archaeal membrane lipids can be well preserved in the environments and geological settings for a long time (Kuypers et al., 2001) due to the stability of their structures. This chemical feature helps to establish a series of proxies to reflect the variations in the environments. Previous culture studies of hyperthermophilic Archaea had already indicated that the relative number of cyclopentane moieties of GDGTs changed with growth temperature (Gliozzi et al., 1983), i.e. the number of cyclopentane moieties increased with increasing temperature. This

temperature adaptation has also been detected in the GDGTs of Thaumarchaeota and forms the basis of a new temperature proxy based on distribution of non-(hyper)thermophlic archaeal membrane lipids in the ocean (Schouten et al., 2002; Eq. 1).

$TEX_{86} = \frac{GDGT2+GDGT3+Cren.iso}{GDGT1+GDGT2+GDGT3+Cren.iso}$ (Schouten et al., 2002) (Eq. 1)

This ratio was determined for a range of marine core top sediments and found to correlate well with annual mean SST (Schouten et al., 2002) (Fig. 1.2). However, this is merely an empirical correlation and there was no direct proof for a functional relationship between temperature and TEX_{86}. Wuchter et al. (2004) found that TEX_{86} is linearly correlated with temperature and that changes in salinity and nutrients do not substantially affect the TEX_{86}. These initial results clearly show that TEX_{86} is a potentially useful SST proxy.

1.2.3. Calibrations of TEX_{86}

The linear regressions of core-top TEX_{86} values versus sea surface temperatures enable us to establish an empirical calibration making TEX_{86} as a (paleo-) temperature proxy (Schouten et al., 2002; Eq. 2). Superseded by a more extensive global core tope dataset (n = 228), Kim et al. (2008) proposed a new calibration (Eq. 3), which was only applicable for SST between 5 and 30 ºC. To make the calibration useable in polar regions, Kim et al. (2010) extended the global core top dataset with core top from mainly polar oceans and improved the correlation that showed a stronger relationship between lower temperature SST and TEX_{86} (Eq. 4). Meanwhile, with enrichment culture data, Kim et al. (2010) suggested a slightly modified form of TEX_{86} for determining SST at temperature > 15 ºC (Eq. 5).

$SST = (TEX_{86} – 0.28)/0.015$ (Eq. 2)

$SST = 56.2 \times TEX_{86} - 10.8$ (Eq. 3)

$SST = 67.5 \times (TEX_{86}^{L}) + 46.9$, $TEX_{86}^{L} = \log[GDGT2/(GDGT1+GDGT2+GDGT3)]$ (Eq. 4)

$SST = 68.4 \times (TEX_{86}^{H}) + 38.6$, $TEX_{86}^{H} = \log[TEX_{86}]$ (Eq. 5)

For all these calibrations, Eq. 5 is well accepted as a more accurate equation to reconstruct the paleo-temperature of low latitude ocean; Eq. 4 is better to be used in high latitude regions.

1.2.4. Problems with TEX_{86}

With increasing application of TEX_{86} in different environments, it has become evident that temperatures derived from this proxy can be biased by several other variables (Schouten et al., 2013) including 1) in situ production of GDGTs in sediments (Lipp and Hinrichs et al., 2009), 2) input of GDGTs from the water column below the photic zone (Kim et al., 2012), 3) seasonal variability (Leider et al., 2010), 4) terrestrial input (Weijers et al., 2006), and 5) selective degradation of polar GDGTs (Schouten et al., 2012). Further bias of TEX_{86} may be attributed to GDGTs produced from other groups of Archaea, such as Euaryarchaeota (Delong et al., 2006), particularly the methanotrophic Archaea associated with gas hydrates (Zhang et al., 2011), or group I.1b Thaumarchaeota of soil origin (Sinninghe Damsté et al., 2012).

1.3 The Pearl River and its estuary

The Pearl River, located in the subtropical or tropical zone with an annual mean air temperature of 21-22 ^{o}C and annual rainfall of 1600-2300mm (Ji et al., 2011), is the second largest river (~ 2214 km) in China and the 14th largest river in the world (Zhao et al., 1990; Cai et

al., 2008). The annual average river discharge ~ 330×10^9 m^3yr^{-1} and sediment deliver of ca. 90 Mt yr^{-1} (Zhao et al., 1990), with 80% during the wet season (Apr.- Sep.) and 20% during the dry season (Oct.- Mar.). The Pearl River system drains to the north South China Sea via three estuaries, Lingdingyang, Modaomen and Huangmaohai and is mainly formed by the confluence of three principal tributaries, namely the West River, the North River and the East River.

Lingdingyang, the largest estuary of the Pearl River Estuary, coupling with the lower Pearl River make up a complex river-estuarine system, with a length of ~ 130 km (40 km of the low Pearl River and the 90 km of the estuary) and a width of 4-58 km (Cai et al., 2004; Rabouille et al., 2008; Chen et al., 1994). The Pearl River estuary receives water from three sources, freshwater from the Pearl River, oceanic water from the South China Sea and coastal water from the South China Coastal Current (Chau and Wong, 1960; Williamson, 1970; Morton and Wu, 1975). In this region, a number of dynamical factors influence hydrodynamic processes and the fate of organic matter, including bottom topography, freshwater discharge, winds, tides and coastal currents that control hydrodynamic processes, circulation and distribution of the physic-chemical parameters such as water pH or salinity. The gravitational circulation between estuarine plume and salt wedge increases the complicacy of the hydrological environment.

The Pearl River estuary (PRE) and adjacent coastal waters display a typical spatial variability of phytoplankton in summer: low biomass and productivity due to high dilution and light limitation caused by high turbidity in the freshwater-dominated estuary; high biomass and productivity at intermediate salinities in the estuarine/coastal plume; and reduced biomass and productivity due to nutrient limitation in the oceanic dominated region (Yin et al., 2004). The water in the PRE is significantly enriched with methane (Chen et al., 2008; Zhou et al., 2009). C3 plants are the dominant vegetation type in this area (Yu et al., 2010). Anthropogenic activities

are strong in the PRE, which increases the ratio of N versus C in total organic matter (Harrison et al., 2008).

1.4 Objective and outline of this thesis

The following thesis work aims is to better understand the environmental and biological factors controlling the variability in TEX_{86} in the Pearl River and its estuary by integrating archaeal membrane lipids with 16S rRNA genes. Specifically I will address 1) the sources of archaeal lipids in the water column and sediments; 2) the factors that may cause biases to TEX_{86} in the transitional zone; and 3) the relationship between Marine Group II Euryarchaeota and GDGTs.

This thesis begins with an investigation of the distribution of TEX_{86} in the water column and surface sediment collected from the lower Pearl River and its estuary (Chapter 2), where I observe that an unusually low TEX_{86}-derived temperature occurred at the transitional area between the Pearl River estuary and the coastal South China Sea. By analysis of archaeal sequence, the change of archaeal community composition is proposed to me the predominant factor controlling the variation of TEX_{86} in this region. However, as lacking of quatification analysis of archaeal DNA, it is hard to identify the possible contributor to the offset of TEX_{86}. To that end, Chapter 3 presents a parallel analysis targeting archaeal tetraether lipids and Marine Group II (MG II) *Euryarchaeota* 16S rRNA gene, showing that MG II are able to produce GDGTs with 1-4 cyclopentane moieties, which may eventually alter TEX_{86} to an unrealistic value.

In summary, this thesis represents a comprehensive combination of organic geochemistry

and molecular DNA technique, with the ultimate objective of providing a new perspective on interpretation of TEX_{86} record in coastal and ocean environments.

1.5 References

Brassell, S. C., G. Eglinton, I. T. Marlowe, U. Pflaumann, and M. Sarnthein (1986), Molecular tratigraphy: A new tool for climatic assessment, Nature, 320, 129-133.

Herbert, T. D., Alkenone Paleotemperature Determinations, in The Ocean and Marine Geochemistry VOL. 6 Treatise on Geochemistry, edited by H. D. Holland and Turekian.K.K., pp. 365-390, Elsevier-Pergamon, Oxford, 2003.

Schouten, S., Hopmans, E.C., Schefuß, E., Sinninghe Damsté, J.S., 2002. Distributional variations in marine crenarchaeotal membrane lipids: a new tool for reconstructing ancient sea water temperatures? Earth Planet. Sci. Lett. 204, 265 – 274.

Sinninghe Damsté, J.S., Hopmans, E.C., Schouten, S., van Duin, A.C.T., Geenevasen, J.A.J., 2002. Crenarchaeol: the characteristic core glycerol dibiphytanyl glycerol tetraether membrane lipid of cosmopolitan pelagic crenarchaeota. J. Lipid Res. 43, 1641 – 1651.

Hopmans, E. C., S. Schouten, R. D. Pancost, M. T. J. Van der Meer, and J. S. Sinninghe Damsté (2000), Analysis of intact tetraether lipids in archaeal cell material and sediments by high performance liquid chromatography/atmospheric pressure chemical ionization mass spectrometry, Rap. Comm. Mass Spectrom., 14, 585-589.

Huguet, C., 2007, TEX_{86} paleothermometry: proxy validation and application in marine sediments. Geologica Ultraiectina, 276.

Schouten, S., Hopmans, E.C., Sinninghe Damsté, J.S., 2013. The organic geochemistry of glycerol dialkyl glycerol tetraether lipids: a review. Org. Geochem. 54, 19–61.

Brochier-Armanet, C., Boussau, B., Gribaldo, S., Forterre, P., 2008. Mesophilic Crenarchaeota: proposal for a third archaeal phylum, the Thaumarchaeota. Nature Reviews in Microbiology 6, 245–252.

Spang, A., Hatzenpichler, R., Brochier-Armanet, C., Rattei, T., Tischler, P., Spieck, E., Streit, W., Stahl, D.A., Wagner, M., Schleper, C., 2010. Distinct gene set in two different lineages of ammonia-oxidizing archaea supports the phylum Thaumarchaeota. Trends in Microbiology 554, 331–340.

Könneke, M., de la Torre, A.E., Walker, J.R., Waterbury, J.B., Stahl, D.A., 2005. Isolation of an autotrophic ammonia-oxidizing marine archaeon. Nature 437, 543–546.

de la Torre, J.R., Walker, C.B., Ingalls, A.E., Könneke, M., Stahl, D.A., 2008. Cultivation of a thermophilic ammonia oxidizing archaeon synthesizing crenarchaeol. Environmental Microbiology 10, 810–818.

Sinninghe Damsté, J.S., Rijpstra, W.I.C., Hopmans, E.C., Jung, M.Y., Kim, J.G., Rhee, S.K., Stieglmeier, M., Schleper, C., 2012b. Intact polar and core glycerol dibiphytanyl glycerol tetraether lipids of Group I.1a and I.1b Thaumarchaeota in soil. Applied and Environmental Microbiology 78, 6866–6874.

Lincoln, S.A., Wai, B., Eppley, J.M., Church, M.J., Summons, R.E., and DeLong, E.F., 2014. Planktonic Euryarchaeota are a significant source of archaeal tetraether lipids in the ocean. Proc. Natl. Acda. Sci. USA 111(27), 9858–9863.

Kuypers, M.M.M., Blokker, P., Erbacher, J., Kinkel, H., Pancost, R.D., Schouten, S., Sinninghe Damsté, J.S., 2001. Massive expansion of marine archaea during a mid-Cretaceous oceanic anoxic event. Science 293, 92–95.

Gliozzi, A., G. Paoli, M. de Rosa, and A. Gambacorta (1983), Effect of isoprenoid cyclization on the transition temperature of lipids in thermophilic archaebacteria., Biochim. Biophys. Acta, 735, 234-242.

Wuchter, C., Schouten, S., Coolen, M.J.L., Sinninghe Damsté, J.S., 2004. Temperaturedependent variation in the distribution of tetraether membrane lipids of marine Crenarchaeota: implications for TEX_{86} paleothermometry. Paleoceanography 19, PA4028. http://dx.doi.org/10.1029/2004PA001041.

Kim, J.-H., Schouten, S., Hopmans, E.C., Donner, B., Sinninghe Damsté, J.S., 2008. Global core-top calibration of the TEX_{86} paleothermometer in the ocean. Geochimica et Cosmochimica Acta 72, 1154–1173.

Kim, J.-H., van der Meer, J., Schouten, S., Helmke, P., Willmott, V., Sangiorgi, F., Koç, N., Hopmans, E.C., Sinninghe Damsté, J.S., 2010b. New indices and calibrations derived from the distribution of crenarchaeal isoprenoid tetraether lipids: implications for past sea surface temperature reconstructions. Geochimica et Cosmochimica Acta 74, 4639–4654.

Kim, J.H., Romero, O.E., Lohmann, L., Donner, B., Laepple, T., Haam, E., Sinninghe Damsté, J.S., 2012. Pronounced subsurface cooling of North Atlantic waters off Northwest Africa during Dansgaard–Oeschger interstadials. Earth and Planetary Science Letters 339–340, 95–102.

Lipp, J.S., Hinrichs, K.-U., 2009. Structural diversity and fate of intact polar lipids in marine sediments. Geochimica et Cosmochimica Acta 73, 6816–6833.

Leider, A., Hinrichs, K.-U., Mollenhauer, G., Versteegh, G.J.M., 2010. Core-top calibration of the lipid-based UK' 37 and TEX_{86} temperature proxies on the southern Italian shelf (SW Adriatic Sea, Gulf of Taranto). Earth and Planetary Science Letters 300, 112–114.

Weijers, J.W.H., Schouten, S., Spaargaren, O.C., Sinninghe Damsté, J.S., 2006. Occurrence and distribution of tetraether membrane in soils: implications for the use of the BIT index and the TEX_{86} SST proxy. Organic Geochemistry 37, 1680–1693.

Schouten, S., Pitcher, A., Hopmans, E.C., Villanueva, L., van Bleijswijk, J., Sinninghe Damsté, J.S., 2012. Distribution of core and intact polar glycerol dibiphytanyl glycerol tetraether lipids in the Arabian Sea Oxygen Minimum Zone: I: Selective preservation and degradation in the water column and consequences for the TEX_{86}. Geochimica et Cosmochimica Acta 98, 228 – 243.

DeLong, E.F., 2006. Archaeal mysteries of the deep revealed. Proceedings of the National Acadamy of Sciences USA 103, 6417–6418.

Zhang, Y.G., Zhang, C.L., Liu, X.L., Li, L., Hinrichs, K.U., Noakes, J.E., 2011. Methane Index: a tetraether archaeal lipid biomarker indicator for detecting the instability of marine gas hydrates. Earth and Planetary Science Letters 307, 525–534.

Ji, X., Sheng, J., Tang, L., Liu, D., Yang, X., 2011. Process study of circulation in the Pearl River Estuary and adjacent coastal waters in the wet season using a triply-nested circulation model. Ocean Modelling 38, 138 – 160.

Zhao, H., 1990. Evolution of the Pearl River Estuary. Ocean Press, Beijing 357pp. (in Chinese).

Cai, W.-J., Guo, X., Chen, C.T. A., Dai, M., Zhang, L., Zhai, W., Lohrenz, S.E., Yin, K., Harrison, P. J. and Wang, Y., 2008. A comparative overview of weathering intensity and

HCO3 - flux of the world¡¯s major rivers with emphasis on the Changjiang, Huanghe, Zhujiang (Pearl) and Mississippi Rivers. Continental Shelf Research 28, 1538-1549.

Rabouille, C., Conley , D.J., Dai, M.H., Cai, W.-J., Chen, C.T.A., Lansard, B., Green, R., Yin, K., Harrison, P.J., Dagg, M., McKee, B., 2008. Comparison of hypoxia among four river-dominated ocean margins: The Changjiang (Yangtze), Mississippi, Pearl, and Rhone rivers. Continental Shelf Research 28, 1527 – 1537.

Chen, J., Xu, S., and Sang, J., 1994. The depositional characteristics and oil potential of the paleo–Pearl River Delta system in the Pearl River Mouth Basin, South China Sea. Tectonophysics 235, 1– 11.

Chau, Y.K., Wong, C.S., 1960. Oceanographic investigations in the northern region of the South China Sea off Hong Kong. Hong Kong University Fisheries Journal 3, 1–25.

Williamson, G.R., 1970. The hydrography and weather of the Hong Kong fishing grounds. Hong Kong Fisheries Bulletin 1, 43–49.

Morton, B., Wu, S.S., 1975. The hydrology of the coastal waters of Hong Kong. Environment Research 10, 319–347.

Yin, K.D., Zhang, J., Qian, P.Y., 2004. Effect of wind events on phytoplankton blooms in the Pearl River estuary during summer. Cont Shelf Res 24, 1909–1923.

Chen, C.T.A., Wang, S.L., Lu, X.X., Zhang, S.R., Lui, H.K., Tseng, H.C., Wang, B.J., Huang, H.I., 2008. Hydrogeochemistry and greenhouse gases of the Pearl River, its estuary and beyond. Quatern. Int. 186, 79–90.

Zhou, H., Yin, X., Yang, Q., Wang, H., Wu, Z., Bao, S., 2009. Distribution source and flux of methane in the western Pearl River Estuary and northern South China Sea. Marine Chemistry 117, 21 – 31.

Yu, F.L., Zong, Y.Q., Lloyd, J.M., Huang, G.Q., Leng, M.J., Kendrick, C., Lamb, A.L., Yim, W.W.S., 2010. Bulk organicδ13C and C/N as indicators for sediment sources in the Pearl River delta estuary, southern China. Estuarine and Coastal Shelf Science 87, 618–630.

Harrison, P.J., Yin, K.D., Lee, J.H.W., Gan, J., Liu, H., 2008. Physical – biological coupling in the Pearl River Estuary. Continental Shelf Research 28, 1405 – 1415.

Fig. 1.1

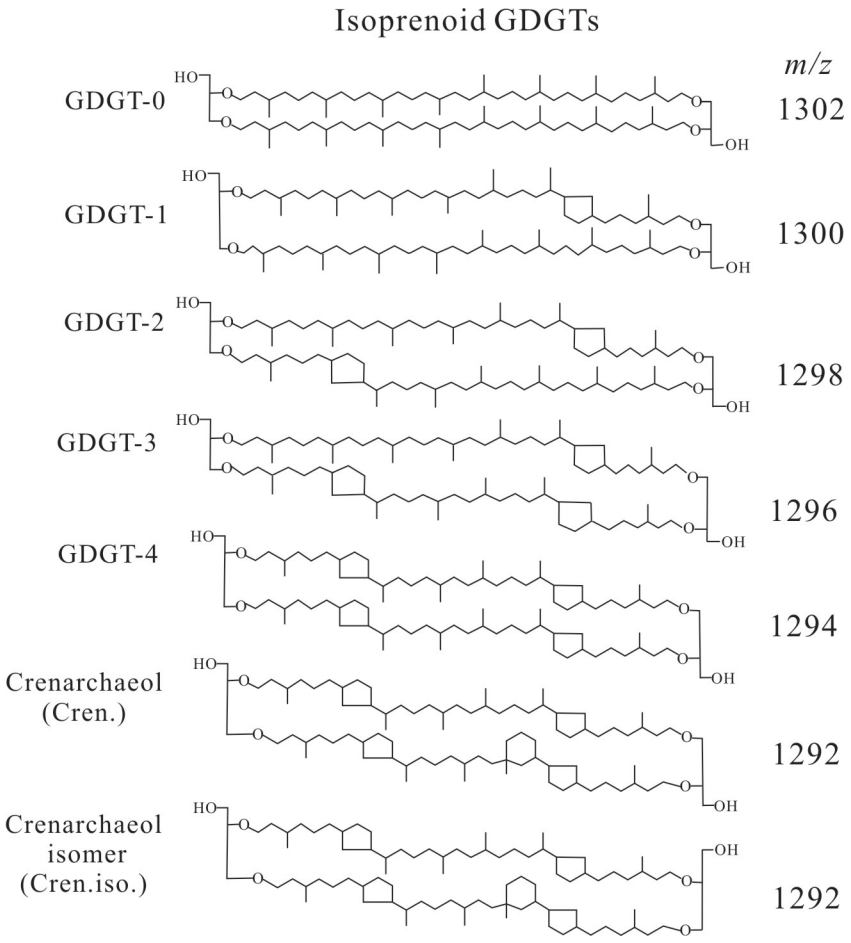

Fig. 1.1. Structures of archaeal core GDGTs described in the text.

Fig. 1.2.

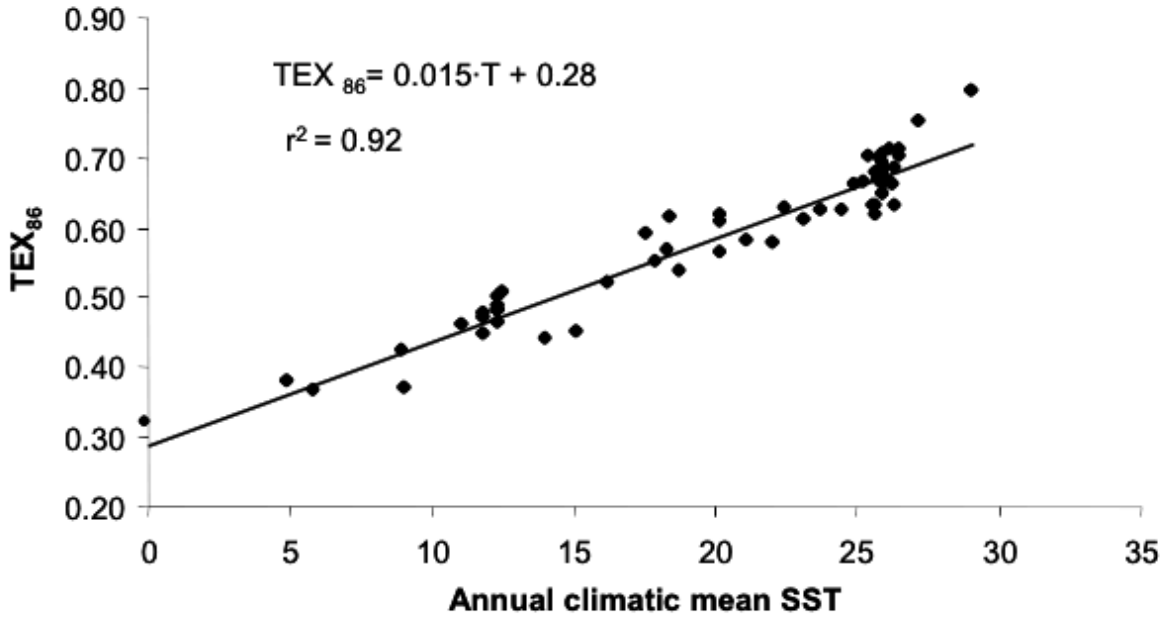

Fig. 1.2. Empirical correlation between TEX_{86} values of core tops and annual mean SST (from Schouten et al., 2002).

CHAPTER 2[1]

UNUSUALLY LOW TEX_{86} VALUES IN THE TRANSITIONAL ZONE BETWEEN PEARL RIVER ESTUARY AND COASTAL SOUTH CHINA SEA: IMPACT OF CHANGING ARCHAEAL COMMUNITY COMPOSITION

[1] Wang, J.X., Y. Wei, P. Wang, Y. Hong, C.L. Zhang. 2015. *Chemical Geology.* 402:18-29.

Reprinted here with permission of the publisher.

Abstract

TEX_{86}, calculated based on the distribution of isoprenoid glycerol dialkyl glycerol tetraethers (GDGTs), is used worldwide for paleotemperature reconstruction in marine and lacustrine environments. Recently, however, increasing evidence showed that TEX_{86} could be affected by multiple environmental variables. In this study, TEX_{86} was calculated for core and polar GDGTs obtained from water column and surface sediments in the lower Pearl River and its estuary. Together with previously published core GDGT data from the coastal and open South China Sea (SCS), a comparison was made between TEX_{86}-derived and satellite-based surface water temperature, which showed a TEX_{86}-temperature minimum that is considerably lower than winter satellite temperature in the transitional zone between the Pearl River estuary and the coastal SCS. TEX_{86} showed significantly positive correlation with GDGT-2 and GDGT-3 in this transitional zone, indicating that they are the primary compounds for the TEX_{86} bias toward cooler temperature. Lipid and molecular DNA data both indicate that the variation in archaeal community composition rather than water depth or seasonality is likely the crucial factor causing the deviation of TEX_{86} in the transitional area. Our study has implications for studies in ancient continental margins where unusually low TEX_{86} temperatures may be observed in the geological record.

Keywords: TEX_{86}; Isoprenoid GDGTs; The lower Pearl River; Estuary; South China Sea

2.1 Introduction

TEX_{86} is a (paleo-) sea surface temperature (SST) proxy based on the distribution of cyclic moieties of isoprenoidal glycerol dialkyl glycerol tetraethers (GDGTs, Fig. 2.1) of archaeal membrane lipids (Schouten et al., 2002). The calibration of TEX_{86} was made empirically using marine core top sediments collected globally (Schouten et al., 2002; Kim et al., 2008, 2010). To date, TEX_{86} has been applied to reconstruct paleo-SST in numerous cases (e.g. Liu et al., 2009; Zhang et al., 2014). However, with increasing application of TEX_{86} in different environments, it appeared that the TEX_{86} value could be affected by factors other than temperature (as reviewed in Pearson and Ingalls, 2013 and Schouten et al., 2013), such as 1) in situ production of GDGTs in sediments (Lipp and Hinrichs, 2009; Liu et al., 2011; Dang et al., 2013), 2) input of GDGTs from the water column below the photic zone (Kim et al., 2012a; Huguet et al., 2007), 3) seasonal variability (Wuchter 2006; Herfort et al., 2006a; Leider et al., 2010), 4) terrestrial input (Weijers et al., 2006; Herfort et al., 2006b, Zhu et al., 2011), and 5) preferential reservation of polar GDGTs (Schouten et al., 2012; Lengger et al., 2012). Further bias of TEX_{86} may be attributed to GDGTs produced from other groups of Archaea, such as marine group II (Lincoln et al., 2014) or methanotrophic (Weijers et al., 2011b; Zhang et al., 2011; Ho et al., 2014) *Euryarchaeota*, or group I.1b *Thaumarchaeota* of soil origin (Sinninghe Damsté et al., 2012).

Recently, analysis of surface sediments from coastal South China Sea (SCS) off the Pearl River (PR) estuary (water depth < 100 m) showed that TEX_{86}-derived temperatures were significantly lower than annual mean SST (Wei et al., 2011). This observation was confirmed by subsequent studies of Ge et al. (2013), Zhang et al. (2013), and Zhou et al. (2014), which examined the TEX_{86} temperature in the sediments from the same geographic region. The latter

two studies favored an interpretation of winter signal imprinted by the low TEX_{86} values. This conclusion was supported by a previous study in the southern North Sea (Herfort et al., 2006a). In contrast, Castañeda et al. (2010) proposed that the TEX_{86} temperature in the coastal area of the Mediterranean Sea reflected summer signal during the Holocene. Leider et al. (2010) found that TEX_{86}-derived temperatures for the nearshore sites were similar to winter SST; whereas, at the most offshore sites, they were close to summer SST. In addition, several other investigations indicated that the TEX_{86}-derived temperatures from the surface sediments of coastal seas reflected temperature signals from different water depths (Lee et al., 2008; Lopes dos Santos et al., 2010). Therefore, it remains unclear what is the predominant factor that controls the variation of TEX_{86} in the coastal marine environment (water depth < 200 m).

In this study we compared the distribution and abundance of archaeal membrane core lipids (CL or CL-GDGTs) and polar lipids (PL or PL-GDGTs) in the suspended particulate matters (SPM), surface sediments, and surrounding soils in the lower Pearl River and its estuary, and then examined the factors controlling the TEX_{86} signals in the estuary and coastal to open SCS by combining our data with those from Zhang et al. (2013), Ge et al. (2013), and Wei et al. (2011). Our results indicated that a TEX_{86} temperature minimum occurred in the transitional zone between the PR estuary and coastal SCS. Together with molecular DNA data from SPM in the surface water, we suggested that the variation in archaeal community composition might be responsible for the unusually low TEX_{86}. Our study warns against the applicability of the TEX_{86} as a paleotemperature proxy for interpretation of low temperature events in ancient continental margins.

2.2 Material and Methods

2.2.1 Sampling

The sampling procedures and analytic methods for water chemistry were described in detail in Zhang et al. (2012). Briefly, eighteen SPM samples and thirteen surface sediments were collected from the lower Pearl River (10 stations) and its estuary (4 stations) (Fig. 2.2) in the summer of 2010. SPM was collected from surface (ca. 1 m) of the lower Pearl River and from surface (ca. 1 m) and near the bottom (ca. 4 – 17 m) of the PR estuary. About 3 – 27 L of surface or bottom water were collected using a submersible pump and filtered onto ashed (450^{o}C, overnight) and pre-weighed glass-fiber filters (Whatman GF/F, 0.7 μm, 142 mm diameter) (Table 2.1). The pH, temperature, and salinity were determined in situ by a Horiba instrument (W-20XD, Kyoto, Japan) (Table 2.2).

Surface sediments (top ca. 10 cm) were collected using a grab sampler at all stations except for the estuarine station PR-13 at which a sediment sample was not collected (Fig. 2.2; Table 2.1). Twenty soil samples (from the top 5-10 cm) were also collected from within the catchment of the lower Pearl River and its estuary (Fig. 2.2).

All samples were frozen immediately in liquid nitrogen and kept at -80°C in the laboratory before analysis. The same samples were used for simultaneous extraction of isoprenoid GDGTs and branched GDGTs; the results for branched GDGTs were reported previously (Zhang et al., 2012); in this study, we present the results of archaeal isoprenoid GDGTs.

2.2.2 Analysis of archaeal isoprenoid GDGTs

Lipid extraction and separation of CL- and PL-GDGTs followed a modified Bligh and Dyer extraction procedure described in Zhang et al. (2012). Briefly, five grams of freeze-dried sediment or the cut pieces of a whole filter were extracted by sonication (10 min, 6X) with a mixture of methanol, dichloromethane (DCM) and phosphate buffer (pH 7.4) (2:1:0.8, v/v/v). The supernatants were combined and carefully evaporated to dryness under a steady stream of N_2 at 35ºC, re-dissolved in a small amount of n-hexane/ethylacetate (1:1,v/v) and separated into an apolar fraction that contained core lipids (CL-GDGTs) and a polar fraction that contained polar lipids (PL-GDGTs), using activated silica gel columns eluted sequentially with n-hexane/ethylacetate (1:1, v/v) and methanol. PL-GDGTs were treated in the following manner: half of the polar fractions (non-hydrolyzed polar fractions) were directly condensed, dissolved in n-hexane/isopropanol (99:1, v/v), and filtered using a PTFE filter that had a pore diameter of 0.45 μm; the other half (hydrolyzed polar fractions) was hydrolyzed (24 h, 70ºC) in 5% HCl/methanol (V/V). DCM and MilliQ water were added, and the DCM fraction was collected (repeated 4X). The DCM fraction was rinsed (6X) with MilliQ water in order to remove acid and dried under N_2 gas. The hydrolyzed fraction was also re-dissolved in n-hexane/isopropanol (99:1, v/v) and filtered through 0.45 μm PTFE filters.

The analysis of non-hydrolyzed polar fractions is to determine any carryover of CL-GDGTs into the polar fraction (Weijers et al., 2011a). In order to analyze PL-GDGTs as CL-GDGTs, the polar fraction was hydrolyzed to cleave off the polar head groups (Pitcher et al., 2009). Thus, the accurate yield of PL-GDGTs in the polar fraction needs to exclude any carryover of CL-GDGTs from the hydrolyzed polar fractions. Because the total polar GDGTs

were calculated based on the difference of yield between hydrolyzed and non-hydrolyzed polar fractions, the precise composition of intact polar lipids was unknown. Thus, we used PL-GDGTs (polar lipid GDGTs) instead of IPL-GDGTs (intact polar lipid GDGTs) as described in Zhang et al. (2012).

All these fractions were analyzed using high performance liquid chromatography/atmospheric pressure chemical ionization-tandem mass spectrometry (HPLC/APCI-MS/MS), which was performed with an Agilent 1200 liquid chromatography equipped with an automatic injector coupled to QQQ 6460 MS and Mass Hunter LC-MS manager software using a procedure modified from Zhang et al. (2012) and Schouten et al. (2007). Separation was achieved with a Prevail Cyano column (2.1 mm × 150 mm, 3 μm; Alltech Deerifled, IL, USA) thermostated at 40ºC. Injection volume was 5 μl. GDGTs were first eluted isocratically with 90% A and 1% B for 5 min, followed by a linear gradient to 18% B in 45 min. Solvent was held for 10 min in 100% B and was then allowed to re-equilibrate in 90% A: 10% B over a period of 10 min. A represents n-hexane and B is a mixture solution of 90% n-hexane and 10% isopropanol.

Detection was performed using positive ion APCI. The $(M+H)^+$ diagnostic of each core isoprenoid GDGT (m/z 1302, 1300, 1298, 1296, 1294, 1292) was monitored via selected ion monitoring (SIM) mode. The conditions for Agilent 6460 ion source were as follows: nebulizer pressure 40 psi, vaporizer temperature 350ºC, drying gas (N_2) flow 5 L/min and temperature 250ºC, capillary voltage 3 kV, corona 4 μA. All fractions were quantified by adding a known amount of an internal C_{46} GDGT standard in the apolar and polar fractions (Huguet et al., 2006). The detection limit for GDGTs was 0.001 ng.

Indices based on the relative abundance of GDGTs were calculated as follows:

$TEX_{86} = ([GDGT\text{-}2] + [GDGT\text{-}3] + [Cren.iso])/([GDGT\text{-}1] + [GDGT\text{-}2] + [GDGT\text{-}3] + [Cren.iso])$ (Schouten et al., 2002) (1)

$TEX_{86}^{H} = \log (TEX_{86})$ (2)

$SST = 68.4 \times TEX_{86}^{H} + 38.6$ (Kim et al., 2010) (3)

with the GDGT numbers corresponding to the GDGT structures in Figure 2.1.

The calibrations of TEX_{86} by Kim et al. (2010) were chosen in this study because of its significant linear correlation with SST in the 15ºC – 28ºC range (cf. Fig. 14 of Schouten et al., 2013) and lower standard error (< ±2.5ºC). On the other hand, using the latest calibration of TEX_{86} based on the core top sediments of < 200 m water depth (Kim et al., 2012a) would result in unrealistic values that are lower than winter temperatures in surface water (Table A1 and Table A2). The analytical error for TEX_{86} was better than ±0.011 for all samples, which corresponded to about ±0.5ºC according to Kim et al. (2010).

2.2.3 DNA analysis

DNA isolation and amplification. Four SPM samples were selected to investigate the archaeal community composition along the lower Pearl River and its estuary, i.e. PR-4, PR-9, PR-12, and PR-14 (Fig. 2.2). Bulk DNA was extracted from SPM samples using PowerSoil™ DNA Isolation Kit (Mo Bio Laboratories, Carlsbad, CA). Archaeal 16S rRNA gene fragments were amplified using primers Arch21F (5'-TTCCGGTTG ATCCYGCCGCCGGA-3') and Arch958R (5'-YCCGGC GTTGAMTCCAATT-3') as previous described (DeLong, 1992). The conditions for amplification of archaeal 16S rRNA genes were as follows: initial denaturation at 95°C for 3 min; 30 cycles of denaturing (1 min at 94°C), annealing (1 min at 55°C), and

extension (1.5 min at 72°C); and a final extension at 72°C for 10 min. The PCR products were purified with a QIAquick PCR Purification kit (Qbiogene Inc., Irvine, CA).

Cloning analysis. The PCR product was ligated into the pMD-18T vector (TaKaRa) and transformed into Escherichia coli DH5α competent cells. The transformed cells were plated on Luria-Bertani plates containing 100 μg/ml of ampicillin, 80 μg/ml of X-Gal (5-bromo-4-chloro-3-indolyl-β-D-galactopyranoside), and 0.5 mM IPTG (isopropyl-β-D-thiogalactopyranoside) and incubated overnight at 37°C, Resulting PCR products were screened for correct size and purity by 1% agarose gel electrophoresis.

Phylogenetic analysis. The 16S rRNA gene sequences were grouped into operational taxonomic units (OTUs) with 3% distance cutoff with the DOTUR program (Schloss & Handelsman, 2005). Sequence similarity searches were performed using the BLAST network service of the NCBI database (http://www.ncbi.nlm.nih.gov/BLAST). The sequences were tested for chimeras by using the Ribosomal Database Project Chimera-Check program and were aligned with Clustal W (Thompson et al., 1997).

Accession number of nucleotide sequences. The sequences have been deposited in the GenBank database under accession numbers: KP769447 - KP769519.

2.2.4 Satellite SST and air temperature

The satellite SST was obtained from the best SST (bSST) data sets from the NOAA advanced very-high-resolution radiometer (AVHRR) (version 5.0; http://pathfinder.nodc.noaa.gov) on a 4 km spatial resolution. Since the temperature reconstructed from the SPM was a snapshot signal, the mean SST of the sampling month (July)

was extracted and averaged from the daily mean bSST for 30 days of July of 2010 using MATLAB. On the other hand, since the top ca. 10 cm sediments in the PR estuary were estimated to represent 6 – 10 yr deposition (Strong et al., 2012), the annual mean SST and winter mean SST used 8-year mean values of annual mean bSST (2003 – 2010) and monthly mean bSST (December – February), respectively. The mean air temperature of the month of July was 30ºC recorded near the city of Guangzhou (Liu et al., 2007).

2.2.5 Statistical analysis

Cluster analysis was performed on CL-GDGTs in the sediments from the lower Pearl River, the PR estuary, and the coastal and open SCS using the base program in R 2.12.1. Data for sediments from the coastal and open SCS were those of Wei et al. (2011), Ge et al. (2013), and Zhang et al. (2013). The relative abundance of CL-GDGTs from all samples was imported into R and the Euclidean method was used to compute the distance matrix and to generate a hierarchical clustering tree. The linear regression analysis was performed by iPython Notebook.

2.3 Results and Discussion

2.3.1 CL- and PL-TEX_{86} temperatures in the lower Pearl River and soils

In the water column of the lower Pearl River, the CL-TEX_{86} temperatures (avg. 25.6 ± 0.6ºC, n = 10) were close to the satellite-based annual mean surface water temperature (SWT)

(24.6 ± 0.1ºC) (Fig. 2.3a). However, the PL-TEX_{86} temperatures (avg. 27.6 ± 1.1ºC, n=10) varied between the satellite-based annual and July mean SWT (Fig. 2.3b).

In the sediments of the lower Pearl River, the CL-TEX_{86} temperatures (avg. 25.2 ± 1.0ºC, n = 10) varied around the annual mean SWT as well (Fig. 2.3c); however, the PL-TEX_{86} temperatures (avg. 20.2 ± 2.9ºC, n=10) were below the annual mean SWT and fluctuated around the winter mean SWT (20.4 ± 0.1ºC) (Fig. 2.3d; Fig. 2.4), which was in contrast to its fluctuation above the annual mean SWT in the SPM samples in the lower Pearl River (Fig. 2.3b).

In summary, the average values of the CL-TEX_{86} temperatures from either SPM or sediment samples were all close to annual mean SWT in the lower Pearl River (Fig. 2.4); whereas, the PL-TEX_{86} temperatures deviated from the annual mean SWT with the SPM samples exhibiting about 3ºC higher and the sediments 4ºC lower than the annual mean SWT (Fig. 2.4).

The TEX_{86} temperatures for soils from the catchment of the lower Pearl River and its estuary were also calculated (using Eq. 3) in order to compare with the signals from the SPM and sediment samples. On average, the TEX_{86} values of the soil samples were significantly higher than those of surface water and surface sediments from the lower Pearl River (Suppl. Table A1, A2, and A3). When translating to temperatures, the CL-TEX_{86} temperatures (avg. 29.0 ± 2.4ºC, n = 20) and PL-TEX_{86} temperatures (avg. 29.6 ± 3.2ºC, n = 20) in the soils were correlated well with the July mean air temperature (30ºC), both of which were 1ºC – 8ºC higher than those from the surface water SPM and the surface sediments in the lower Pearl River (Fig. 2.4).

The significant difference in TEX_{86} temperatures between soils and the SPM samples (Fig. 2.4) indicates a substantial amount of in situ production of GDGTs in the lower Pearl River, which is consistent with previous studies showing in situ production of crenarchaeol in the water column of the Amazon River (Kim et al., 2012b; Zell et al., 2013a, b) and in the Yangtze River

(Yang et al., 2013). Furthermore, the TEX_{86} temperature from PL-GDGTs in the SPM reflects water temperature during the collecting season (July). This is in line with previous observation that TEX_{86} temperature in the Yangtze River appeared to have a good correlation with in situ river temperature (Yang et al., 2013).

In contrast with the short time scale (ca. days or even months) of SPM in the water column, sediments represent a relatively long time accumulation, i.e. ca. 6-10 yrs for our sediment samples according to Strong et al. (2012). Hence, the CL- and PL-GDGTs in the surface sediments of the lower Pearl River may have multiple sources, including: 1) terrestrial input from surrounding soil, 2) vertical export from water column, 3) lateral transport from the upland, or 4) in situ production in the surface sediment.

Here we assess each of the above potential sources. 1) The substantial difference in TEX_{86} and the amount of total GDGTs between the surface sediments and soils (Fig. 2.4; Table 2.2) suggest that soil input in the surface sediment may be insignificant. 2) Due to the similarity in CL-TEX_{86} temperature between the SPM and surface sediments, most CL-GDGTs in the sediments are likely from the surface water. Yet, this interpretation cannot explain the offset of PL-TEX_{86} temperature between the SPM and the surface sediments. 3) Strong et al. (2012) suggested that most of terrestrial organic matter in the PR estuary were predominantly contributed by the cooler upland region based on the evidence that annual mean air temperature derived from the branched GDGTs-based proxies were cooler than a given annual mean air temperature in the lowland Pearl River catchment. If that is the case, the PL-GDGTs in the surface sediment of the lower Pearl River may be derived from a cooler upland region because of the occurrence of low PL-TEX_{86} temperature (Fig. 2.3d & Fig. 2.4). This is counter intuitive as the CL-GDGTs should also register this cooler signal from upland, which is not the case in this

study (more discussion in the next section). 4) Since the PL-TEX_{86} temperatures in the sediments were cooler than the annual mean SST even though sampling occurred in summer, it seems reasonable to assume that the dominant component of PL-GDGTs may be from in situ production in the sediments that are expected to have lower in situ temperature than the water column.

Overall, our data suggest that CL-TEX_{86} in the surface sediment is unlikely to be influenced by the relatively low abundance of PL-GDGTs produced in situ in the water column and surface sediments (Table 2.2). Consequently, the CL-TEX_{86} may have the potential to be employed as a palaeothermometer in the surface sediment of the lower Pearl River.

2.3.2 CL- and PL-TEX_{86} temperatures in the PR estuary

Variations in TEX_{86} temperature in the SPM and the surface sediments of the PR estuary were different from those in the lower Pearl River (Fig. 2.3). In the surface water of the PR estuary, the CL-TEX_{86} temperature fell between annual and winter mean SWT, whereas the PL-TEX_{86} temperature ranged between July and annual mean SWT (Fig. 2.3a & 2.3b). In the bottom water, the CL-TEX_{86} temperature approached the winter mean SWT, whereas PL-TEX_{86} temperature varied between annual and winter mean SWT (Fig. 2.3a & 2.3b). One exception was the PL-TEX_{86} temperature at the station PR-11, which was close to the satellite-based July mean SWT (Fig. 2.3b). Overall, the CL- and PL-TEX_{86} temperatures were consistently higher in the surface water than in the bottom water in the PR estuary, with the lowest average value occurring in the CL-GDGTs from the bottom water (Fig. 2.4).

In the sediments of the PR estuary, the CL-TEX_{86} temperature tended to decrease from close to the annual mean SWT at the station PR-11 to even slightly below the winter mean SWT at the station PR-14 (Fig. 2.3c). However, the PL-TEX_{86} temperature varied between the annual and winter mean SWT (Fig. 2.3d). Overall, CL- and PL-TEX_{86} temperatures were lower than the annual mean SWT, with the former being even lower than the winter temperature toward the open SCS (Fig. 2.4).

Comparison of CL- and PL-TEX_{86} in the SPM and the surface sediments of the PR estuary indicates that the CL-TEX_{86} signal in the surface sediments of the PR estuary is predominantly contributed by the CL-TEX_{86} in the water column. The seaward station, PR-14, appeared to be mainly contributed by CL-TEX_{86} signal in the bottom water (Fig. 2.3d), where, typically after the station PR-12, the water column seemed to be stratified according to the salinity and the water temperature (Table 2.2). This is consistent with previous interpretations that TEX_{86} signal in the surface sediment was mainly from suspended particulate organic matter in the water column in the southern North Sea (water depth < 50 m) (Herfort et al., 2006a), and that, with increasing water depth, it even reflects the temperature of slightly deeper water in the Amazon shelf and slope (Zell et al., 2014). Further evidence comes from the comparison of the abundance of CL- and PL-crenarchaeol between the low Pearl River and its estuary. The abundance of crenarchaeol from the surface sediment of the PR estuary (CL = 279.7 ± 345.6 ng/g, n = 3; PL = 33.4 ± 38.7 ng/g, n = 3) was significantly higher than that from the lower Pearl River (CL = 47.7 ± 29.2 ng/g, n = 10; PL = 6.6 ± 3.3 ng/g, n = 10) (Table 2.2). This is consistent with the distribution of crenarchaeol in the SPM, i.e. the crenarchaeol concentration from the SPM in PR estuary (CL = 11.4 ± 6.4 ng/g, n = 8; PL = 16.3 ± 14.6 ng/g, n = 8) was up to 10-times higher than those from the lower Pear River (CL = 5.7 ± 5.0 ng/g, n = 10; PL = 1.6 ± 1.2 ng/g, n = 10) (Table 2.2),

implying that the archaeal lipids in the surface sediments of the PR estuary are predominantly derived from the water column.

2.3.3 Possible mechanisms for the unusually low TEX_{86} in the transitional zone between the PR estuary and the coastal SCS

In the coastal area of northern South China Sea off the Pearl River estuary (water depth < 200 m), the low temperature signals calculated based on the CL-TEX_{86} in the sediments were interpreted as impact of terrestrial input or reflecting winter temperature (Wei et al., 2011; Ge et al., 2013; Zhang et al., 2013; Zhou et al., 2014). In order to determine the predominant factor(s) causing a CL-TEX_{86} bias toward low temperature signal in the transitional zone between the PR estuary and coastal SCS, the CL-TEX_{86} values from this study, in combination with data sets from Wei et al. (2011), Ge et al. (2013), Zhang et al. (2013), were plotted against water depth (Fig. 2.5; Table 2.1). The results showed that TEX_{86} temperature did not reflect winter SWT as previous suggestions (Ge et al., 2013; Zhang et al., 2013; Zhou et al., 2014), but exhibited a trend of discrepancy between the TEX_{86} temperature estimates and the satellite-based winter temperatures in the transitional zone (at water depth of ca. 20 – 30 m) (Fig. 2.5). Although the TEX_{86} temperatures from Zhou et al. (2014) were relatively higher than those from other studies (Ge et al., 2013; Zhang et al., 2013) in the coastal SCS, which may result from different sampling season and/or different methods of lipid extraction, they decreased from above the winter SWT to below the winter SWT as well (Table 2.1 of Zhou et al., 2014), showing a similar trend of discrepancy along the transitional zone (Fig. 2.5). However, in the open South China Sea (water depth of 1000 – 4000 m), the TEX_{86} temperature matched roughly the annual mean

SST (Fig. 2.5). The inconsistency between TEX_{86} temperature and winter SWT in the sediments of coastal SCS suggests that seasonality seems unlikely to be a major factor controlling the GDGT distribution at water depth < 200 m, particularly in the transitional zone between the PR estuary and the coastal SCS.

In order to evaluate which compounds may give rise to the deviation of TEX_{86} (eqn. 1) toward the transitional zone between the PR estuary and the coastal SCS, fractional abundances (to total GDGTs) of the GDGT-1, GDGT-2, GDGT-3, and crenarchaeol regioisomer were assessed. The deviation of TEX_{86} in the transitional zone was linearly correlated with the fractional abundance of GDGT-2 and GDGT-3 (Fig. 2.6a & 2.6b) and reached the lowest points at the water depth of 20 – 30 m (Fig. 2.6c & 2.6d). Compared with the data from the open South China Sea (Wei et al., 2011; Ge et al., 2013), the fractional abundance of GDGT-2 was lower in the transitional zone (Fig. 2.6c), whereas the fractional abundance of GDGT-3 in the whole depth profile of the transitional zone was no less than that from the open South China Sea (Fig. 2.6d), suggesting that the GDGT-2 and GDGT-3 are key components causing the bias of TEX_{86} in the transitional zone. Similar observations were made by Taylor et al. (2013) and Hernandez-Sanchez et al. (2014) for other marine environments. On the other hand, the variation of GDGT-1 and crenarchaeol regioisomer exhibited no correlation with TEX_{86} in this region (data not shown), suggesting that these two compounds may have little impact on the variation of TEX_{86} in the transitional zone.

The unusually low CL-TEX_{86} in the transitional zone is an important observation in our study, which may be explained by four scenarios: 1) variation in CL-GDGT composition with water depth; 2) terrestrial input of CL-GDGTs; 3) preferential diagenesis of GDGTs; and 4) contribution of diverse members of the planktonic archaeal community. Regarding scenario 1,

the TEX_{86} signal was not linearly correlated with water depth in the transitional zone (Fig. 2.5), which indicates that water depth is not a key factor controlling the variation of CL-TEX_{86}. For scenario 2, the comparison in TEX_{86} temperature between surface sediments in the lower Pearl River and its estuary and the soils (Fig. 2.4) has clearly indicated that terrestrial input had little impact on the distribution of TEX_{86} in the sediments of the PR estuary, which is also demonstrated by the low BIT values (< 0.2) in the estuarine station PR-14 and the seaward coastal stations (Fig. 2.5). For scenario 3, although it is difficult to identify the degradation of GDGTs in the transitional zone, a recent study showed that the PR estuary was not characterized by extensive loss of organic matter through degradation (Strong et al., 2012). Furthermore, previous studies indicated that the distribution of core GDGTs in the sediments was not significantly affected by oxic degradation (Schouten et al., 2004; Kim et al., 2009; Turich et al., 2013).

Scenario 4 concerns with the variation in GDGTs within different thaumarchaeotal populations (e.g. fresh water vs. marine *Thaumarchaeota*) and the change in total archaeal community composition (e.g. *Euryarchaeota* vs. *Thaumarchaeota*) (Taylor et al., 2013; Hernandez-Sanchez et al., 2014 and refs. therein). The ratio of GDGT-2 to GDGT-3 ([2/3] ratio) was significantly lower in the PR estuary and coastal SCS than in the open South China Sea (Fig. 2.6). A similar observation using global modern core-top sediments and SPM in the modern water column was reported by Taylor et al. (2013). Hernandez-Sanchez et al. (2014) also noted the increase of the [2/3] ratio with water depth in subsurface and deep water of southeast Atlantic Ocean and suggested that this trend was related to the variation of thaumarchaeotal community composition, which arises from the evidence of the linear correlations between the

concentrations of core GDGT-2 & 3 and core crenarchaeol, a known biomarker of *Thaumarchaeota* (Sinninghe Damsté et al., 2002).

In respect to the core lipids within the PR estuary, however, our data exhibited no correlation between the concentrations of GDGT-2 & GDGT-3 and crenarchaeol (Table 2.3). Even though both PL-GDGT-2 and PL-GDGT-3 in the PR estuary appeared to be correlated with crenarchaeol to a certain degree, the correlation was not as strong as those exhibited in the lower Pearl River (Table 2.3), where PL-GDGTs were suggested as in situ production in the water column as discussed above. This indicates that *Thaumarchaeota* may not be the sole archaeal source to govern the distribution of GDGTs in the PR estuary given the insignificant impact of terrestrial input and preferential preservation.

Alternatively, the variation in archaeal community composition is likely the factor contributing to the unusually low TEX_{86} discrepancy in the surface sediments in the transitional zone. This is supported by the cluster analysis based on the distribution of CL-GDGTs in the sediments from different aquatic settings (Fig. 2.7). The cluster analysis identified four distinct aquatic settings, including 1) fresh water group (lower PR); 2) estuarine group (the PR estuary); 3) shallow water group (coastal South China Sea); and 4) deep water group (open South China Sea) (Fig. 2.7). The shallow water group (coastal SCS) was characterized by the highest fractional abundance of crenarchaeol and inconsistently distributed crenarchaeol regioisomer, whereas the estuarine group (the PR estuary) had a lower fractional abundance of crenarchaeol than the shallow water group, but a higher fractional abundance of GDGT-0 (Fig. 2.7). We hypothesize that changing characteristics of CL-GDGT distribution in the transitional zone between coastal SCS and the PR estuary is probably driven by the change in archaeal community composition.

To further evaluate this hypothesis, 16S rRNA gene clone libraries were analyzed to characterize the overall archaeal community in the surface water of the lower Pearl River and its estuary (Fig. 2.8 & Table A4). We assume that CL-GDGTs in the surface sediments are predominantly derived from the water column (Fig. 2.4). The results showed that the predominant archaeal population in the river water was *Methanosarcinales* in the upper end of the lower Pearl River (PR-9) and MCG in the lower end of the lower Pearl River (PR-4), which were distinct from the PR estuary (PR-12 & PR-14) where MG I.1a *Thaumarchaeota* predominantly occurred in the water column (Fig. 2.8). Intriguingly, MG II *Euryarchaeota* notably increased by 15% from the estuarine station PR-12 to PR-14; whereas it was absent in the riverine station PR-4 and PR-9 (Fig. 2.8). This is consistent with previous studies showing that MG II predominantly occurred in the surface water of the Pearl River estuary (Liu et al., 2014) and the Yangtze River estuary (Liu et al., 2011). Xie et al. (2014) further demonstrated that salinity was the dominating factor controlling the change in archaeal community composition and their ecological function in the sediments of the lower Pearl River and its estuary based on the archaeal 16S rRNA gene from the surface sediments.

These results suggest that MG II *Euryarchaeota* may be another source in addition to *Thaumarchaeota* for the GDGT pool in the PR estuary. A similar observation was made by Turich et al. (2007) for other marine environments. Recently, Lincoln et al. (2014) presented evidence indicating that MG II *Euryarchaeota* were significant contributors to the GDGT pool (including crenarchaeol) in North Pacific Subtropical Gyre. Thus it is possible that MG II can be a major source of GDGTs in the marine system where *Euryarchaeota* occur abundantly, particularly in the coastal region (Pernthaler et al., 2002; Galand et al., 2010; Hugoni et al., 2013). On the other hand, the lack of MG II based on the genetic analysis in the surface sediments of

coastal stations (Wang et al., 2014) may indicate that these organisms predominantly live in the water column and their DNA are decomposed after settling down in sediments, which thus cannot be used as evidence for excluding the contribution of MG II to the GDGT pool in the sediments at these locations. However, since none of the MG II *Euryarchaeota* has been isolated, their exact lipid profiles are unknown. Enrichment and isolation of MGII would be critical for resolving this issue in future research.

2.4 Conclusions

This study presents the spatial distribution of CL- and PL-TEX_{86} in the water column and sediment from the lower Pearl River to the PR estuary and coastal and open South China Sea. Terrestrial input of CL- and PL-GDGTs has little impact on the distribution and abundance of CL- and PL-GDGTs in the lower Pearl River and the PR estuary. In the water column, CL- and PL-GDGTs are largely from in situ production in the lower Pearl River and from a combination of fresh water and seawater in the PR estuary. However, the small fraction of PL-GDGTs in sediments does not seem to impact the distribution of CL-GDGTs. Thus, the CL-TEX_{86} in the surface sediments of lower Pearl River may have the potential to be used as a paleothermometer in the lower Pearl River. GDGT-2 and GDGT-3 are crucial components toward unusually low TEX_{86} values in the transitional zone between the PR estuary and the coastal SCS (water depth ranging 10 – 200 m), which may be contributed by non-thaumarchaeotal species, such as Marine Group II *Euryarchaeota*. Consequently low temperature events based on TEX_{86} in ancient continental margins should be interpreted with extreme caution.

2.5 References

Castañeda, I.S., Schefuß, E., Pätzold, J., Sinninghe Damsté, J.S., Weldeab, S., Schouten, S., 2010. Millennial-scale sea surface temperature changes in the Eastern Mediterranean (Nile River Delta Region) over the last 27,000 years. Paleoceanography 25, PA1208. http://dx.doi.org/10.1029/2009PA001740.

Dang, H., Zhou, H., Yang, J., Ge, H., Jiao, N., Luan, X., Zhang, C.L., Klotz, M.G., 2013. Thaumarchaeotal signature gene distribution in sediments of the northern South China Sea: an indicator o the metabolic intersection of the marine carbon, nitrogen, and phosphorus cycles? Appl. Environ. Microbiol. 79, 2137–2147.

DeLong E.F., 1992. Archaea in coastal marine environments. Proc. Natl. Acad. Sci. USA 89, 5685–5689.

Galand, P.E., Gutierrez-Provecho, C., Massana, R., Gasol, J., Casamayor, E.O., 2010. Interannual recurrence of archaeal assemblages in the coastal NW Mediterranean Sea. Limnol. Oceanogr. 55, 2117–2125.

Ge, H.M., Zhang, C.L., Dang, H.Y., Zhu, C., Jia, G.D., 2013. Distribution of tetraether lipids in surface sediments of the northern South China Sea: implications for TEX_{86} proxies. Geosci. Front. 4, 223–229.

Herfort, L., Schouten, S., Boon, J.P., Sinninghe Damsté, J.S., 2006a. Application of the TEX_{86} temperature proxy in the southern North Sea. Org. Geochem. 37, 1715–1726.

Herfort, L., Schouten, S., Boon, J.P., Woltering, M., Baas, M., Weijers, J.W.H., Sinninghe Damsté, J.S., 2006b. Characterization of transport and deposition of terrestrial organic matter in the southern North Sea using the BIT index. Limnol. Oceanogr. 51, 2196–2205.

Hernandez-Sanchez, M.T., Woodward, E.M.S., Taylor, K.W.R., Henderson, G.M., Pancost, R.D., 2014. Variations in GDGT distributions through the water column in the South East Atlantic Ocean. Geochim. Cosmochim. A. 132, 337–348.

Ho, S.L., Mollenhauer G., Fietz, S., Martinez-Garcia, A., Lamy, F., Rueda, G., Schipper, K., Meheust, M., Rosell-Mele, A., Stein, R., Tiedemann, R., 2014. Appraisal of TEX_{86} and TEX_{86}^{L} thermometries in subpolar and polar regions. Geochim. Cosmochim. A. 131, 213–226.

Hugoni, M., Taib, N., Debroas, D., Domaizon, I., Dufournel, I.J., Bronner, G., Salter, I., Agogue, H., Mary, I., and Galand, P.E., 2013. Structure of the rare archaeal biosphere and seasonal dynamics of active ecotypes in surface coastal waters. Proc. Natl. Acad. Sci. USA 110(15), 6004–6009.

Hopmans, E.C., Weijers, J.W.H., Schefuss, E., Herfort, L., Sinninghe Damsté, J.S., Schouten, S., 2004. A novel proxy for terrestrial organic matter in sediments based on branched and isoprenoid tetraether lipids. Earth Planet. Sci. Lett. 224, 107–116.

Huguet, C., Hopmans, E.C., Febo-Ayala, W., Thompson, D.H., Sinninghe Damsté, J.S., Schouten, S., 2006. An improved method to determine the absolute abundance of glycerol dibiphytanyl glycerol tetraether lipids. Org. Geochem. 37, 1036–1041.

Huguet, C., Schimmelmann, A., Thunell, R., Lourens, L.J., Sinninghe Damsté, J.S., Schouten, S., 2007. A study of the TEX_{86} paleothermometer in the water column and sediments of the Santa Barbara Basin, California. Paleoceanography. http://dx.doi.org/10.1029/2006PA001310.

Kim, J.-H., Schouten, S., Hopmans, E.C., Donner, B., Sinninghe Damsté, J.S., 2008. Global core-top calibration of the TEX_{86} paleothermometer in the ocean. Geochim. Cosmochim. A. 72, 1154–1173.

Kim, J.-H., Huguet, C., Zonneveld, K.A.F., Versteegh, G.J.M., Roeder, W., Sinninghe Damsté, J.S., Schouten, S., 2009. An experimental field study to test the stability of lipids used for TEX_{86} and U_K^{37} palaeothermometry. Geochim. Cosmochim. A. 73, 2888–2898.

Kim, J.-H., van der Meer, J., Schouten, S., Helmke, P., Willmott, V., Sangiorgi, F., Koç, N., Hopmans, E.C., Sinninghe Damsté, J.S., 2010. New indices and calibrations derived from the distribution of crenarchaeal isoprenoid tetraether lipids: implications for past sea surface temperature reconstructions. Geochim. Cosmochim. A. 74, 4639–4654.

Kim, J.H., Romero, O.E., Lohmann, L., Donner, B., Laepple, T., Haam, E., Sinninghe Damsté, J.S., 2012a. Pronounced subsurface cooling of North Atlantic waters off Northwest Africa during Dansgaard–Oeschger interstadials. Earth Planet. Sci. Lett. 339–340, 95–102.

Kim, J.H., Zell, C., Moreira-Turcq, P., Pérez, M.A.P., Abril, G., Mortillaro, J.M., Weijers, J.W.H., Meziane, T., Sinninghe Damsté, J.S., 2012b. Tracing soil organic carbon in the lower Amazon River and its tributaries using GDGT distributions and bulk organic matter properties. Geochim. Cosmochim. A. 90, 163–180.

Lee, K.Y., Kim, J.H., Wilke, I., Helmke, P., Schouten, S., 2008. A study of the alkenone, TEX_{86}, and planktonic foraminifera in the Benguela Upwelling System: implications for past sea surface temperature estimates. Geochem. Geophys. Geosyst. 9, Q10019. http://dx.doi.org/10.1029/2008GC002056.

Leider, A., Hinrichs, K.-U., Mollenhauer, G., Versteegh, G.J.M., 2010. Core-top calibration of the lipid-based UK' 37 and TEX_{86} temperature proxies on the southern Italian shelf (SW Adriatic Sea, Gulf of Taranto). Earth Planet. Sci. Lett. 300, 112–114.

Lengger, S.K., Hopmans, E.C., Reichart, G.-J., Nierop, K.G.J., Sinninghe Damsté, J.S., Schouten, S., 2012. Distribution of core and intact polar glycerol dibiphytanyl glycerol tetraether lipids in the Arabian Sea Oxygen Minimum Zone. II: evidence for selective preservation and degradation in sediments and consequences for the TEX_{86}. Geochim. Cosmochim. A. 98, 244–258.

Lincoln, S.A., Wai, B., Eppley, J.M., Church, M.J., Summons, R.E., and DeLong, E.F., 2014. Planktonic Euryarchaeota are a significant source of archaeal tetraether lipids in the ocean. Proc. Natl. Acda. Sci. USA 111(27), 9858–9863.

Lipp, J.S., Hinrichs, K.-U., 2009. Structural diversity and fate of intact polar lipids in marine sediments. Geochim. Cosmochim. A. 73, 6816–6833.

Liu, M., Xiao, T., Wu, Y., Zhou, F., and Zhang, W., 2011. Temporal distribution of the archaeal community in the Changjiang Estuary hypoxia area and the adjacente East China Sea as determined by denaturing gradiente gel electrophoresis and multivariate analysis. Can. J. Microbiol. 57, 504–513.

Liu, J., Yu, S., Zhao, M., He, B. & Zhang, X.-H., 2014. Shifts in archaeaplankton community structure along ecological gradients of Pearl Estuary. FEMS Microbiol. Ecol. 90(2), 424–435.

Liu, Z., Pagani, M., Zinniker, D., DeConto, R., Huber, M., Brinkhuis, H., Shah, S.R., Leckie, M., Pearson, A., 2009. Global cooling during the Eocene–Oligocene climate transition. Science 323, 1187–1190.

Liu, X.L., Lipp, J.S., Hinrichs, K. - U., 2011. Distribution of intact and core GDGTs in marine sediments. Org. Geochem. 42, 368–375.

Liu, Z., Colin, C., Phon Le, K., Tong, S., Chen, Z., and Trentesaux, A., 2007. Climatic and tectonic con- trols on weathering in south China and Indochina Peninsula: clay mineralogical and geochemical investi- gations from the Pearl, Red, and Mekong drainage basins. Geochem. Geophys. Geosyst. 8, 1–18.

Lopes dos Santos, R., Prange, M., Castañeda, I.S., Schefuß, E., Mulitza, S., Schulz, M., Niedermeyer, E.M., Sinninghe Damsté, J.S., Schouten, S., 2010. Glacial– interglacial variability in Atlantic meridional overturning circulation and thermocline adjustments in the tropical North Atlantic. Earth Planet. Sci. Lett. 300, 407–414.

Pearson, A. and Ingalls, A.E., 2013. Assessing the use of archaeal lipids as marine environmental proxies. Ann. Rev. Earth Planet. Sci. 41, 359–384.

Pernthaler, A., Preston, C.M., Pernthaler, J., DeLong, E.F., and Amann, R., 2002. Comparison of fluorescently labeled oligonucleotide and polynucleotide probes for the detection of pelagic marine bacteria and archaea. Appl. Environ. Microbiol. 68, 661–667.

Pitcher, A., Hopmans, E.C., Schouten, S., Sinninghe Damsté, J.S., 2009. Separation of core and intact polar archaeal tetraether lipids using silica columns: insights into living and fossil biomass contributions. Org. Geochem. 40, 12–19.

Schloss, P.D. & Handelsman, J., 2005. Introducing DOTUR, a computer program for defining operational taxonomic units and estimating species richness. Appl. Environ. Microbiol. 71, 1501–1506.

Schouten, S., Hopmans, E.C., Schefuß, E., Sinninghe Damsté, J.S., 2002. Distributional variations in marine crenarchaeotal membrane lipids: a new tool for reconstructing ancient sea water temperatures? Earth Planet. Sci. Lett. 204, 265–274.

Schouten, S., Hopmans, E.C., Sinninghe Damsté, J.S., 2004. The effect of maturity and depositional redox conditions on archaeal tetraether lipid palaeothermometry. Org. Geochem. 35, 567–571.

Schouten, S., Huguet, C., Hopmans, E.C., Sinninghe Damsté, J.S., 2007. Improved analytical methodology of the TEX_{86} paleothermometry by high performance liquid chromatography/atmospheric pressure chemical ionization–mass spectrometry. Anal. Chem. 79, 2940–2944.

Schouten, S., Pitcher, A., Hopmans, E.C., Villanueva, L., van Bleijswijk, J., Sinninghe Damsté, J.S., 2012. Distribution of core and intact polar glycerol dibiphytanyl glycerol tetraether lipids in the Arabian Sea Oxygen Minimum Zone: I: Selective preservation and degradation in the water column and consequences for the TEX_{86}. Geochim. Cosmochim. A. 98, 228–243.

Schouten, S., Hopmans, E.C., Sinninghe Damsté, J.S., 2013. The organic geochemistry of glycerol dialkyl glycerol tetraether lipids: a review. Org. Geochem. 54, 19–61.

Sinninghe Damsté, J.S., Hopmans, E.C., Schouten, S., van Duin, A.C.T., Geenevasen, J.A.J., 2002. Crenarchaeol: the characteristic core glycerol dibiphytanyl glycerol tetraether membrane lipid of cosmopolitan pelagic crenarchaeota. J. Lipid Res. 43, 1641–1651.

Sinninghe Damsté, J.S., Rijpstra, W.I.C., Hopmans, E.C., Jung, M.Y., Kim, J.G., Rhee, S.K., Stieglmeier, M., Schleper, C., 2012. Intact polar and core glycerol dibiphytanyl glycerol

tetraether lipids of Group I.1a and I.1b Thaumarchaeota in soil. Appl. Environ. Microbiol. 78, 6866–6874.

Strong, D.J., Flecker, R., Valdes, P.J., Wilkinson, I.P., Rees, J.G., Zong, Y.Q., Lloyd, J.M., Garrett, E., Pancost, R.D., 2012. Organic matter distribution in the modern sediments of the Pearl River Estuary. Org. Geochem. 49, 68–82.

Taylor, K.W.R., Huber, M., Hollis, C.J., Hernandez-Sanchez, M.T., Pancost, R.D., 2013. Re-evaluating modern and palaeogene GDGT distributions: Impalications for SST reconstructions. Global Planet. Change 108, 158–174.

Thompson, J.D., Gibson, T.J., Plewniak, F., Jeanmougin, F. & Higgins, D.G., 1997. The CLUSTAL_X windows interface: flexible strategies for multiple sequence alignment aided by quality analysis tools. Nucleic acids res. 25, 4876–4882.

Turich, C., Freeman, K.H., Bruns, M.A., Conte, M., Jones, A.D., Wakeham, S.G., 2007. Lipids of marine Archaea: patterns and provenance in the water-column and sediments. Geochim. Cosmochim. A. 71, 3272–3291.

Turich, C., Schouten, S., Thunell, R.C., Varela, R., Astor, Y., Wakeham, S.G., 2013. Comparison of TEX_{86} and U^{K}_{37} temperature proxies in sinking particles in the cariaco Basin. Deep-Sea Res. I 78, 115–133.

Wang, P., Wei, Y., Li, T., Li, F., Meng, J., and Zhang, C.L., 2014. Archaeal diversity and spatial distribution in the surface sediment of the South China Sea. Geomicrobiol. J. 31(1), 1–11.

Wei, Y., Wang, J., Liu, J., Dong, L., Li, L., Wang, H., Wang, P., Zhao, M., Zhang, C.L., 2011. Spatial variations in Archaeal lipids of surface water and core-top sediments in the South China Sea: implications for paleoclimate studies. Appl. Environ. Microbiol. 77, 7479–7489.

Weijers, J.W.H., Schouten, S., Spaargaren, O.C., Sinninghe Damsté, J.S., 2006. Occurrence and distribution of tetraether membrane in soils: implications for the use of the BIT index and the TEX_{86} SST proxy. Org. Geochem. 37, 1680–1693.

Weijers, J.W.H., Bernhardt, B., Peterse, F., Werne, J.P., Dungait, J.A.J., Schouten, S., Sinninghe Damsté, J.S., 2011a. Absence of seasonal patterns in MBT–CBT indices in mid-latitude soils. Geochim. Cosmochim. A. 75, 3179–3190.

Weijers, J.W.H., Lima, K.H.L., Aquilina, A., Sinninghe Damsté, J.S., Pancost, R.D., 2011b. Biogeochemical controls on glycerol dialkyl glycerol tetraether lipid distributions in sediments characterized by diffusive methane flux. Geochem. Geophys. Geosyst. 12, Q10010. http://dx.doi.org/10.1029/2011GC003724.

Wuchter, C., Schouten, S., Wakeham, S.G., Sinninghe Damsté, J.S., 2006. Archaeal tetraether membrane lipid fluxes in the northeastern Pacific and the Arabian Sea: implications for TEX_{86} paleothermometry. Paleoceanography 21, PA4208. http://dx.doi.org/10.1029/2006PA001279.

Xie, W., Zhang, C.L., Zhou, X., Wang, P., 2014. Salinity-dominated change in community structure and ecological function of Archaea from the lower Pearl River to coastal South China Sea. Environ. Appl. Microbiol. Biotechnol. DOI: 10.1007/s00253-014-5838-9.

Yang, G., Zhang, C.L., Xie, S., Chen, Z., Gao, M., Ge, Z., Yang, Z., 2013. Microbial glycerol dialkyl glycerol tetraethers from river water and soil near the Three Gorges Dam on the Yangtze River. Org. Geochem. 56, 40–50.

Zell, C., Kim, J.-H., Moreira-Turcq, P., Abril, G., Hopmans, E.C., Bonnet, M.P., Sobrinho, R.L., and Sinninghe Damste´, J.S., 2013a. Disentangling the origins of branched tetraether lipids

and crenarchaeol in the lower Amazon River: Implications for GDGT-based proxies. Limnol. Oceanogr. 58, 343–353.

Zell, C., Kim, J.-H., Abril, G., Sobrinho, R.L., Dorhout, D., Moreira-Turcq, P., Sinninghe Damsté, J.S., 2013b. Impact of seasonal hydrological variation on the distributions of tetraether lipids along the Amazon River in the central Amazon basin: implications for the MBT/CBT paleothermometer and the BIT index. Front. Terr. Microbiol. 4. http://dx.doi.org/10.3389/fmicb.2013.00228.

Zell, C., Kim, J.-H., Hollander, D., Lorenzoni, L., Baker, P., Silva, C.G., Nittrouer, C., Sinninghe Damsté, J.S., 2014. Sources and distributions of branched and isoprenoid tetraether lipids on the Amazon shelf and fan: Implications for the use of GDGT-based proxies in marine sediments. Geochim. Cosmochim. A. 139, 293–312.

Zhang, C.L., Wang, J., Wei, Y., Zhu, C., Huang, L., Dong, H., 2012. Production of branched tetraether lipids in the lower Pearl River and estuary: effects of extraction methods and impact on bGDGT proxies. Front. Terr. Microbiol. 2. http://dx.doi.org/10.3389/fmicb.2011.00274.

Zhang, J., Bai, Y., Xu, S., Lei, F., Jia, G., 2013. Alkenone and tetraether lipids reflect different seasonal seawater temperatures in the coastal northern South China Sea. Org. Geochem. 58, 115–120.

Zhang, Y.G., Zhang, C.L., Liu, X.L., Li, L., Hinrichs, K.U., Noakes, J.E., 2011. Methane Index: a tetraether archaeal lipid biomarker indicator for detecting the instability of marine gas hydrates. Earth Planet. Sci. Lett. 307, 525–534.

Zhang, Y.G., Pagani, M., Liu, Z., 2014. A 12 – million – year temperature history of the tropical Pacific Ocean. Science.344, 84–87.

Zhou, H., Hu, J., Spiro, B., Peng, P., Tang, J., 2014. Glycerol dialkyl glycerol tetraethers in surficial coastal and open marine sediments around China: Indicators of sea surface temperature and effects of their sources. Palaeogeogr. Palaeoclimatol. Palaeoecol. 395, 114–121.

Zhu, C., Weijers, J.W.H., Wagner, T., Pan, J.M., Chen, J.F., Pancost, R.D., 2011. Sources and distributions of tetraether lipids in surface sediments across a large riverdominated continental margin. Org. Geochem. 42, 376–386.

Fig. 2.1

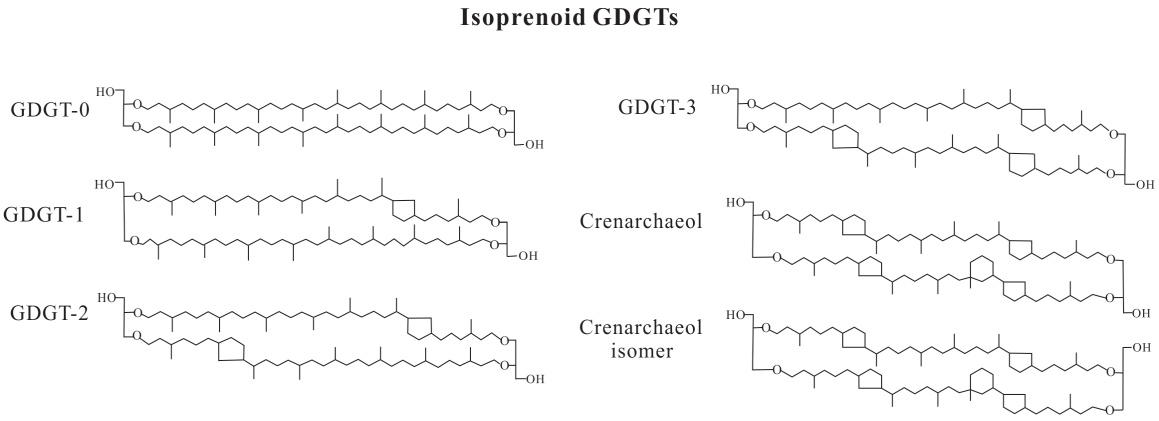

Figure 2.1. Structures of archaeal core GDGTs described in the text.

Fig. 2.2

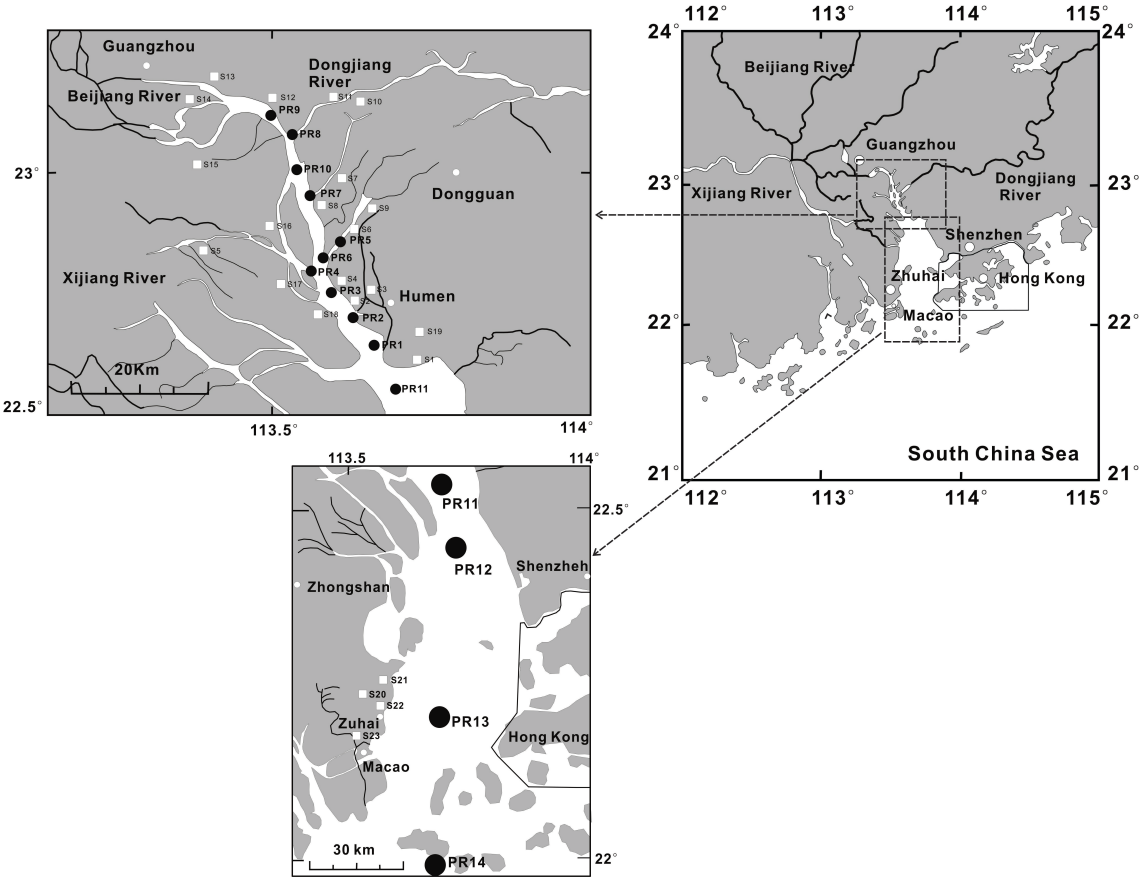

Figure 2.2. Map of sampling locations of the lower Pearl River and the PR estuary. Panel A shows suspended particulate matter (SPM) samples from the water column of the lower Pearl River (black solid circles, PR1 – PR10). Panel B shows SPM samples from the water column of the PR estuary (black solid circles, PR11 – PR14). The surface sediment samples were collected at the same locations at which SPM samples were collected except for the station PR-13. Soil samples in the drainage basin of the lower PR and the PR estuary are shown in white squares. This map is modified from Zhang et al. (2012) and permission has been obtained from The Frontiers Publisher.

Fig. 2.3

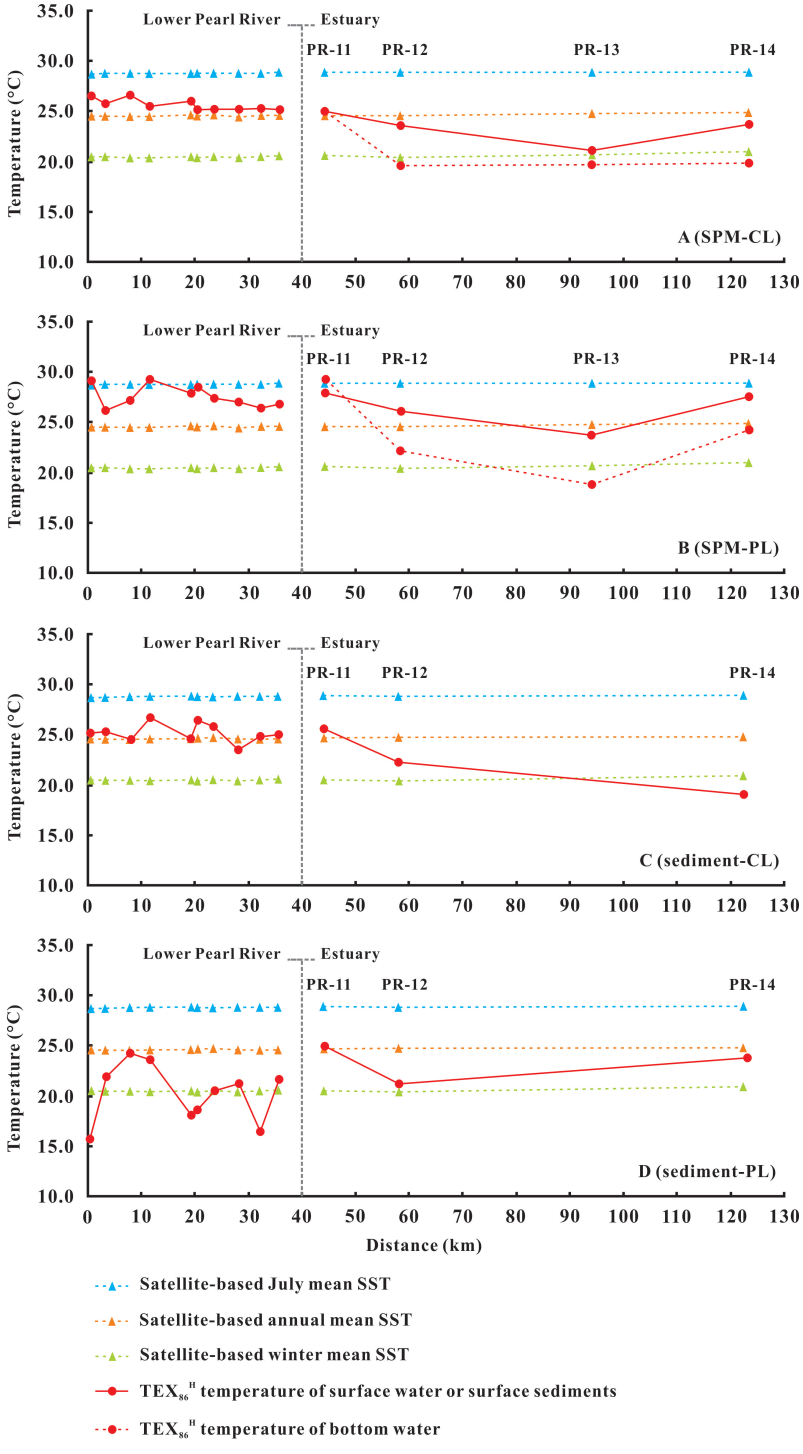
Lower Pearl River
Estuary
PR-11
PR-12
PR-13
PR-14
Temperature (°C)
A (SPM-CL)
B (SPM-PL)
C (sediment-CL)
D (sediment-PL)
Distance (km)
Satellite-based July mean SST
Satellite-based annual mean SST
Satellite-based winter mean SST
TEX86H temperature of surface water or surface sediments
TEX86H temperature of bottom water

Figure 2.3. Distance profiles of TEX_{86} temperature compared to the satellite-based annual mean SWT (yellow dashed line), satellite-based July mean SWT (blue dashed line), and satellite-based winter mean SWT (green dashed line). A: CL-TEX_{86} temperature from SPM in the surface water (red solid line) and bottom water (red dashed line); B: PL-TEX_{86} temperature from SPM in the surface water (red solid line) and bottom water (red dashed line); C: CL-TEX_{86} temperature in the surface sediments (red solid line); D: PL-TEX_{86} temperature in the surface sediments (red solid line). Triangular symbols are satellite-based temperatures at each sampling site; circular symbols are TEX_{86}-derived temperatures. PR-11, PR-12, PR-13, and PR-14 are station names in the Pearl River estuary. The distance profile starts from Guanghzou as 0 km; the lower Pearl River is 40 km long from Guangzhou to Humen (Fig. 2.2).

Fig. 2.4

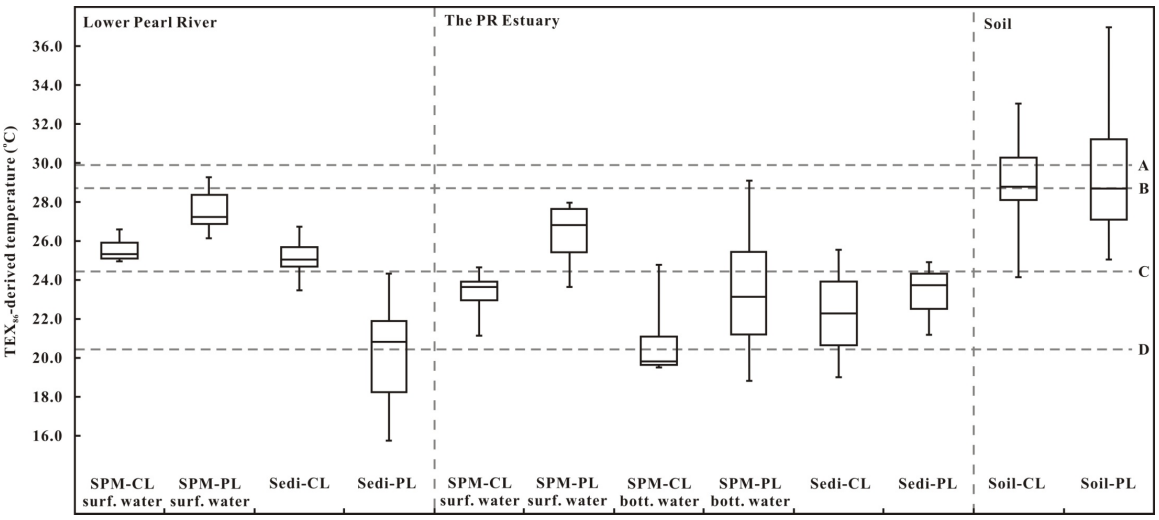

Figure 2.4. TEX_{86}-derived temperatures from SPM samples, surface sediments and soils in comparison to satellite-based mean surface water temperatures (July, annual, and winter) and monthly mean air temperature in July in the sampling area. Dashed line A: Monthly mean air temperature in July (30ºC); dashed line B: Satellite-based July mean water surface temperature (28.78 ± 0.04ºC); dashed line C: Satellite-based annual mean water surface temperature (24.61 ± 0.09ºC); dashed line D: Satellite-based winter mean water surface temperature (20.49 ± 0.16ºC). CL, core lipids; PL, polar lipids.

Fig. 2.5

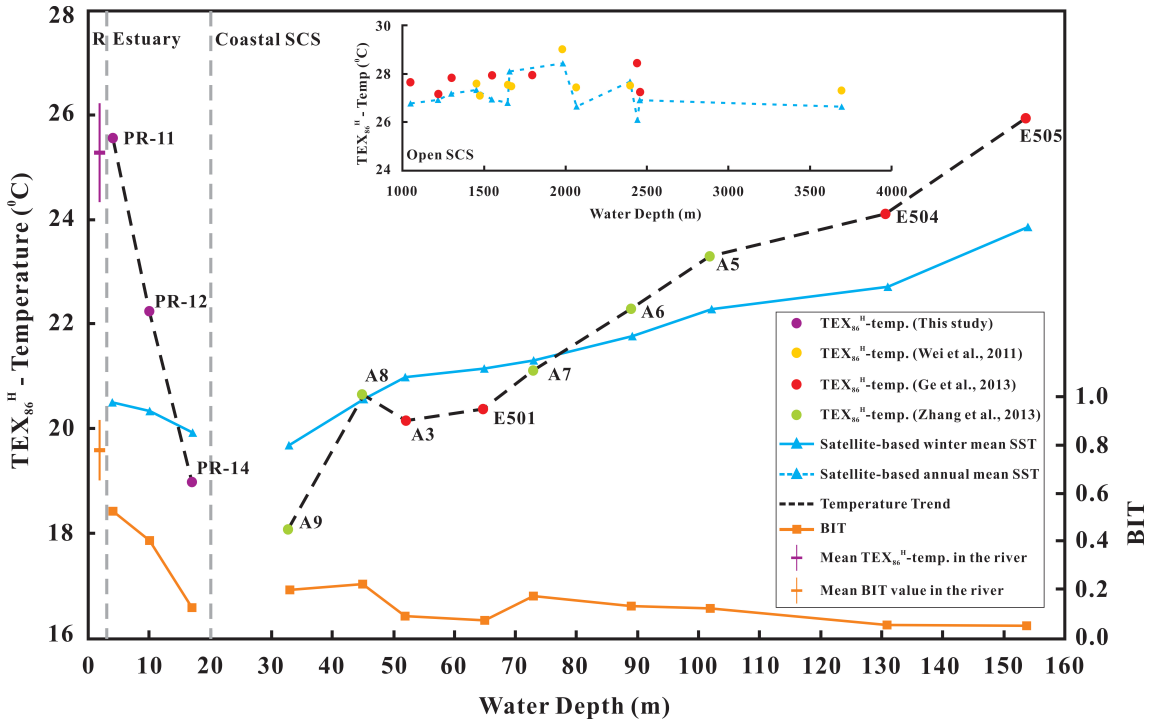

Figure 2.5. The discrepancy between TEX_{86} temperature estimates (circles with station names) and satellite-based WST/SST (triangle) in the sediments from the transitional zone. The transitional zone is defined as an area from the PR estuary to the coastal SCS. The insert figure is TEX_{86} temperatures from core-tope sediments in the open South China Sea plotted against water depth. The horizontal purple bar represents the mean value of TEX_{86} temperatures in the surface sediments of the lower Pearl River (R); the vertical purple bar represents the range of TEX_{86} temperatures in the surface sediments of the lower Pearl River. BIT index (Branched and Isoprenoid Tetraether index) was proposed to evaluate terrestrial soil organic matter contribution to oceanic settings (Hopmans et al., 2004). The BIT data in the lower Pearl River (mean value, yellow bar) and the Pearl River estuary (yellow square) are from Zhang et al. (2012); those in the

coastal sea (yellow square) are from Zhang et al. (2013) and Ge et al. (2013). The detailed sample information is in Table 2.1.

Fig. 2.6

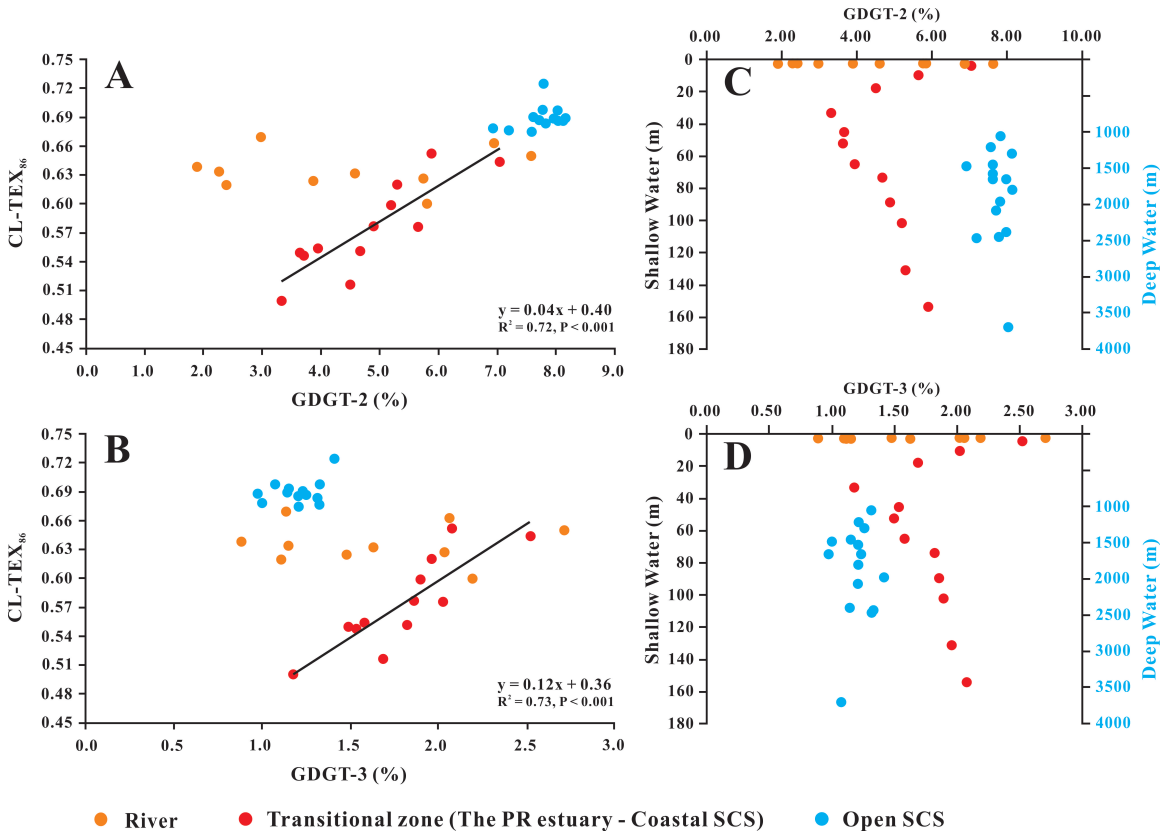

Figure 2.6. Relationships between the fractional abundance of GDGT-2 and GDGT-3 and CL-TEX_{86} (A, B) and the distribution of fractional abundance of GDGT-2 and GDGT-3 versus water depth (C, D). Red solid circles represent sediments from the transitional zone (between estuary and the coastal SCS); yellow solid circles, river surface sediments; blue solid circles, core-tope sediments from the open SCS; solid line, linear regression of data from the transitional zone. The sediment data in the river and the estuary are from this study; the other sediment data (coastal and open SCS) are from Zhang et al. (2013), Ge et al. (2013), and Wei et al. (2011). The detailed sample information is in Table 2.1.

Fig. 2.7

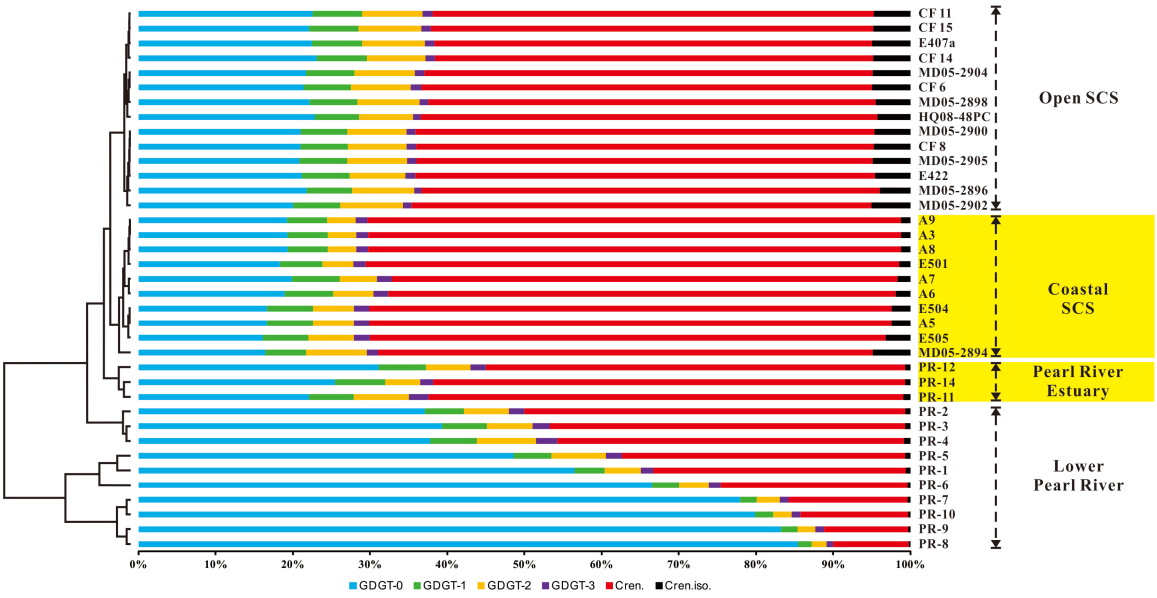

Figure 2.7. Cluster analysis of the relative abundance of core GDGTs in the sediments from the lower Pearl River and its estuary, coastal SCS, and the open SCS. The data in the river and the estuary are from this study. The other data (coastal and open SCS) are from Wei et al. (2011) (HQ08-48PC, MD05-2894, MD05-2896, MD05-2398, MD05-2900, MD05-2902, MD05-2903, MD05-2905), Ge et al. (2013) (A3, CF6, CF8, CF11, CF14, CF15, E407a, E422, E501, E504, E505), Zhang et al. (2013) (A5, A6, A7, A8, A9). The detailed sample information shows in Table 2.1. The yellow highlight area represents the transitional zone. The structures of the GDGTs as in Figure 2.1.

Fig. 2.8

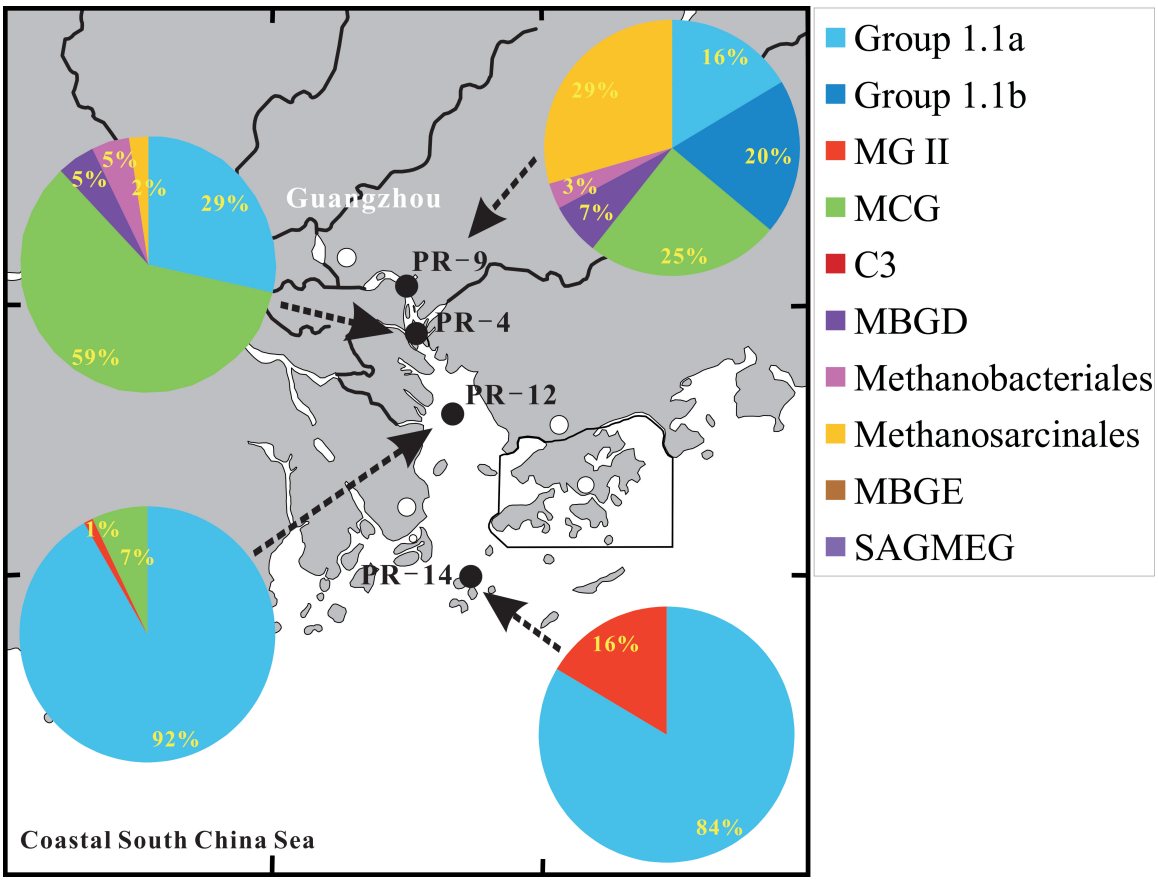

Figure 2.8. The distribution of archaeal community composition based on 16S rRNA gene clone libraries from the lower Pearl River to the coastal SCS. PR-9 and PR-4 were from surface water of the lower Pearl River; PR-12 and PR-14 were from surface water of the PR estuary.

Table 2.1

Table 2.1. Basic information on geographic coordinates, water depths, volumes of water filtered (for SPM samples), and intervals of sediment samples from the lower Pearl River, the Pearl River estuary, and the coastal and open South China Sea (SCS).

Sample ID	Sampling Date	Latitude (N)	Longtitude (E)	Water Depth (m)	SPM (L)	Sediment (cm)	Reference
Lower Pearl River							
PR-1[a]	Jul. 2010	22°47.126′	113°37.812′	8	3	surface sedi. (0-10[c])	This study
PR-2	Jul. 2010	22°49.036′	113°36.926′	3	3	surface sedi. (0-10)	This study
PR-3	Jul. 2010	22°50.339′	113°35.086′	15	6	surface sedi. (0-10)	This study
PR-4	Jul. 2010	22°52.225′	113°32.462′	12	7	surface sedi. (0-10)	This study
PR-5	Jul. 2010	22°54.392′	113°35.234′	12	7	surface sedi. (0-10)	This study
PR-6	Jul. 2010	22°54.790′	113°33.809′	8	7	surface sedi. (0-10)	This study
PR-7	Jul. 2010	22°58.252′	113°33.147′	7	7	surface sedi. (0-10)	This study
PR-8	Jul. 2010	22°02.916′	113°31.388′	6	7	surface sedi. (0-10)	This study
PR-9	Jul. 2010	22°03.478′	113°29.645′	15	8	surface sedi. (0-10)	This study
PR-10	Jul. 2010	22°59.787′	113°31.842′	7	8	surface sedi. (0-10)	This study
Pearl River estuary							
PR-11	Jul. 2010	22°42.967′	113°40.119′	5	SW[b]: 10 BW: 10	surface sedi. (0-10)	This study
PR-12	Jul. 2010	22°35.698′	113°42.594′	10	SW: 11 BW: 11	surface sedi. (0-10)	This study
PR-13	Jul. 2010	22°16.270′	113°41.921′	15	SW: 16 BW: 10	n.a.[d]	This study
PR-14	Jul. 2010	22°00.270′	113°41.986′	18	SW: 21 BW: 27	surface sedi. (0-10)	This study
Coastal SCS							
A5	Aug. 2009	21.0º	115.0º	102	n.a.	downcore (24)	Zhang et al. (2013)
A6	Aug. 2009	21.25º	114.7º	89	n.a.	downcore (34)	Zhang et al. (2013)
A7	Aug. 2009	21.5º	114.5º	73	n.a.	downcore (20)	Zhang et al. (2013)
A8	Aug. 2009	21.8º	114.2º	45	n.a.	downcore (48)	Zhang et al. (2013)
A9	Aug. 2009	22.0º	114.0º	33	n.a.	downcore (52)	Zhang et al. (2013)
A3	Aug. 2009	21°50.525′	114°23.163′	52	n.a.	core top (0-5)	Ge et al. (2013)
E501	Aug. 2007	18°59.995′	110°41.835′	65	n.a.	core top (0-5)	Ge et al. (2013)
E504	Aug. 2007	19°0.102′	111°18.096′	131	n.a.	core top (0-5)	Ge et al. (2013)
E505	Aug. 2007	18°59.897′	111°29.029′	154	n.a.	core top (0-5)	Ge et al. (2013)
Open SCS							
CF 11	Aug. 2007	19°43.341′	114°34.477′	1050	n.a.	core top (0-5)	Ge et al. (2013)
CF 14	Aug. 2007	19°54.256′	115°12.971′	1120	n.a.	core top (0-5)	Ge et al. (2013)
CF 15	Aug. 2007	19°59.581′	110°41.837′	1300	n.a.	core top (0-5)	Ge et al. (2013)
CF 8	Aug. 2007	18°1.908′	111°3.710′	1548	n.a.	core top (0-5)	Ge et al. (2013)
E407	Aug. 2007	18°29.810′	112°0.017′	1800	n.a.	core top (0-5)	Ge et al. (2013)
CF 6	Aug. 2007	22°0.316′	119°30.060′	2441	n.a.	core top (0-5)	Ge et al. (2013)
E422	Aug. 2007	18°0.341′	112°0.793′	2456	n.a.	core top (0-5)	Ge et al. (2013)
MD05-2894	Apr./Mar. 2010	7°2.25′	111°33.11′	1982	n.a.	core top (<5)	Wei et al. (2011)
MD05-2896	Apr./Mar. 2010	8°49.50′	111°26.47′	1657	n.a.	core top (<5)	Wei et al. (2011)
MD05-2898	Apr./Mar. 2010	13°47.39′	112°11.03′	2395	n.a.	core top (<5)	Wei et al. (2011)
MD05-2900	Apr./Mar. 2010	14°23.33′	110°41.47′	1455	n.a.	core top (<5)	Wei et al. (2011)
MD05-2902	Apr./Mar. 2010	17°57.07′	114°57.33′	3697	n.a.	core top (<5)	Wei et al. (2011)
MD05-2903	Apr./Mar. 2010	19°27.32′	116°15.15′	2066	n.a.	core top (<5)	Wei et al. (2011)
MD05-2905	Apr./Mar. 2010	20°08.17′	117°21.61′	1647	n.a.	core top (<5)	Wei et al. (2011)
HQ08-48PC	Apr./Mar. 2010	16°57.513′	110°31.581′	1474	n.a.	core top (<5)	Wei et al. (2011)

[a]PR, the Pearl River, which is followed by station numbers. The sampling stations are shown in Fig. 2.
[b]"SW" or "BW" means "surface water" or "bottom water", respectively.
[c]Approximately 10 cm. See text for more details.
[d]Not available.

Table 2.2

Table 2.2. Temperature (Temp.), pH, salinity (Sal.), and concentrations of total GDGTs and crenarchaeol for suspended particulate matters (SPM) in the water column and surface sediments collected from the lower Pearl River and its estuarya. The GDGTs from soil within the catchment of the lower Pearl River and its estuary are also included. All the lipid data are from this study.

Sample ID[b]		Temp. (°C)	pH	Sal. (%)	GDGTs_SPM (ng/l)[c]				GDGTs_Sediments (ng/g)				Sample ID	GDGTs_Soil (ng/g)			
					CL	CL-Cren.	PL	PL-Cren.	CL	CL-Cren.	PL	PL-Cren.		CL	CL-Cren.	PL	PL-Cren.
Lower Pearl River													PR-Soil-1	8.7	5.6	2.6	0.6
PR-1		29.8	5.2	0.0	71.0	17.9	72.9	4.3	196.2	63.7	146.6	10.9	PR-Soil-2	45.7	27.3	3.5	0.1
PR-2		30.4	5.4	0.0	35.3	10.3	54.2	2.9	67.2	32.7	70.5	7.4	PR-Soil-3	322.5	111.0	141.9	21.0
PR-3		30.1	5.3	0.0	28.8	5.2	43.5	1.5	234.2	106.3	139.4	13.1	PR-Soil-4	43.3	25.4	3.2	0.1
PR-4		30.3	5.7	0.0	14.5	4.9	15.8	1.9	26.2	11.6	14.7	1.7	PR-Soil-5	30.2	12.5	6.4	0.7
PR-5		30.2	5.2	0.0	15.4	3.3	21.9	0.9	60.0	21.8	89.1	4.3	PR-Soil-6	16.8	7.1	3.5	0.6
PR-6		30.3	5.2	0.0	23.5	3.3	31.9	0.9	333.7	80.2	353.1	7.7	PR-Soil-7	5.0	2.0	0.7	0.1
PR-7		30.2	5.2	0.0	23.7	5.7	31.9	1.3	202.0	30.9	300.8	5.1	PR-Soil-8	12.0	5.0	2.3	0.6
PR-8		30.2	5.4	0.0	70.2	3.5	70.3	0.9	357.4	34.8	446.9	4.4	PR-Soil-9	335.7	178.9	19.1	1.7
PR-9		30.7	5.8	0.0	19.9	1.7	40.3	0.8	332.6	36.0	533.7	5.6	PR-Soil-10	83.3	21.6	16.8	1.9
PR-10		31.3	5.8	0.0	15.5	1.5	40.8	0.6	424.3	58.8	544.8	6.0	PR-Soil-11	7.1	4.1	1.7	0.4
Pearl River Estuary													PR-Soil-12	36.7	13.0	8.5	1.0
PR-11	S	30.1	6.3	0.1	7.6	3.0	9.2	2.7	66.4	40.2	20.9	5.4	PR-Soil-13	662.9	23.4	184.7	0.3
	B	30.0	6.3	0.1	7.4	2.7	8.8	2.2					PR-Soil-14	38.1	14.6	6.8	1.1
PR-12	S	31.0	6.7	0.0	22.4	13.6	36.0	8.7	228.6	122.9	82.7	17.2	PR-Soil-15	83.4	55.9	13.4	6.7
	B	28.0	7.3	2.2	37.9	17.3	64.1	36.2					PR-Soil-16	68.0	43.6	5.4	0.4
PR-13	S	30.5	7.4	0.8	7.4	4.6	26.5	16.5	n.a.[d]	n.a.	n.a.	n.a.	PR-Soil-17	5.1	2.7	3.4	1.0
	B	28.7	7.3	2.0	26.4	16.6	61.3	36.5					PR-Soil-18	71.7	35.6	11.2	4.9
PR-14	S	30.1	8.1	1.5	10.6	7.2	15.4	10.4	1119.0	675.9	189.8	77.6	PR-Soil-19	29.2	5.6	4.1	0.9
	B	24.2	7.6	3.6	41.1	26.4	31.3	17.1					PR-Soil-20	27.3	13.6	5.7	1.9

[a]Temperature, pH, and salinity are from Zhang et al. (2012).
[b]PR, the Pearl River, which is followed by station numbers; the letter "S" or "B" after station number means "surface" or "bottom", respectively. The sampling stations are shown in Fig. 2.
[c]CL, total core GDGTs; CL-Cren, Core Crenarchaeol; PL, total polar GDGTs; PL-Cren, Polar Crenarchaeol.
[d]Not available.

Table 2.3

Table 2.3. Linear regression analysis between the abundances of GDGT-2 or GDGT-3 and crenarhcaeol for core lipids (CL) and polar lipids (PL). PR, the lower Pearl River; PRE, the Pearl River estuary.

		CL		PL	
		PR (n = 10)	PRE (n = 8)	PR (n = 10)	PRE (n = 8)
GDGT-2	R	0.98	0.17	0.98	0.73
&	r^2	0.96	0.03	0.97	0.54
Crenarchaeol	P-value	0.000	0.689	0.000	0.038
GDGT-3	R	0.97	0.02	0.94	0.79
&	r^2	0.93	0.00	0.89	0.62
Crenarchaeol	P-value	0.000	0.962	0.000	0.020

CHAPTER 3[2]

CONTRIBUTION OF MARINE GROUP II *EURYARCHAEOTA* TO CYCLOPENTYL TETRAETHERS IN THE PEARL RIVER ESTUARY AND COASTAL SOUTH CHINA SEA: IMPACT ON TEX_{86} PALEOTHERMOMETER

[2] Wang, J.X., C.L. Zhang, W. Xie, Y.G. Zhang, P. Wang. Submitted to *Biogeosciences*, 07/15/2015.

Abstract

TEX_{86} (TetraEther indeX of glycerol dialkyl glycerol tetraethers (GDGTs) with 86 carbon atoms) has been widely applied to reconstruct (paleo-) sea surface temperature (SST). While Marine Group I (MG I) *Thaumarchaeota* have been commonly believed to be the source for GDGTs, Marine Group II (MG II) *Euryarchaeota* have recently been suggested to contribute significantly to the GDGT pool in the ocean. However, little is known how the MG II-derived GDGTs may influence TEX_{86} in marine sediment record. In this study, we characterize MG II-produced GDGTs and assess the likely effect of these tetraether lipids on TEX_{86}. Analyses of core lipid (CL-) and intact polar lipid (IPL-) based GDGTs, 454 sequencing and quantitative polymerase chain reaction (qPCR) targeting MG II were performed on suspended particulate matter (SPM) and surface sediments collected along a salinity gradient from the lower Pearl River (river water) and its estuary (mixing water) to the coastal South China Sea (seawater). The results showed that the community composition varied along the salinity gradient with MG II as the second dominant group in the mixing water and seawater. qPCR data indicated that the abundance of MG II in the mixing water was three to four orders of magnitude higher than the river water and seawater. Significant linear correlations were observed between the gene abundance ratio of MG II vs. total archaea and the relative abundance of GDGTs-1, -2, -3, or -4 as well as the ring index based on these compounds, which collectively suggest that MG II may actively produce GDGTs in the water column. These results also show strong evidence that MG II synthesizing GDGTs with 1-4 cyclopentane moieties may bias TEX_{86} in the water column and sediments. This study highlights that valid interpretation of TEX_{86} in sediment record, particularly in coastal oceans, needs to consider the contribution from MG II *Euryarchaeota*.

3.1 Introduction

TEX_{86} is a popular temperature proxy in paleoclimatological studies (Schouten et al., 2013; Pearson and Ingalls, 2013). It is based upon relative distribution of isoprenoid glycerol dialkyl glycerol tetraethers (GDGTs; see Fig. S1 for structures) (Schouten et al., 2002), which ubiquitously occur in marine and terrestrial environments. The global core-top calibrations of TEX_{86} are empirically correlated with annual mean sea surface temperature (SST) (Schouten et al., 2002; Kim et al., 2008, 2010; Tierney and Tingley, 2014), with the assumption that the majority of sedimentary GDGTs are produced by planktonic Thaumarchaeota (Schouten et al., 2002; Kim et al., 2008). However, mounting evidence indicates anomalies or discrepancies in TEX_{86}-derived SST in coastal seas and open ocean, which have been interpreted as additional contribution of GDGTs from, such as, terrestrial input (e.g. Weijers et al., 2006), subsurface (e.g. Lee et al., 2008) and/or marine sediment production (e.g. Liu et al., 2011).

A great deal of efforts has been made to assess TEX_{86} accuracy in marine and lake sediments. For example, TEX_{86} values are cautioned when branched and isoprenoid tetraether (BIT) index > 0.2 (Zhu et al., 2011), ratio of GDGT-2/crenarchaeol > 0.4 (Weijers et al., 2011b), Methane Index > 0.5 (Zhang et al., 2011), ratio of GDGT-0/Crenarchaeol > 2 (Blaga et al., 2009), or %GDGT-2 > 45 (Sinninghe Damsté et al., 2012). Recently, based on assessment of the relationship between the weighted average number of cyclopentane rings in all GDGTs (ring index, RI) and TEX_{86} from the published core-top sediments, Zhang et al. (in review) established a significant correlation between TEX_{86} and RI, given by $RI = 3.32*(TEX_{86})^2 - 0.77*TEX_{86} + 1.59$ ($\pm 2\sigma \sim 0.3$). This relationship reflects the physiological adaptation of marine archaea by synthesizing GDGTs with more rings (higher RI values) when their ambient environment is

warm (high TEX_{86} values). Deviations from this relationship suggest that temperature is no longer the dominant factor governing the GDGT distribution under the circumstances when the response of GDGTs to temperature is different from the modern analog as defined by the global core-top dataset.

The TEX_{86}-related GDGTs (GDGT-1, -2, -3, and crenarchaeol regioisomer) in marine water column are commonly derived from the Marine Group I (MG I) *Thaumarchaeota* (e.g. Schouten et al., 2008; Pitcher et al., 2011a), as it is one of the dominant groups of planktonic archaea in the ocean (Karner et al., 2001). In particular, crenarchaeol, containing one cyclohexane and four cyclopentane moieties, is considered as a specific biomarker for MG I *Thaumarchaeota* (Sinninghe Damsté et al., 2002; Schouten et al., 2008). Marine Group II *Euryarchaeota* are another abundant planktonic archaea inhabiting predominantly coastal water and (near) surface water of open oceans (e.g. Delong et al., 1992; Galand et al., 2010; Hugoni et al., 2013). Recently, this cosmopolitan group has been suggested to be another major source of GDGTs (including crenarchaeol) in the ocean (Lincoln et al., 2014a), which supported an earlier hypothesis about GDGT-producing MG II (Turich et al., 2007); however, concrete evidence, such as culturing study focusing on MG II, has been lacking (Schouten et al., 2014; Lincoln et al., 2014b).

Because of the absence of MG II enrichments or cultures, little is known about the characteristic of the MG II-produced GDGTs in water column and how these tetraethers might bias TEX_{86} in marine sediment. Recently, unusually low TEX_{86} values in the estuarine and coastal region of South China Sea (SCS) are hypothesized to relate to the production of GDGTs by MG II *Euyarchaeota* (Wang et al., 2015). However, the lack of direct link between archaeal lipids and DNA prevented the drawing of a more concrete conclusion.

In this study, we investigate the archaeal community compositions, present the distribution of TEX_{86} and Ring Index (RI), and evaluate the relationship between MG II and core lipid (CL-) and intact polar lipid (IPL-) based GDGTs in the suspended particulate matter (SPM) and surface sediments collected along a salinity gradient from the lower Pearl River (PR) and its estuary to the coastal South China Sea. Our goal was to test the hypothesis that a large portion of the isoprenoid GDGTs are produced by MG II *Euryarchaeota*, which might influence the applicability of TEX_{86} in coastal marine environments where MG II are abundant. In addition to total CL-GDGTs, total IPL-GDGTs obtained through acid hydrolysis (IPL-H or total IPL), and IPL-GDGTs with only phosphate head groups from base hydrolysis (IPL-OH or phospho IPL), were also examined in order to better correlate with the qPCR data of MG II *Euryarchaeota* and total *Archaea*. The results indicate that MG II may produce GDGTs having 1-4 cyclopentane moieties. Contribution of the MG II-produced GDGTs with more cyclopentane rings appears to bias TEX_{86}, shown by their GDGT distribution deviating from the RI-TEX_{86} relationship identified from the global core-top dataset used for TEX_{86}-SST calibration (Zhang et al., in review). As a result, the TEX_{86}-derived temperature in these samples significantly deviates from the actual SSTs. Our results have important implications for a better understanding of the production of marine GDGTs, and the use of TEX_{86} as a paleothermometer for probing past changes of climate.

3.2 Material and Methods

3.2.1 Sample collection

The sampling locations and sampling information for SPM and surface sediments are shown in Figure 1 and Table 1, respectively. SPM samples (n = 18) and surface sediments (n = 8) were collected along a salinity gradient from the lower Pearl River and its estuary to the coastal South China Sea in the summer of 2011. River water SPM samples were collected from the surface (station R1 to R6) and the bottom (station R1 and R2) of the water column in the lower Pearl River. Mixing water SPM samples were collected from three water layers (surface, middle and bottom) and from three tidal periods (high tide, slack tide and low tide) at station M located in the PR estuary. Seawater SPM samples were collected from four water layers (surface, subsurface, middle and bottom) at station S in the coastal SCS (Fig. 1). The depth of the sampling layers in the water column is given in Table 1. About 4 to 103 liters of water were filtered onto ashed (450^{o}C, overnight) glass-fiber filters (Whatman GF/F, 0.7 μm, 142 mm diameter) using an in situ submersible pump. The pH, temperature, and salinity were determined in situ by a Horiba instrument (W-20XD, Kyoto, Japan) (Table 1).

Surface sediments (top *ca.* 10 cm) were collected at all stations using a grab sampler (Fig. 1; Table 1). All samples were frozen immediately in liquid nitrogen and kept at -80°C in the laboratory before analysis.

3.2.2 GDGT analysis and indices

GDGT extraction and separation. The SPM samples (n = 18) and surface sediments (n = 8) were freeze dried and extracted using a modified Bligh and Dyer method (Blight and Dyer, 1959); the separation of core lipids and intact polar lipids followed the procedure described in Weijers et al. (2011a). Briefly, the total lipid extract (TLE) was obtained by extraction (10 min each, 6 times) of SPM (1 filter) or sediments (5 g) with a single-phase solvent mixture of methanol, dichloromethane (DCM) and phosphate buffer (2:1:0.8, v/v/v; pH 7.4). The TLE was separated over an activated silica gel column eluted with n-hexane/ethylacetate (1:1, v/v) and methanol for CL and IPL, respectively. For GDGT quantification, a known amount of an internal C46 GDGT standard was added into the CL fraction or IPL fraction (Huguet et al., 2006).

The polar head groups were cleaved off through hydrolyzation, which allows indirect analysis of IPL as CL (Pitcher et al., 2009; Weijers et al., 2011a). Briefly, 1/3 IPL fraction (non-hydrolyzed IPL fractions) was directly condensed; another 1/3 IPL fraction was hydrolyzed (2 h) in 1.5 N HCl in methanol, which is called acid-hydrolyzed IPL fraction (IPL-H). DCM and MilliQ water were added, and the DCM fraction was collected (repeated 4 times). The DCM fraction was rinsed (6 times) with MilliQ water in order to remove acid and dried under N2 gas. The last 1/3 IPL fraction was subjected to base hydrolysis (2 h) in a 1N KOH in methanol/H2O mixture (95:5, v/v), which is called base-hydrolyzed IPL fraction (IPL-OH). The recovery of IPL-OH was similar to that of IPL-H. Together with the condensed CL fraction, the four fractions were dissolved in n-hexane/isopropanol (99:1, v/v), and filtered using a PTFE filter that had a pore diameter of 0.45 μm. The analysis of non-hydrolyzed IPL fractions is to determine any carryover of CL into the IPL fraction. IPL-H reflects total IPL, which includes both

phosphate head groups and glycosidic head groups; IPL-OH represents the IPL with phosphate head group only (phospho IPL) (Weijers et al., 2011a).

GDGT analysis. GDGTs from all treatments were analyzed using high performance liquid chromatography/atmospheric pressure chemical ionization-tandem mass spectrometry (HPLC/APCI-MS/MS), which was performed with an Agilent 1200 liquid chromatography equipped with an automatic injector coupled to QQQ 6460 MS and Mass Hunter LC-MS manager software using a procedure carried out in the same way as described by Zhang et al. (2012). Separation was achieved by using a Prevail Cyano column (2.1 mm × 150 mm, 3 μm; Alltech Deerifled, IL, USA) with n-hexane (solvent A) and a mixture of n-hexane/isopropanol 90/10 (v/v) (solvent B). The (M+H)+ ions of each core isoprenoid GDGT (m/z 1302, 1300, 1298, 1296, 1294, 1292) was monitored via selected ion monitoring (SIM) mode (Schouten et al., 2007).

Indices based on the fractional abundance of GDGTs were calculated as follows:

TEX_{86} = ([GDGT-2] + [GDGT-3] + [Cren.iso])/([GDGT-1] + [GDGT-2] + [GDGT-3] + [Cren.iso]) (Schouten et al., 2002) (1)

Ring Index1 (RI1) = ([GDGT-1]+2*[GDGT-2]+3*[GDGT-3]+4*[Cren.]+4*[Cren.iso])/100 (Zhang et al., in review) (2)

Ring Index (RI) = ([GDGT-1]+2*[GDGT-2]+3*[GDGT-3]+4*[GDGT-4]+4*[Cren.iso])/100 (3)

with the GDGT numbers corresponding to the GDGT structures in Fig. B1. Note that RI1 is originally proposed by Zhang et al. (in review), which is defined as the weighted average number of cyclopentyl rings in GDGTs (the six-ringed moiety in crenarchaeol is thus not included in the equation of RI1). RI is modified from RI1, in which the fractional abundance of crenarchaeol is

replaced by GDGT-4 in order to eliminate the influence of crenarchaeol on weighted average number of cyclopentane rings in GDGTs (see section 3.2 for more details).

3.2.3 DNA analysis

DNA Extraction and qPCR of archaeal 16S rDNA. The SPM samples (n = 12) and surface sediments (n = 3) from station R1 (river water), station M (mixing water), and station S (seawater) were selected for the DNA analysis. The frozen filters were washed 3 times by phosphate buffered saline (pH 7.4). The supernatants were centrifuged under 11000 g for 10 min. The sediments were collected and transferred into the FastDNA SPIN Kit tubes (MP Biomedical, OH, USA). The DNA was extracted following the protocol of FastDNA SPIN Kit. The DNA samples were dissolved with a final elution in 100μl de-ionized water and were preserved at -80 ℃ until further processing. The quantitative PCR primers were Arch_334F (5' ACGGGGCGCAGCAGGCGCGA3') /Arch_518R (5' ATTACCGCGGCTGCTGG 3') for archaeal 16S gene quantification (Bano et al., 2004) and GII-554-f (5' GTCGMTTTTATTGGGCCTAA3') and Eury806-r (5' CACAGCGTTTACACCTAG 3') for MG II 16S gene quantification (Massana et al., 1997; Teira et al., 2004). The qPCR analysis of this gene was performed at 95℃ for 30 s and 40 cycles at 94℃ for 30 s, 55℃ for total Archaea (53℃ for MG II) for 30 s and 68℃ for 1 min.

454 sequencing. SPM samples (n = 3), which respectively represent river water, mixing water and seawater, are selected to conduct pyrosequence targeting archaeal 16S rDNA. Different from qPCR primers, we chose the primers targeted on longer sequences to get more confident phylogenetic composition of those samples. The primer were Arch_344F (5'

ACGGGGCGCAGCAGGCGCGA 3') / Arch_915R (5' GTGCTCCCCCGCCAATTCCT 3') (Gantner et al., 2011). The pyrosequencing was conducted on the Roche GS FLX + (454) system by Majorbio Bio-Pharm Technology Co., Ltd. (Shanghai, China). We use the Mothur (version 1.29.2) (Schloss et al., 2009) to filter the raw pyrosequencing data. The selected sequences were analyzed using QIIME standard pipeline (Caporaso et al., 2010). Taxonomy was assigned using the Ribosomal Database Project (RDP) classifier 2.2 (minimum confidence of 80%) (Cole et al., 2009).

3.2.4 Satellite-derived surface water temperature (SWT)

The satellite-derived SWT was derived from the data sets on a spatial resolution of 4-km from the NOAA advanced very-high-resolution radiometer (AVHRR) (version 5.2; http://www.nodc.noaa.gov/SatelliteData/pathfinder4km/) according to Wang et al. (2015). The June mean SWT was obtained from the daily averaged values of 30 days in June 2011 (sampling month) using MATLAB. The annual mean SWT and winter mean SWT represent 8-years mean values of annual mean temperature (2004 – 2011) and monthly mean temperature (December – February), respectively, as the surface sediment (top ca. 10 cm) collected in this study may represent a deposition of 6 – 10 yr based on an estimation from Strong et al. (2012).

3.2.5 Statistical analysis

Cluster analysis was performed on CL-GDGTs and phospho IPL-GDGTs in the SPM samples collected from the lower Pearl River, the PR estuary and coastal South China Sea using

the base program in R 2.12.1. The fractional abundance of GDGTs from all samples was imported into R and the Euclidean method was used to compute the distance matrix and to generate a hierarchical clustering tree. The linear regression analysis was conducted from iPython Notebook. The Canoco software (version 4.5) was used to perform the redundancy analysis (RDA), which was to assess the relationship between archaeal tetraether lipids, GDGT-based indices and environmental parameters.

3.3 Results and Discussion

3.3.1 Archaeal community compositions

The phylogenetic classification of archaeal sequences exhibited that methanogens were the predominant group in the fresh water (station R1) and MG I Thaumarchaeota mainly occurred in the salty water (stations M & S) (Fig. 3.2). A significant proportion of MG II Euryarchaeota was present at station M in the PR estuary and station S in the coastal SCS; whereas it was absent at station R1 in the lower Pearl River (Fig. 3.2). These results are in agreement with the previous observations showing that MG I Thaumarchaeota and MG II Euryarchaeota dominated in planktonic archaeal communities in the marine-influenced region of the Pearl River estuary (Liu et al., 2014; Wang et al., 2015), the Yangtze River estuary (Liu et al., 2011), and the Jiulong River estuary (Hu et al., 2015). This is also supported by cluster analysis based on fractional abundances of CL- and phospho IPL-GDGTs in the water column along the salinity gradient, as GDGT-0 and Crenarchaeol were the dominant archaeal tetraether lipids in the river water and mixing/sea water, respectively (Fig. B2). The overwhelming change in archaeal community

composition from the lower Pearl River to the PR estuary was suggested to be predominantly controlled by salinity (Xie et al., 2014). Since the purpose of this study was to explore how MG II influenced TEX_{86} in the water column and surface sediments, the following results and discussion focus on the PR estuary and coastal SCS where MG II are present.

3.3.2 TEX_{86}-derived temperature and Ring Index

The TEX_{86}-derived temperature was calculated based on the calibration of Kim et al. (SST = 68.4*log (TEX_{86}) + 38.6; 2010). The results exhibited that CL-TEX_{86} temperatures from either SPM or surface sediments were close to the satellite-based annual mean SWT in the lower Pearl River and its estuary; whereas those from the coastal SCS were lower than the winter mean SWT (Fig. 3). The correspondence between the CL-TEX_{86} temperature in the SPM and sediment along the salinity gradient indicates that the TEX_{86} signal in the sediment is predominantly from water column, which is consistent with previous studies in the PR estuary (Wang et al., 2015) and other coastal settings (Herfort et al., 2006; Zell et al., 2014).

Total IPL-TEX_{86} temperatures in the water column were consistently below either June mean SWT or in situ instrumental measurements, although the sampling season was summer (Fig. 3). In the PR estuary and coastal SCS, the phospho IPL-TEX_{86} (IPL-OH-TEX_{86}) was lower than the total IPL-TEX_{86} (IPL-H-TEX_{86}); whereas, it was very close to the CL-TEX_{86} (Fig. 3; Table 1). Since phosphate head groups can be degraded faster than the glycosidic head groups, the phospho IPL is considered to be a better reflection of the living microbes (Harvey et al., 1986; Schouten et al., 2010); on the other hand, the CL may be mostly derived from the easier degrading phospho IPL, thus causing their TEX_{86} values to be similar. Furthermore, in the same

study area, variation in TEX_{86} has been suggested to attribute to the change in archaeal community composition in the water column, in which the unusually low TEX_{86}-derived temperature in the coastal SCS was speculated to link to MG II *Euryarchaeota* (Wang et al., 2015).

Since the TEX_{86} can be influenced by factors other than temperature as shown in Fig. 3, the Ring Index was proposed to be able to evaluate the accuracy of TEX_{86} in the marine sediments (Zhang et al., in review). Here, the CL- and IPL-TEX_{86} values were plotted against RI (RI_1, eq. 2) using the SPM and surface sediments in this study and from previous studies (Wei et al., 2011; Ge et al., 2013; Zhang et al., 2013; Wang et al., 2015). The results exhibited that SPM and surface sediments from the open South China Sea were predominantly assembled within the RI_1-TEX_{86} -confined zone ($RI_1 = 3.32*(TEX_{86})^2 - 0.77*TEX_{86} + 1.59, \pm 2\sigma = 0.3$; Zhang et al., in review); whereas, the majority of samples from coastal SCS and the PR estuary fell outside the calibration zone (Fig. 4). Furthermore, all the SPM samples in the mixing water and seawater were scattered above the confined zone (Fig. 4), suggesting that ring index values in the PR estuary and coastal SCS were unexpectedly elevated. This implies that more cyclopentane-containing GDGTs seem to contribute to the GDGT pool in the water column of the PR estuary and coastal SCS.

To further assess the distribution of RI in the SPM and to explore other contributor(s) to the cyclopentyl GDGT pool in the study area, mean values of CL-, total IPL-, and phospho IPL-RI were examined (Fig. 5). Note that crenarchaeol was excluded from the ring index calculation (RI, eq. 3) in order to limit its overwhelming influence on the index. The re-defined RI equation makes it more sensitive to the variation of cyclopentane-containing GDGTs that may be contributed from other archaeal group(s). This is also in agreement with the cluster analysis

based on the same dataset, showing that the GDGTs with 1-4 cyclopentane moieties belonged to the same cluster group (Fig. S2). Compared with the river water and seawater, the highest ring index value for either CL (avg. 0.39 ± 0.08) or IPL (avg. 0.48 ± 0.07 for total IPL; avg. 0.47 ± 0.10 for phospho IPL) occurred at station M in the mixing water (Fig. 5; Table 1), with the PR estuary (station M) appears to be a hot spot of the additional input of GDGTs with cyclopentane moieties. Further confirmation comes from the comparison of the fractional abundance of the CL- and phospho IPL-GDGTs in the cluster analysis, showing that the sum of the GDGTs with 1-4 cyclopentane moieties in the mixing water cluster was significantly higher than that from the seawater cluster or river water cluster (Fig. S2). In the mixing water station, the mean values of total IPL-RI and phospho IPL-RI had no significant difference; and both were higher than the CL-RI (Fig. 5). However, in the seawater station, the total IPL-RI (0.34 ± 0.07) was more elevated than the phospho IPL-RI (0.22 ± 0.01) and the CL-RI (0.24 ± 0.04) (Fig. 5). This distribution pattern of RI at station S in the seawater corresponded to the TEX_{86}-temperature distribution in the SPM and sediments (Fig. 3), suggesting that cyclopentane-containing GDGTs appear to be able to alter TEX_{86} record in the water column, or even in the surface sediment, where the vertical transportation of GDGTs from the water column predominantly occurs.

3.3.3 Relationship between MG II and cyclopentane-containing GDGTs

The abundances of MG II *Euryarchaeota* 16S rRNA gene and total *Archaea* 16S rRNA gene were examined in the SPM and surface sediments of the river water (station R1), mixing water (station M), and seawater (station S) (Table 1). In the water column, the abundance of MG II 16S rRNA gene in the mixing water station averaged $5.4 \pm 6.5 \times 10^8$ copies L^{-1} (n = 5), which

was three orders of magnitude higher than that in the river water (avg. $1.5 \pm 2.1 \times 10^5$ copies L^{-1}, n = 2) and seawater (avg. $1.8 \pm 3.0 \times 10^5$ copies L^{-1}, n = 3) (Fig. 5). In the surface sediment, however, no significant difference in the abundance of MG II was observed (Table 1). Although it is unclear what factors exactly control the distribution of MG II *Euryatchaeota* in the water column and sediments, salinity apparently played an important role (Table 1) and perhaps competition for nutrients (e.g. ammonium and phosphate; Fig. S3) ought to be considered as well.

Furthermore, the ratio of the abundances of MG II *Euryarchaeota* 16S rRNA gene to total *Archaea* 16S rRNA gene ([MG II]/[Archaea] ratio) in the mixing water station (avg. 0.23 ± 0.08, n = 5) was significantly higher than that in the seawater (avg. 0.09 ± 0.07, n = 3); yet, the [MG II]/[Archaea] ratio in the river water was negligible (avg. < 0.0001) (Fig. 5). This observation further confirms that the PR estuary (mixing zone, salinity avg. 16.6) is a hot spot for the occurrence of MG II *Euryarchaeota* along the salinity gradient from the low Pearl River to the coastal SCS.

The above observations provide the opportunity to evaluate the relationship between Ring Index and MG II. On one hand, the presence of (more labile) phospho IPL-GDGTs (Table 1) implies that in situ production of isoprenoid GDGTs occurs in the water column along the Pearl River and its estuary to the coastal SCS. The elevated value of phospho IPL-RI in the mixing water, thus, indicates that higher relative proportions of GDGTs with 1-4 cyclopentane moieties were produced in situ in the PR estuary by the source microorganism(s). On the other hand, the MG II 16S rRNA gene copy numbers and the [MG II]/[Archaea] ratio follow practically identical patterns with the distribution of the CL- and IPL-RI along the salinity gradient (Fig. 5). Linear regression analysis then confirmed the positive relationship between phospho IPL-derived RI and the [MG II]/[Archaea] ratio along the salinity gradient ($R^2 = 0.61$, $P < 0.01$; Fig. 6f).

Therefore, it is reasonable to hypothesize that MG II *Euryarchaeota* preferentially synthesize GDGTs with 1-4 cyclopentane moieties in this region, resulting in an elevated value of RI. However, since no more samples to quantify the abundance of MG I *Thaumarchaeota* in this study, further work will focus on comparing the proportion of cyclopentane-containing GDGTs contributed between MG I and MG II in water column and sediment.

The correspondence between MG II *Euryarchaeota* and RI in the water column along the salinity gradient is an important observation in this study. To further constrain the characteristic of MG II *Euryarhcaeota*-produced GDGTs, linear regression analysis was conducted between fractional abundance of GDGTs and [MG II]/[Archaea] ratio in the SPM along the salinity gradient. In respect to the RI-related GDGTs (Eq. 3), our data exhibited a significantly positive linear correlation between [MG II]/[Archaea] ratio and the fractional abundance of phospho IPL-based GDGT with 1-4 cyclopentane moieties (Fig. 6a-d); whereas it appears to be less correlated with the fractional abundance of crenarchaeol regioisomer (Fig. 6e). Similar trends of the linear correlations were also shown between [MG II]/[Archaea] ratio and the CL- and total IPL-GDGT with 1-4 cyclopentane moieties, with a less significant correlation between [MG II]/[Archaea] ratio and total IPL-based crenarchaeol regioisomer (Table 2). In contrast, with respect to phospho IPL-based GDGT-0 or crenarchaeol, our data exhibited no correlation between [MG II]/[Archaea] ratio and the fractional abundance of these membrane lipids (Fig. 6g, h; Table 2). Crenarchaeol has been proved to be a biomarker of MG I *Thaumarchaeota* (Schouten et al., 2008, 2012; Pitcher et al., 2011a, b). Although MG II were suggested to be another source of crenarchaeol in the ocean (Lincoln et al., 2014a), our study shows the absence of a significant correlation between the distribution of MG II and crenarchaeol (Fig. 6h), suggesting that MG II may not be a major source of crenarchaeol in Pearl River estuary.

On the other hand, comparison of the slopes and the R^2 values of the regression equations (Fig. 6a-e) show that GDGT-1 has a stronger correlation with MG II *Euryarhcaeota* in the study area. If MG II preferentially synthesize GDGT-1, additional contribution of the GDGT-1 to the water column of the PR estuary and the coastal SCS is capable of causing a substantial decrease of the TEX_{86} value. Moreover, Wang et al. (2015) suggested that the decreased ratio of GDGT-2 to GDGT-3 contributes to the offset of TEX_{86} in the surface sediments of this area; on the contrary, the increased ratio of GDGT-2 over GDGT-3 in the deep-water column seems to be responsible for a warm bias of TEX_{86}-derived temperature in other marine environments (Taylor et al., 2013; Hernandez-Sanchez et al., 2014). A recent study by Kim et al. (2015) suggested that the co-variation of an increase in GDGT-2 & crenarchaeol regioisomer and a decrease in GDGT-1 & GDGT-3 altered TEX_{86}-derived temperature toward higher values in the deep-water surface sediments of the Mediterranean Sea. Considering the above, along with the new observations in this study (Fig. 5 & 6), it seems feasible that planktonic Euryarchaeota bias TEX_{86} by changing the distribution of TEX_{86}-related GDGTs (especially the GDGTs with 1-3 cyclopentant rings) in the estuary and coastal area.

3.4 Conclusions

This study assesses the relationship between GDGTs with cyclopentane moieties and MG II *Euryarchaeota* along a salinity gradient from river water to seawater. The correlation between the percentage of MG II over total archaeal population and GDGT-1, -2, -3, or -4 as well as RI implies that MG II can produce GDGTs with 1-4 cyclopentane moieties. The production of GDGTs from MG II changes the proportion of ringed GDGTs in the total GDGT pool, which

may bias TEX_{86}. On the other hand, apparent evidence shows that MG II *Euryarchaeota* do not seem to be a significant source of crenarchaeol. However, validation of the production of GDGTs by MG II may have to wait until a pure culture is available.

3.5 References

Blaga, C. I., Reichart, G. J., Heiri, O., Sinninghe Damsté, J. S.: Tetraether membrane lipid distributions in lake particulate matter and sediments: a study of 47 European lakes along a North–South transect, J. Paleolimnol., 41, 523–540, 2009.

Bligh, E.G. and Dyer W.J.: A rapid method of total lipid extraction and purification, Can. J. Biochem. Physiol., 37, 911–917, 1959.

Bano, N., Ruffin, S., Ransom, B., Hollibaugh, J. T.: Phylogenetic composition of Arctic Ocean archaeal assemblages and comparison with Antarctic assemblages, Appl. Environ. Microbiol., 70, 781–789, 2004.

Caporaso, J. G., Kuczynski, J., Stombaugh, J., Bittinger, K., Bushman, F. D., Costello, E. K., Fierer, N., Pena, A. G., Goodrich, J. K., Gordon, J. I.: QIIME allows analysis of high-throughput community sequencing data, Nat. Methods, 7, 335–336, 2010.

Cole, J.R., Wang, Q., Cardenas, E., Fish, J., Chai, B., Farris, R. J., Kulam-Syed-Mohideen, A. S., McGarrell, D. M., Marsh, T., Garrity, G. M., Tiedje, J. M.: The Ribosomal Database Project: improved alignments and new tools for rRNA analysis, Nucleic Acids Res., 37, D141–D145, 2009.

DeLong E. F.: Archaea in coastal marine environments, Proc. Natl. Acad. Sci., USA 89, 5685–5689, 1992.

Galand, P. E., Gutierrez-Provecho, C., Massana, R., Gasol, J., Casamayor, E. O.: Interannual recurrence of archaeal assemblages in the coastal NW Mediterranean Sea, Limnol. Oceanogr., 55, 2117–2125, 2010.

Gantner, S., Andersson, A. F., Alonso-Saez, L., Bertilsson, S.: Novel primers for 16S rRNA-based archaeal community analyses in environmental samples, J. Microbiol. Methods, 84, 12–18, 2011.

Ge, H., Zhang, C. L., Dang, H. Y., Zhu, C., Jia, G. D.: Distribution of tetraether lipids in surface sediments of the northern South China Sea: implications for TEX_{86} proxies, Geosci. Front., 4, 223–229, 2013.

Harvey, H. R., Fallon, R. D., Patton, J. S.: The effect of organic matter and oxygen on the degradation of bacterial membrane lipids in marine sediments, Geochim. Cosmochim. A., 50, 795–804, 1986.

Herfort, L., Schouten, S., Boon, J. P., Sinninghe Damsté, J. S.: Application of the TEX_{86} temperature proxy in the southern North Sea, Org. Geochem., 37, 1715–1726, 2006.

Hernandez-Sanchez, M. T., Woodward, E. M. S., Taylor, K. W. R., Henderson, G. M., Pancost, R. D.: Variations in GDGT distributions through the water column in the South East Atlantic Ocean, Geochim. Cosmochim. A., 132, 337–348, 2014.

Hugoni, M., Taib, N., Debroas, D., Domaizon, I., Dufournel, I.J., Bronner, G., Salter, I., Agogue, H., Mary, I., and Galand, P. E.: Structure of the rare archaeal biosphere and seasonal dynamics of active ecotypes in surface coastal waters, Proc. Natl. Acad. Sci., USA 110(15), 6004–6009, 2013.

Hu, A., Hou, L., Yu, C. –P.: Biogeography of planktonic and benthic archaeal communities in a subtropical eutrophic estuary of China, Microbio. Ecol., 1–14, 2015.

Huguet, C., Hopmans, E. C., Febo-Ayala, W., Thompson, D. H., Sinninghe Damsté, J. S., Schouten, S.: An improved method to determine the absolute abundance of glycerol dibiphytanyl glycerol tetraether lipids, Org. Geochem., 37, 1036–1041, 2006.

Karner, M., DeLong, E. F., Karl, D. M.: Archaeal dominance in the mesopelagic zone of the Pacific Ocean, Nature, 409, 507–510, 2001.

Kim, J.-H., Schouten, S., Hopmans, E. C., Donner, B., Sinninghe Damsté, J. S.: Global core-top calibration of the TEX_{86} paleothermometer in the ocean, Geochim. Cosmochim. A., 72, 1154–1173, 2008.

Kim, J. -H., van der Meer, J., Schouten, S., Helmke, P., Willmott, V., Sangiorgi, F., Koç, N., Hopmans, E. C., Sinninghe Damsté, J. S.: New indices and calibrations derived from the distribution of crenarchaeal isoprenoid tetraether lipids: implications for past sea surface temperature reconstructions, Geochim. Cosmochim. A., 74, 4639–4654, 2010.

Kim, J. H., Schouten, S., Rodrigo-Gamiz, M., Rampen, S., Marino, G., Huguet, C., Helmke, P., Buscail, R., Hopmans, E. C., Pross, J., Sangiorgi, F., Middelburg, J. B. M., Sinninghe Damsté, J. S.: Influence of deep-water derived isoprenoid tetraether lipids on the TEX_{86}^{H} paleothermometer in the Mediterranean Sea, Geochim. Cosmochim. A., 150, 125–141, 2015.

Lee, K. E., Kim, J. –H., Wilke, I., Helmke, P., Schouten, S.: A study of the alkenone, TEX_{86}, and planktonic foraminifera in the Benguela Upwelling System: Implications for past sea surface temperature estimates, Geochem. Geophys. Geosyst., 9 (10), Q10019, 2008.

Lincoln, S. A., Wai, B., Eppley, J. M., Church, M. J., Summons, R. E., and DeLong, E. F.: Planktonic Euryarchaeota are a significant source of archaeal tetraether lipids in the ocean, Proc. Natl. Acda. Sci. USA, 111(27), 9858–9863, 2014a.

Lincoln, S. A., Wai, B., Eppley, J. M., Church, M. J., Summons, R. E., and DeLong, E. F.: Reply to Schouten et al.: Marine Group II planktonic Euryarchaeota are significant contributors to tetraether lipids in the ocean, Proc. Natl. Acda. Sci. USA, 111(41), E4286, 2014b.

Liu, M., Xiao, T., Wu, Y., Zhou, F., and Zhang, W.: Temporal distribution of the archaeal community in the Changjiang Estuary hypoxia area and the adjacente East China Sea as determined by denaturing gradiente gel electrophoresis and multivariate analysis, Can. J. Microbiol., 57, 504–513, 2011.

Liu, J., Yu, S., Zhao, M., He, B. & Zhang, X. -H.: Shifts in archaea plankton community structure along ecological gradients of Pearl Estuary, FEMS Microbiol. Ecol., 90, 424–435, 2014.

Liu, X. L., Lipp, J. S., Hinrichs, K. - U.: Distribution of intact and core GDGTs in marine sediments, Org. Geochem., 42, 368–375, 2011.

Massana, R., Murray, A. E., Preston, C. M., DeLong, E. F.: Vertical distribution and phylogenetic characterization of marine planktonic Archaea in the Santa Barbara Channel, Appl. Environ. Microbiol., 63(1), 50–56, 1997.

Pearson, A. and Ingalls, A. E.: Assessing the use of archaeal lipids as marine environmental proxies, Ann. Rev. Earth Planet. Sci., 41, 359–384, 2013.

Pitcher, A., Hopmans, E. C., Schouten, S., Sinninghe Damsté, J. S.: Separation of core and intact polar archaeal tetraether lipids using silica columns: insights into living and fossil biomass contributions, Org. Geochem., 40, 12–19, 2009.

Pitcher, A., Hopmans, E. C., Mosier, A. C., Francis, C. A., Reese, S. K., Schouten, S., Sinninghe Damsté, J. S.: Distribution of core and intact polar tetraether lipids in enrichment cultures of Thaumarchaeota from marine sediments, Appl. Environ. Microbiol., 77, 3468–3477, 2011a.

Pitcher, A., Villanueva, L., Hopmans, E. C., Schouten, S., Reichart, G. J., Sinninghe Damsté, J. S.: Niche segregation of ammonia-oxidizing archaea and anammox bacteria in the Arabian Sea oxygen minimum zone, ISME J., 5, 1896–1904, 2011b.

Schloss, P. D., Westcott, S. L., Ryabin, T., Hall, J. R., Hartmann, M., Hollister, E. B., Lesniewski, R. A., Oakley, B. B., Parks, D. H., Robinson, C. J.: Introducing mothur: open-source, platform-independent, community-supported software for describing and comparing microbial communities, Appl. Environ. Microbiol., 75, 7537–7541, 2009.

Schouten, S., Hopmans, E. C., Schefuß, E., Sinninghe Damsté, J. S.: Distributional variations in marine crenarchaeotal membrane lipids: a new tool for reconstructing ancient sea water temperatures?, Earth Planet. Sci. Lett., 204, 265–274, 2002.

Schouten, S., Huguet, C., Hopmans, E. C., Sinninghe Damsté, J. S.: Improved analytical methodology of the TEX_{86} paleothermometry by high performance liquid chromatography/atmospheric pressure chemical ionization–mass spectrometry, Anal. Chem., 79, 2940–2944, 2007.

Schouten, S., Hopmans, E. C., Baas, M., Boumann, H., Standfest, S., Könneke, M., Stahl, D.A., Sinninghe Damsté, J. S.: Intact membrane lipids of ‘‘Candidatus Nitrosopumilus maritimus’’, a cultivated representative of the cosmopolitan mesophilic Group I Crenarchaeota, Appl. Environ. Microbiol., 74, 2433–2440, 2008.

Schouten, S., Middelburg, J. J., Hopmans, E. C., Sinninghe Damsté, J.S.: Fossilization and degradation of intact polar lipids in deep subsurface sediments: a theoretical approach, Geochim. Cosmochim. A., 74, 3806–3814, 2010.

Schouten, S., Pitcher, A., Hopmans, E.C., Villanueva, L., van Bleijswijk, J., Sinninghe Damsté, J. S.: Distribution of core and intact polar glycerol dibiphytanyl glycerol tetraether lipids in

the Arabian Sea Oxygen Minimum Zone: I: Selective preservation and degradation in the water column and consequences for the TEX_{86}, Geochim. Cosmochim. A., 98, 228–243, 2012.

Schouten, S., Hopmans, E. C., Sinninghe Damsté, J. S.: The organic geochemistry of glycerol dialkyl glycerol tetraether lipids: a review, Org. Geochem., 54, 19–61, 2013.

Schouten, S., Villanueva, L., Hopmans, E, C., van der Meer, M. T. J., Sinninghe Damsté, J. S.: Are Marine Group II Euryarchaeota significant contributors to tetraether lipids in the ocean?, Proc. Natl. Acda. Sci. USA, 111(41), E4285, 2014.

Sinninghe Damsté, J. S., Hopmans, E. C., Schouten, S., van Duin, A. C. T., Geenevasen, J. A. J.: Crenarchaeol: the characteristic core glycerol dibiphytanyl glycerol tetraether membrane lipid of cosmopolitan pelagic crenarchaeota, J. Lipid Res., 43, 1641–1651, 2002.

Sinninghe Damsté, J. S., Ossebaar, J., Schouten, S., Verschuren, D.: Distribution of tetraether lipids in the 25-kyr sedimentary record of Lake Challa: extracting reliable TEX_{86} and MBT/CBT palaeotemperatures from an equatorial African lake, Quaternary Sci. Rev., 50, 43–54, 2012.

Strong, D. J., Flecker, R., Valdes, P. J., Wilkinson, I. P., Rees, J. G., Zong, Y. Q., Lloyd, J. M., Garrett, E., Pancost, R. D.: Organic matter distribution in the modern sediments of the Pearl River Estuary, Org. Geochem., 49, 68–82, 2012.

Taylor, K.W.R., Huber, M., Hollis, C. J., Hernandez-Sanchez, M. T., Pancost, R. D.: Re-evaluating modern and palaeogene GDGT distributions: Impalications for SST reconstructions, Global Planet. Change, 108, 158–174, 2013.

Teira, E., Reinthaler, T., Pernthaler, A., Pernthaler, J., and Herndl, G. J.: Combining catalyzed reporter deposition- fluorescence in situ hybridization and microautoradiography to detect

substrate utilization by Bacteria and Archaea in the deep ocean, Appl. Environ. Microbiol., 70: 4411–4414, 2004.

Turich, C., Freeman, K. H., Bruns, M. A., Conte, M., Jones, A. D., Wakeham, S. G.: Lipids of marine Archaea: patterns and provenance in the water-column and sediments, Geochim. Cosmochim. A., 71, 3272–3291, 2007.

Wang, J. -X., Wei, Y., Wang, P., Hong, Y., Zhang, C. L.: Unusually low TEX_{86} values in the transitional zone between Pearl River estuary and coastal South China Sea: Impact of changing archaeal community composition, Chem. Geol., 402, 18 – 29, 2015.

Wei, Y., Wang, J. X., Liu, J., Dong, L., Li, L., Wang, H., Wang, P., Zhao, M., Zhang, C. L.: Spatial variations in Archaeal lipids of surface water and core-top sediments in the South China Sea: implications for paleoclimate studies, Appl. Environ. Microbiol., 77, 7479–7489, 2011.

Weijers, J. W. H., Schouten, S., Spaargaren, O. C., Sinninghe Damsté, J. S.: Occurrence and distribution of tetraether membrane in soils: implications for the use of the BIT index and the TEX_{86} SST proxy, Org. Geochem., 37, 1680–1693, 2006.

Weijers, J. W. H., Bernhardt, B., Peterse, F., Werne, J. P., Dungait, J. A. J., Schouten, S., Sinninghe Damsté, J. S.: Absence of seasonal patterns in MBT–CBT indices in mid-latitude soils, Geochim. Cosmochim. A., 75, 3179–3190, 2011a.

Weijers, J. W. H., Lima, K. H. L., Aquilina, A., Sinninghe Damsté, J. S., Pancost, R.D.: Biogeochemical controls on glycerol dialkyl glycerol tetraether lipid distributions in sediments characterized by diffusive methane flux, Geochem. Geophys. Geosyst., 12, 2011b.

Wuchter, C., Schouten, S., Wakeham, S. G., Sinninghe Damsté, J. S.: Archaeal tetraether membrane lipid fluxes in the northeastern Pacific and the Arabian Sea: implications for TEX_{86} paleothermometry, Paleoceanography, 21, PA4208., 2006.

Xie, W., Zhang, C. L., Zhou, X., Wang, P.: Salinity-dominated change in community structure and ecological function of Archaea from the lower Pearl River to coastal South China Sea. Environ., Appl. Microbiol. Biotechnol., 98(18), 7971–7982, 2014.

Zell, C., Kim, J. -H., Hollander, D., Lorenzoni, L., Baker, P., Silva, C. G., Nittrouer, C., Sinninghe Damsté, J. S.: Sources and distributions of branched and isoprenoid tetraether lipids on the Amazon shelf and fan: Implications for the use of GDGT-based proxies in marine sediments, Geochim. Cosmochim. A., 139, 293–312, 2014.

Zhang, C. L., Wang, J. –X., Wei, Y., Zhu, C., Huang, L., Dong, H.: Production of branched tetraether lipids in the lower Pearl River and estuary: effects of extraction methods and impact on bGDGTs proxies. Front. Terr. Microbiol., 2, http://dx.doi.org/10.3389/fmicb.2011.00274, 2012.

Zhang, J., Bai, Y., Xu, S., Lei, F., Jia, G.: Alkenone and tetraether lipids reflect different seasonal seawater temperatures in the coastal northern South China Sea, Org. Geochem., 58, 115–120, 2013.

Zhang, Y. G., Zhang, C. L., Liu, X.L., Li, L., Hinrichs, K. -U., Noakes, J. E.: Methane Index: a tetraether archaeal lipid biomarker indicator for detecting the instability of marine gas hydrates, Earth Planet. Sci. Lett., 307, 525–534, 2011.

Zhang, Y. G., Pagani, M., and Wang, Z.: Ring Index: A new strategy to evaluate the integrity of TEX_{86} paleothermometry, Paleoceanography, in review.

Zhu, C., Weijers, J.W.H., Wagner, T., Pan, J. M., Chen, J. F., Pancost, R. D.: Sources and distributions of tetraether lipids in surface sediments across a large riverdominated continental margin, Org. Geochem., 42, 376–386, 2011.

Fig. 3.1

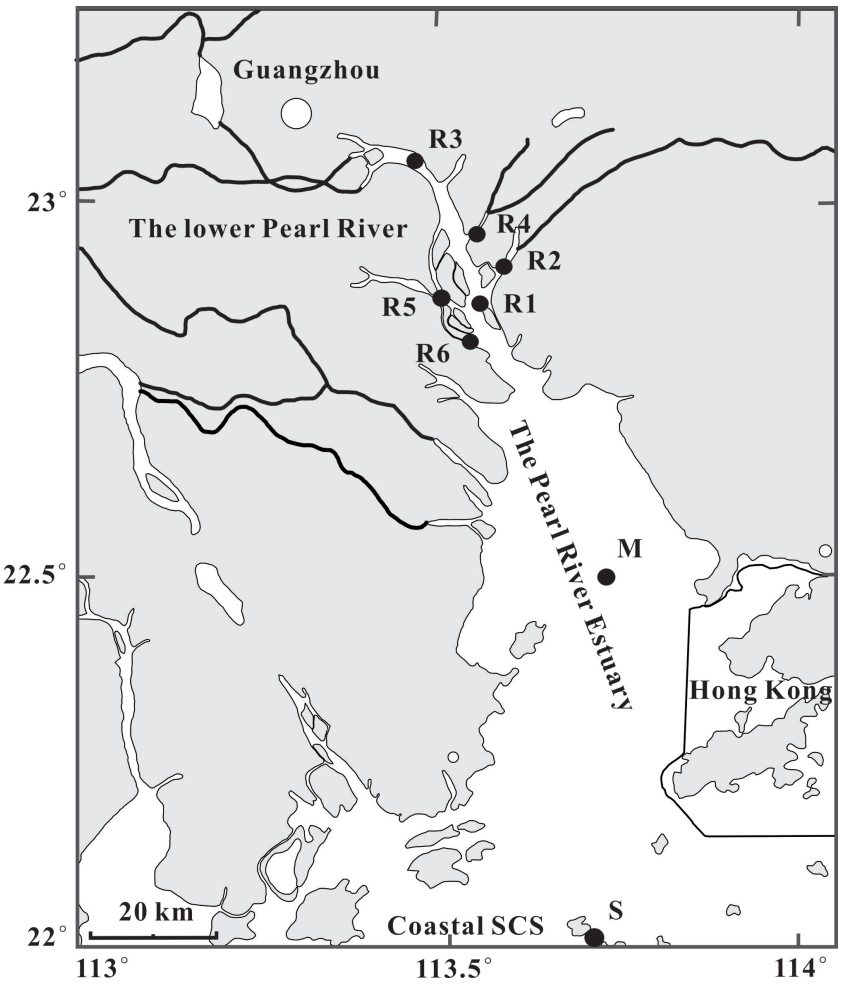

Figure 3.1. Map showing location of sites (dark circle) in the lower Pearl River (PR), the PR estuary, and coastal South China Sea (SCS). Abbreviations: R, River water, which is followed by the station #; M, mixing water; S, seawater. The station S includes four water layers (surface, subsurface, middle, and bottom). The station M includes three water layers (surface, middle and bottom). The surface water of the station M were also collected at the high tide, slack tide, and low tide period. The station R1 and R2 include two water layer (surface and bottom). Surface sediments were collected at each sampling sites.

Fig. 3.2

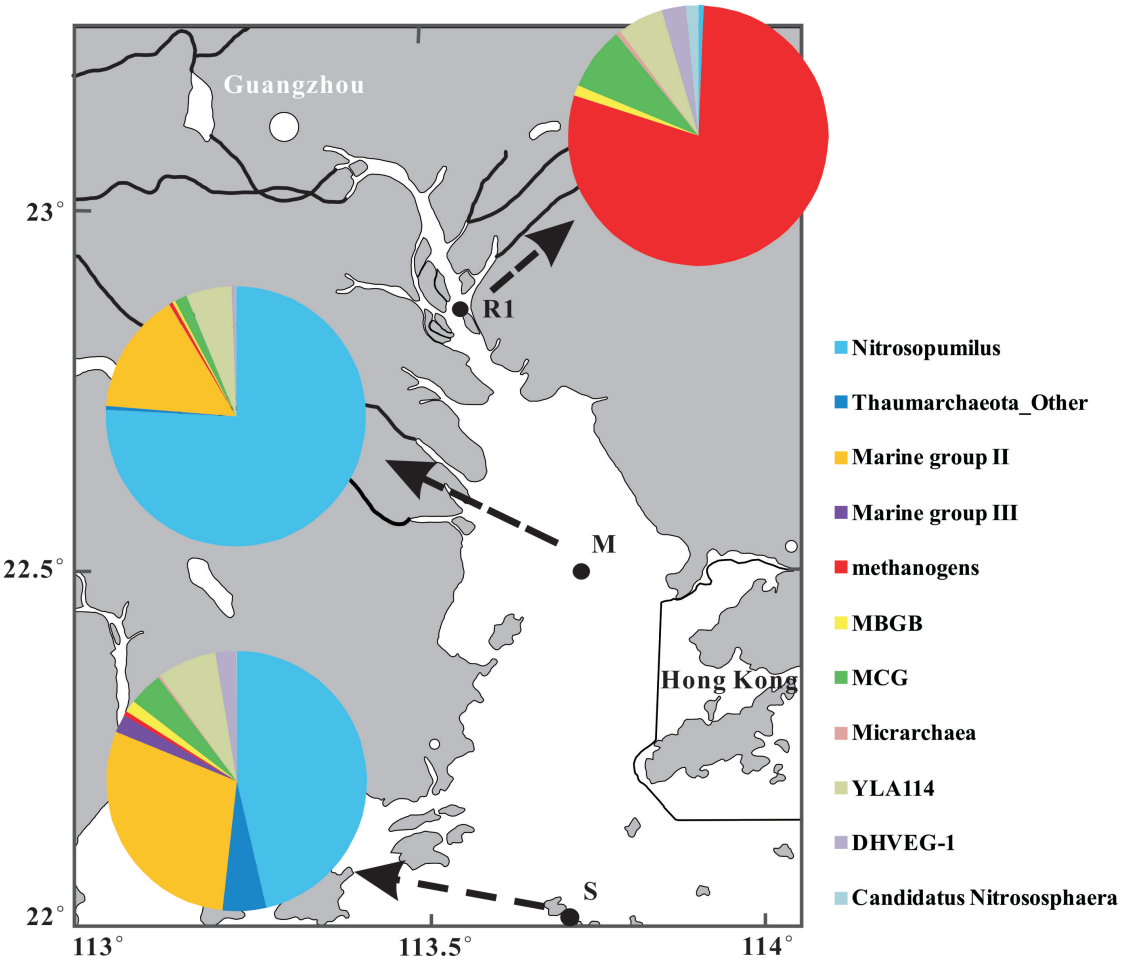

Fig. 3.2. The distribution of archaeal community composition based on 454 sequencing along the salinity gradient at the lower Pearl River (river water, station R1), The PR estuary (mixing water, station M), and coastal South China Sea (seawater, station S).

Fig. 3.3

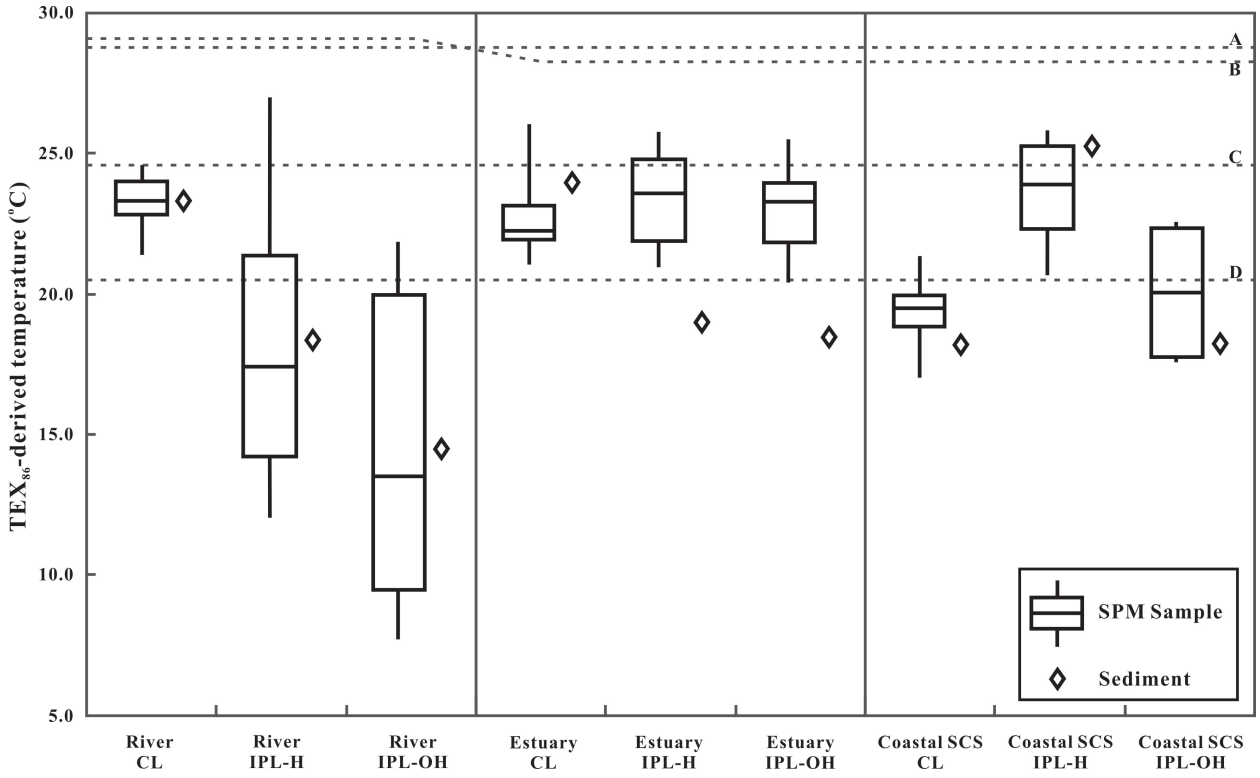

Fig. 3.3. Mean values of TEX_{86}-derived temperatures in SPM and surface sediments from the lower Pearl River (R), the PR estuary (M), and coastal SCS (S). CL, core lipids; IPL-H, intact polar lipid based upon acid hydrolysis; IPL-OH, intact polar lipid based upon base hydrolysis. Dashed lines A, June mean surface water temperature (SWT) (28.4 ± 0.07^{o}C); dashed line B, in situ instrumental temperature (29.1^{o}C, in the river water; 28.2^{o}C in the mixing water and seawater); dashed line C, annual mean SWT (24.71 ± 0.11^{o}C); dashed line D, winter SWT (20.54 ± 0.10^{o}C).

Fig. 3.4

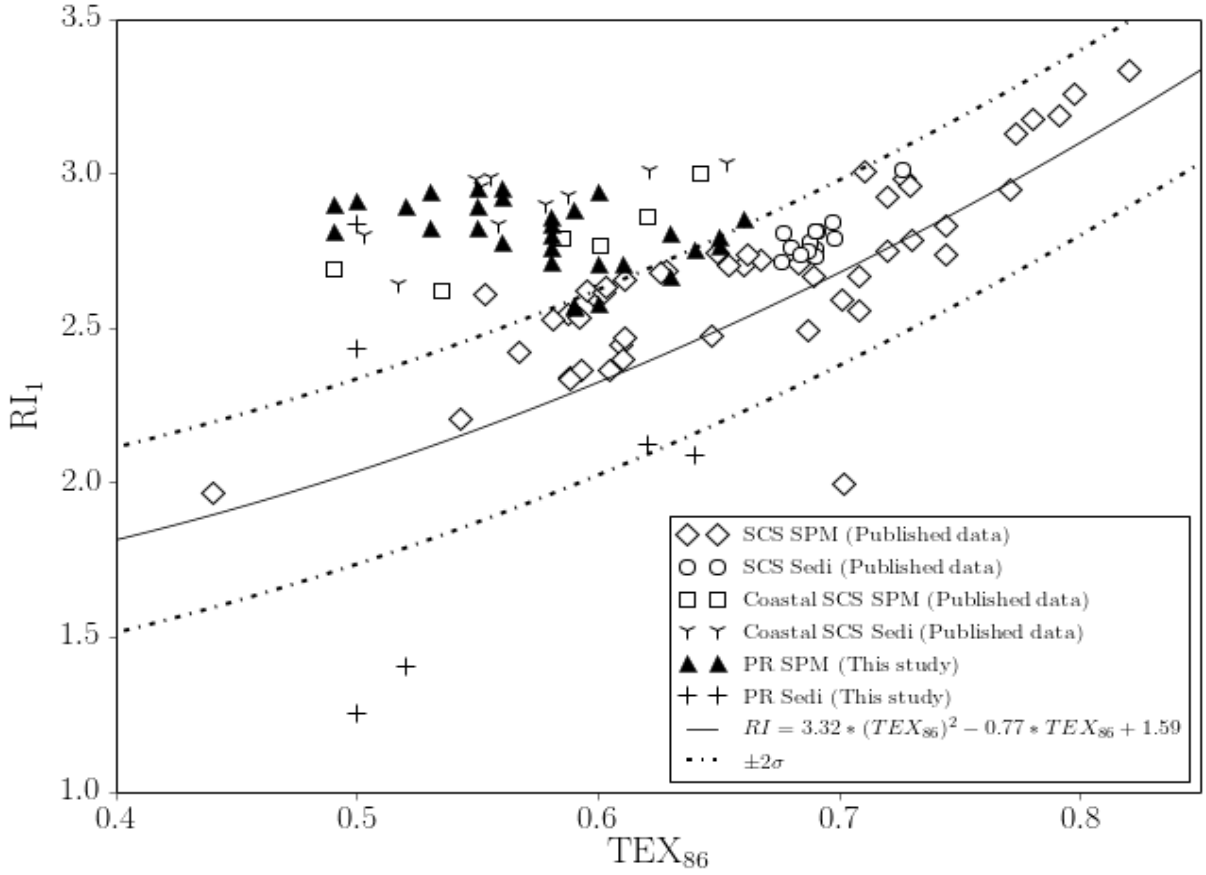

Fig. 3.4. TEX_{86} of the SPM samples and surface sediments plotted against RI1. The blue dashed line represents the RI-TEX_{86} calibration from Zhang et al. (in review). The SCS SPM/sediments and coastal SCS SPM/sediments (black points) are from Wei et al. (2011), Ge et al. (2013), Zhang et al. (2013), and Wang et al. (2015). The colored points are from this study.

Fig. 3.5

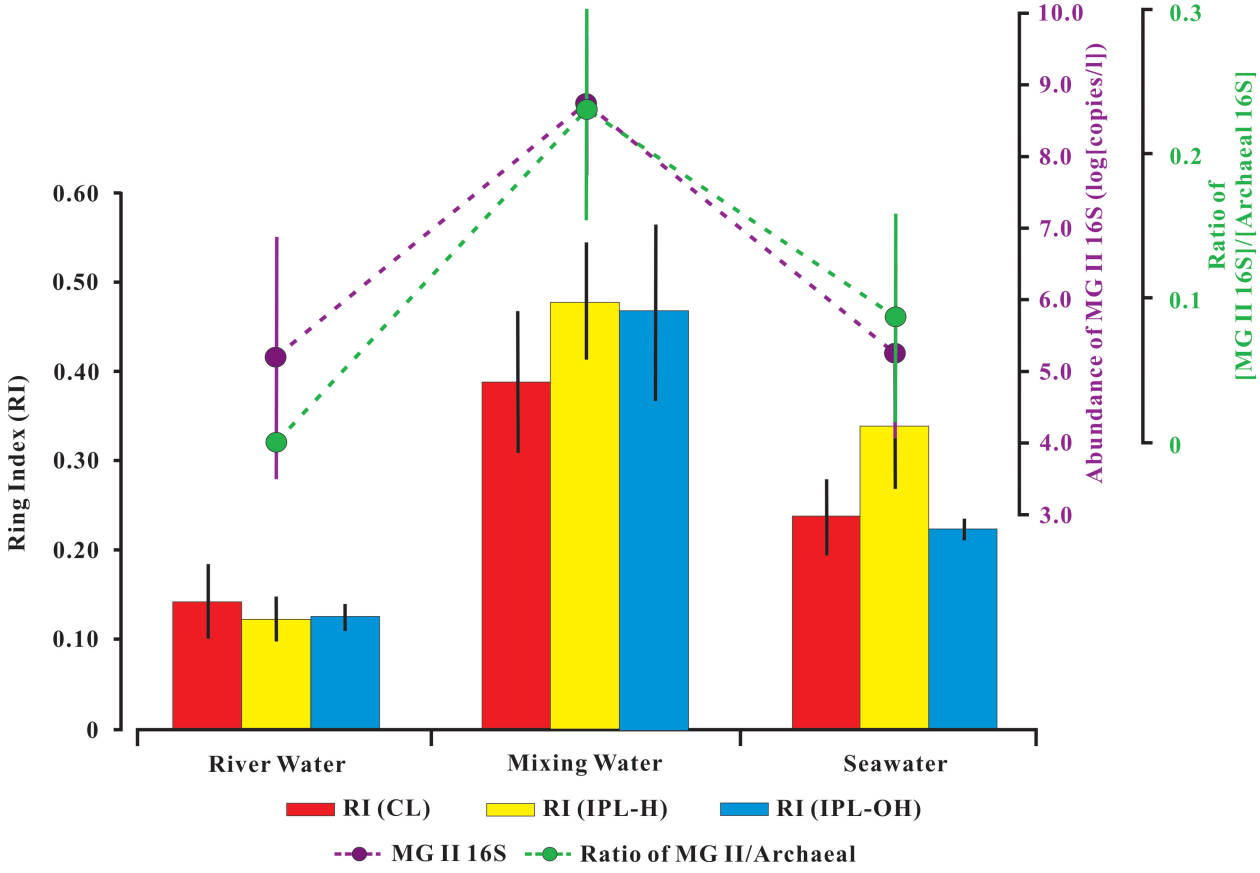

Fig. 3.5. Distribution of the mean values of the Ring Index (bars) calculated from CL, IPL-H and IPL-OH, the abundance of 16S rRNA genes (purple marked line), and the ratio of MG II 16S to Archaeal 16S (green marked line) along the salinity gradient from the river water to seawater. Individual value is shown in Table 3.1.

Fig. 3.6

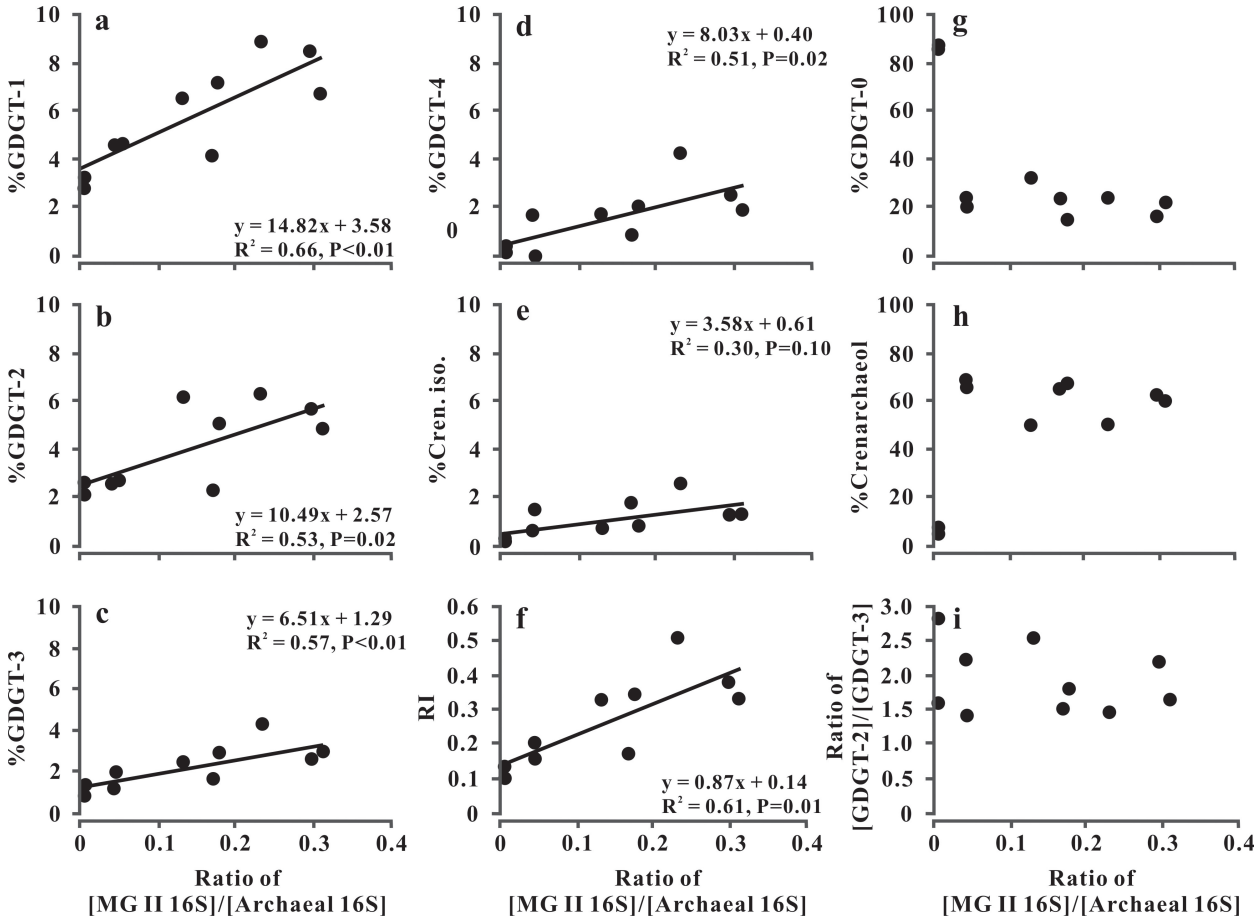

Fig. 3.6. Fractional abundance (%) of GDGTs, RI, and ratio of GDGT-2 to GDGT-3 vs. the ratio of MG II 16S to Archaeal 16S. SPM samples collected from the lower Pearl River, the PR estuary, and the coastal SCS.

Table 3.1

Table 3.1. Basic information, abundance of isoprenoid GDGTs, TEX_{86}, Ring Index, and 16S rRNA gene for suspended particulate matters (SPM) in the water column and surface sediments collected from the lower Pearl River, the Pearl River estuary, and coastal northern South China Sea. Basic information includes location, sampling date, water depth, temperature (Temp.), and salinity (Sal.).

Sample ID[a]	Longitude (E)	Latitude (N)	Sampling date (mm/dd/yyyy)	Depth[b] (m)	Temp. (℃)	Sal.	pH	iGDGTs (ng/l)[c]			TEX_{86}			Ring Index (RI)			Archaeal 16S	MGII 16S
								CL	IPL-H	IPL-OH	CL	IPL-H	IPL-OH	CL	IPL-H	IPL-OH		
River water SPM																		
R1_sur	113°34.249′	22°52.647′	06/21/2011	1.5	29.7	0.2	7.25	188.6	201.5	16.7	0.59	0.50	0.57	0.19	0.15	0.12	2.1E+09	3.0E+05
R1_bott	113°34.249′	22°52.647′	06/21/2011	6.0	29.6	0.2	7.25	221.3	128.1	8.9	0.60	0.56	0.54	0.16	0.12	0.15	3.6E+08	1.2E+03
R2_sur	113°36.680′	22°56.338′	06/21/2011	1.5	29.0	0.1	6.95	64.8	82.5	6.8	0.56	0.42	0.49	0.16	0.15	0.11	-[d]	-
R2_bott	113°36.680′	22°56.338′	06/21/2011	6.0	29.0	0.1	6.90	266.6	426.5	27.9	0.60	0.45	0.38	0.14	0.10	0.12	-	-
R3	113°28.726′	23°04.339′	06/22/2011	1.5	29.4	0.1	7.46	79.8	150.2	8.0	0.57	0.41	0.38	0.07	0.09	0.14	-	-
R4	113°33.507′	22°58.409′	06/22/2011	1.5	29.6	0.2	7.28	19.1	30.6	3.3	0.63	0.57	0.37	0.26	0.13	0.20	-	-
R5	113°29.941′	22°53.588′	06/22/2011	1.5	28.5	0.1	7.28	20.0	30.4	2.0	0.61	0.48	0.35	0.37	0.40	0.34	-	-
R6	113°33.088′	22°44.811′	06/22/2011	1.5	27.8	0.1	6.92	49.1	21.8	1.2	0.62	0.68	0.53	0.15	0.19	0.25	-	-
Mixing water SPM																		
M_lt	113°45.098′	22°27.206′	06/18/2011	1.5	-	-	-	25.9	105.0	2.4	0.66	0.55	0.53	0.52	0.47	0.43	2.0E+07	6.1E+06
M_st	113°45.098′	22°27.206′	06/18/2011	1.5	-	-	-	35.3	97.3	1.4	0.58	0.65	0.60	0.36	0.61	0.61	1.3E+09	3.1E+08
M_ht	113°45.098′	22°27.206′	06/18/2011	1.5	-	-	-	21.9	86.8	2.8	0.59	0.56	0.55	0.43	0.46	0.38	6.9E+07	1.2E+07
M_sur	113°45.098′	22°27.206′	06/18/2011	1.5	28.7	11.1	8.03	18.9	67.0	1.9	0.58	0.60	0.63	0.36	0.44	0.65	-	7.2E+07
M_mid	113°45.098′	22°27.206′	06/18/2011	5.0	28.3	15.6	7.93	102.6	73.4	5.2	0.61	0.64	0.59	0.35	0.47	0.36	6.0E+09	7.9E+08
M_bott	113°45.098′	22°27.206′	06/18/2011	9.0	27.6	23.0	7.89	107.4	76.7	6.0	0.56	0.60	0.58	0.30	0.42	0.38	5.1E+09	1.6E+09
Sea water SPM																		
S_sur	113°70.448′	22°05.165′	06/15/2011	1.5	29.6	29.5	8.63	1.1	0.7	0.1	0.52	0.65	0.58	0.28	0.39	0.22	1.0E+05	4.8E+03
S_subs	113°70.448′	22°05.165′	06/15/2011	5.0	29.5	29.7	8.64	2.1	1.1	0.1	0.56	0.63	0.58	0.27	0.33	0.24	3.1E+06	5.3E+05
S_mid	113°70.448′	22°05.165′	06/15/2011	10.0	28.6	31.7	8.45	12.6	13.5	0.6	0.49	0.55	0.50	0.20	0.24	0.23	9.8E+04	4.4E+03
S_bott	113°70.448′	22°05.165′	06/15/2011	18.0	25.4	33.7	7.92	21.4	9.6	0.7	0.53	0.59	0.49	0.20	0.39	0.21	-	-
Sediment																		
Sedi-R1	113°34.249′	22°52.647′	06/21/2011	8.0	-	-	7.46	461.8	142.8	9.5	0.58	0.37	0.30	0.27	0.38	0.41	2.8E+10	1.2E+06
Sedi-R2	113°36.680′	22°56.338′	06/21/2011	7.0	-	-	7.68	687.5	289.2	17.0	0.56	0.35	0.31	0.23	0.22	0.26	-	-
Sedi-R3	113°28.726′	23°04.339′	06/22/2011	9.0	-	-	7.29	800.3	233.5	19.6	0.57	0.43	0.36	0.15	0.23	0.30	-	-
Sedi-R4	113°33.507′	22°58.409′	06/22/2011	7.0	-	-	7.50	881.0	149.7	9.7	0.58	0.51	0.38	0.33	0.75	0.62	-	-
Sedi-R5	113°29.941′	22°53.588′	06/22/2011	8.0	-	-	7.58	621.7	84.2	7.3	0.62	0.52	0.37	0.33	0.66	0.43	-	-
Sedi-R6	113°33.088′	22°44.811′	06/22/2011	8.0	-	-	7.66	120.2	103.8	6.2	0.67	0.35	0.42	0.42	0.65	0.74	-	-
Sedi-M	113°45.098′	22°27.206′	06/18/2011	12.0	-	-	7.60	200.4	67.7	2.3	0.62	0.52	0.50	0.38	0.69	0.42	1.1E+10	1.7E+06
Sedi-S	113°70.448′	21°95.165′	06/15/2011	20.0	-	-	7.40	5003.6	267.3	20.8	0.50	0.64	0.50	0.19	0.73	0.34	1.3E+10	4.8E+06

[a]R, River (the lower Pearl River), which is followed by the station numbers; sur and bott represent surface water and bottom water. M, Mixing water (the Pearl River estuary); lt, low tide; st, slack tide; ht, high tide; mid means middle layer water. S, Sea water (northern South China Sea); subs represents subsurface water.
[b]For the SPM samples collected from the water column, the depth is referred to the sampling water depth; For the sediments, the depth indicates the river water depth.
[c]CL, core lipids; IPL-H, intact polar lipid (IPL) derived core lipids upon acid (H) hydrolysis; IPL-OH, IPL-derived core lipids derived upon base (OH) hydrolysis.
[d]-, data are not available or not examined.

Table 3.2

Table 3.2. Regression analysis between the ratio of MG II16S to Archaeal 16S and the fractional abundance of GDGTs, RI, and the ratio of GDGT-2 to GDGT-3.

	16S Ratio vs. CL[a]		16S Ratio vs. IPL-H		16S Ratio vs. IPL-OH	
	R^2	P value	R^2	P value	R^2	P value
%GDGT-0	0.43	0.04	0.47	0.03	0.44	0.04
%GDGT-1	0.52	0.02	0.63	0.01	0.68	0.00
%GDGT-2	0.54	0.02	0.47	0.03	0.53	0.02
%GDGT-3	0.43	0.04	0.54	0.02	0.57	0.01
%GDGT-4	0.52	0.02	0.62	0.01	0.51	0.02
%Cren.	0.32	0.09	0.39	0.05	0.30	0.10
%Cren.iso	0.48	0.03	0.02	0.72	0.35	0.07
RI	0.54	0.02	0.61	0.01	0.61	0.01
GDGT 2/3	0.16	0.25	0.34	0.08	0.06	0.49

[a]16S ration, the ratio of MG II 16S to archaeal 16S. CL, core lipdis; IPL-H, intact polar lipids derived upon acid hydrolysis; IPL-OH, intact polar lipids derived upon base hydrolysis.

CHAPTER 4

SUMMARY

Reconstruction of paleo-sea surface temperature (SST) is of primary importance for the study of paleoclimate changes, paleo-ecological variation, and ocean circulation. In the last decade, TEX_{86} (TetraEther indeX of glycerol dialkyl glycerol tetraethers (GDGTs) with 86 carbons) has been a popular temperature proxy in paleoclimate studies. Although the global core-top calibrations of TEX_{86} are empirically correlated with annual mean SST, mounting evidence indicates anomalies or discrepancies in TEX_{86}-derived SST in the coastal seas and open ocean. The main objective of this thesis was to constrain the predominant factor controlling the variation of TEX_{86} in the estuary and coastal region of South China Sea (SCS). To do this we focused on 1) finding the source of archaeal GDGTs, 2) investigating the archaeal community compositions and 3) evaluating the relationship between archaeal lipids and molecular DNA in the water column and surface sediments of the lower Pearl River and its estuary.

Regarding the source of archaeal GDGTs, the results suggested that terrestrial input of archaeal tetraether lipids has little impact on the distribution and abundance of GDGTs in the lower Pearl River and its estuary. In situ production of archaeal lipids predominantly contributes to the GDGT pool in the water column and sediments in this region. Vertical transportation plays a dominant role in the export of GDGTs from water column to the surface sediments.

The archaeal community composition is overwhelmingly changed from the lower Pearl River to the PR estuary, with methanogens and Marine Group I (MG I) Thaumarchaeota being

the predominant groups, respectively. A significant proportion of Marine Group II (MG II) Euryarchaeota was present in the PR estuary and coastal SC. This is consistent with the cluster analysis based on the fractional abundances of GDGTs in the water column of the lower PR and its estuary, which showing that GDGT-0 and crenarchaeol predominantly distributed in the river water end and salty water end, respectively. The quantitative polymerase chain reaction (qPCR) of MG II and total Archaea suggests that the PR estuary is a hot spot for the occurrence of MG II Euryarchaeota along the salinity gradient from the low Pearl River to the coastal SCS.

The unusually low TEX_{86} in the transitional zone from the PR estuary to the coastal SCS is an important observation in this study. The accuracy of TEX_{86} can be assessed by Ring Index (RI), which is significantly correlated with the ratio of MG II Euryarchaeota to total Archaea. GDGT-2 and GDGT-3 are crucial components to contribute to the discrepancy between TEX_{86}-derived temperature and satellite-based temperature. Linear correlation between the TEX_{86}-related GDGTs (GDGT-1, -2, -3) and [MGII]/[Archaea] ratio strongly suggests that a significant proportion of cyclopentane moieties-containing GDGTs (GDGTs with 1-4 rings) can be produced by MG II Euryarchaeota, another abundant planktonic archaea inhabiting predominantly (near) surface water of coastal and open ocean. These MG II-produced tetraether lipids may alter the GDGT pool in the water column and surface sediments. This mechanism may further influence TEX_{86} in the sediment record.

Our study implies that low temperature events based on TEX_{86} in ancient continental margins should be interpreted with extreme caution. MG II-produced GDGTs provide an alternative interpretation for the TEX_{86} anomalies or discrepancies in sediment record. Moreover, cultivation techniques focusing on MG II will be necessary to substantiate the conclusion proposed in this thesis.

APPENDICES

A. SUPPLEMENTAL TABLES IN CHAPTER TWO

Table A1

Table A1. Fractional abundance of archaeal isoprenoid GDGTs, TEX_{86}, and TEX_{86}-derived temperatures for SPM samples collected from the water column of the lower Pearl River and the Pealr River estuary.

Sample ID[a]		Fractional abundance of archaeal isoprenoid GDGTs (%)							TEX_{86}	TEX_{86}^H	SST-TEX_{86}^H (^oC,2010[c])	SST-TEX_{86}^H (^oC,2012[c])	Sat-Ann.[d] (^oC)	Sat-Jul. (^oC)	Sat-Win. (^oC)
		GDGT-0	GDGT-1	GDGT-2	GDGT-3	GDGT-4	Cren[b]	Cren.iso.[b]							
Lower Pearl River - core lipids															
PR-1-CL		64.8	3.4	3.7	1.6	0.6	25.2	0.6	0.63	-0.20	25.11	19.91	24.58	28.80	20.58
PR-2-CL		60.0	3.6	4.1	1.7	0.7	29.2	0.6	0.64	-0.20	25.20	19.99	24.63	28.76	20.50
PR-3-CL		74.8	2.4	2.7	1.2	0.5	17.9	0.4	0.64	-0.20	25.12	19.92	24.54	28.76	20.35
PR-4-CL		53.8	4.1	4.5	1.9	1.2	33.8	0.7	0.63	-0.20	25.09	19.90	24.68	28.76	20.50
PR-5-CL		70.4	2.7	2.9	1.2	0.7	21.7	0.4	0.63	-0.20	24.97	19.80	24.63	28.76	20.33
PR-6-CL		80.1	1.8	2.2	1.0	0.5	14.1	0.3	0.65	-0.18	25.95	20.59	24.68	28.76	20.50
PR-7-CL		67.5	2.7	3.1	1.3	0.8	24.0	0.4	0.64	-0.19	25.39	20.14	24.51	28.76	20.40
PR-8-CL		92.6	0.8	0.8	0.4	0.3	5.0	0.2	0.65	-0.19	25.77	20.44	24.53	28.73	20.43
PR-9-CL		85.8	1.6	1.9	1.0	0.6	8.7	0.4	0.66	-0.18	26.45	20.99	24.53	28.73	20.43
PR-10-CL		86.5	1.1	1.1	0.7	0.6	9.7	0.3	0.67	-0.18	26.61	21.12	24.51	28.76	20.40
Pearl River estuary - core lipids															
PR-11-CL	S	47.5	4.7	5.0	2.0	1.2	38.8	0.8	0.62	-0.20	24.63	19.53	24.61	28.80	20.54
	B	49.4	4.5	4.8	2.0	1.4	37.1	0.8	0.63	-0.20	24.78	19.65			
PR-12-CL	S	37.1	6.3	6.2	2.3	1.4	45.7	1.0	0.60	-0.22	23.59	18.69	24.64	28.84	20.36
	B	25.3	6.2	4.5	1.8	0.7	60.9	0.6	0.53	-0.28	19.61	15.52			
PR-13-CL	S	22.0	6.6	5.4	2.2	1.4	61.7	0.6	0.56	-0.25	21.16	16.76	24.77	28.84	20.64
	B	21.8	6.6	4.7	2.2	1.3	62.8	0.6	0.53	-0.28	19.66	15.56			
PR-14-CL	S	13.1	6.6	7.0	2.5	2.0	68.3	0.6	0.61	-0.22	23.69	18.77	24.78	28.88	20.95
	B	22.4	6.0	4.7	1.5	0.6	64.2	0.6	0.53	-0.27	19.86	15.71			
Lower Pearl River - polar lipids															
PR-1-PL		87.7	1.8	1.7	1.5	0.9	5.9	0.6	0.67	-0.17	26.82	21.28	24.58	28.80	20.58
PR-2-PL		88.3	1.8	1.6	1.4	0.9	5.4	0.6	0.66	-0.18	26.39	20.93	24.63	28.76	20.50
PR-3-PL		92.2	1.2	1.2	0.9	0.6	3.5	0.4	0.68	-0.17	27.00	21.43	24.54	28.76	20.35
PR-4-PL		78.5	2.5	2.6	1.9	1.5	12.1	0.9	0.69	-0.16	27.41	21.75	24.68	28.76	20.50
PR-5-PL		92.2	0.9	1.1	0.8	0.6	4.0	0.4	0.71	-0.15	28.53	22.65	24.63	28.76	20.33
PR-6-PL		93.8	0.9	1.0	0.7	0.4	2.8	0.3	0.70	-0.16	27.96	22.19	24.68	28.76	20.50
PR-7-PL		92.2	0.8	1.1	0.8	0.6	4.2	0.3	0.73	-0.14	29.29	23.25	24.51	28.76	20.40
PR-8-PL		96.7	0.6	0.6	0.5	0.3	1.2	0.2	0.66	-0.18	26.16	20.75	24.53	28.73	20.43
PR-9-PL		95.1	0.7	0.8	0.7	0.5	2.0	0.3	0.72	-0.14	28.91	22.95	24.53	28.73	20.43
PR-10-PL		95.7	0.7	0.7	0.6	0.4	1.6	0.3	0.68	-0.17	27.05	21.46	24.51	28.76	20.40
Pearl River estuary - polar lipids															
PR-11-PL	S	56.1	3.7	5.1	2.6	2.3	29.2	1.0	0.70	-0.16	27.96	22.19	24.61	28.80	20.54
	B	61.4	3.1	4.5	2.4	2.3	25.2	1.1	0.73	-0.14	29.11	23.11			
PR-12-PL	S	59.2	5.1	5.1	2.7	2.0	24.1	1.8	0.65	-0.18	26.03	20.65	24.64	28.84	20.36
	B	23.4	7.2	5.8	2.9	3.3	56.5	0.9	0.57	-0.24	21.99	17.42			
PR-13-PL	S	15.5	7.1	7.0	3.1	4.3	62.3	0.7	0.60	-0.22	23.64	18.74	24.77	28.84	20.64
	B	21.2	7.9	5.0	2.7	2.9	59.6	0.7	0.51	-0.29	18.84	14.90			
PR-14-PL	S	9.7	5.9	8.8	3.5	3.9	67.5	0.8	0.69	-0.16	27.54	21.86	24.78	28.88	20.95
	B	25.9	6.7	6.8	2.8	1.9	54.8	1.1	0.62	-0.21	24.24	19.22			

[a]PR, the Pearl River, which is followed by station numbers; the letter "S" or "B" after station number means "surface" or "bottom", respectively. CL, core lipid; PL, polar lipid. The sampling stations are shown in Fig. 2.

[b] Cren., Crenarchaeol; Cren.iso., Crenarchaeol regioisomer.

[c]The calibration is from Kim et al. (2010) or Kim et al. (2012).

[d]Sate-Ann, satellite-based annual mean surface water temperature; Sate-Jul, satellite-based July mean surface water temperature; Sate-Win, satellite-based winter mean surface water temperature.

Table A2

Table A2. Fractional abundance of arhcaeal isoprenoid GDGTs, TEX_{86}, and TEX_{86}-derived temperatures for the surface sediments collected from the lower Pearl River and the Pearl River estuary.

Sample ID[a]	Fractional abundance of archaeal isoprenoid GDGTs (%)							TEX_{86}	TEX_{86}^{H}	SST-TEX_{86}^{H} (^{o}C,2010[c])	SST-TEX_{86}^{H} (^{o}C,2012[c])	Sat-Ann.[d] (^{o}C)	Sat-Jul. (^{o}C)	Sat-Win. (^{o}C)
	GDGT-0	GDGT-1	GDGT-2	GDGT-3	GDGT-4	Cren[b]	Cren.iso.[b]							
Lower Pearl River - core lipids														
PR-1-CL	56.0	3.9	4.6	1.6	0.8	32.5	0.6	0.63	-0.20	25.01	19.83	24.58	28.80	20.58
PR-2-CL	36.6	5.0	5.7	2.0	1.2	48.7	0.7	0.63	-0.20	24.76	19.63	24.63	28.76	20.50
PR-3-CL	38.7	5.7	5.8	2.2	1.5	45.4	0.6	0.60	-0.22	23.48	18.61	24.54	28.76	20.35
PR-4-CL	37.3	6.0	7.6	2.7	1.5	44.2	0.8	0.65	-0.19	25.84	20.49	24.68	28.76	20.50
PR-5-CL	48.1	4.9	6.9	2.1	1.1	36.3	0.6	0.66	-0.18	26.45	20.98	24.63	28.76	20.33
PR-6-CL	66.1	3.4	3.9	1.5	0.7	24.0	0.4	0.63	-0.20	24.65	19.54	24.68	28.76	20.50
PR-7-CL	77.4	2.2	3.0	1.1	0.7	15.3	0.3	0.67	-0.17	26.73	21.21	24.51	28.76	20.40
PR-8-CL	85.0	1.7	1.9	0.9	0.5	9.7	0.2	0.64	-0.19	25.29	20.06	24.53	28.73	20.43
PR-9-CL	82.6	2.1	2.3	1.1	0.8	10.8	0.3	0.63	-0.20	25.08	19.89	24.53	28.73	20.43
PR-10-CL	79.3	2.3	2.4	1.1	0.7	13.9	0.3	0.62	-0.21	24.43	19.37	24.51	28.76	20.40
Pearl River estuary - core lipids														
PR-11-CL	21.7	5.7	7.0	2.5	1.7	60.6	0.8	0.64	-0.19	25.56	20.27	24.61	28.80	20.54
PR-12-CL	30.8	6.1	5.6	2.0	1.1	53.8	0.6	0.58	-0.24	22.27	17.64	24.64	28.84	20.36
PR-14-CL	25.2	6.4	4.5	1.7	1.1	60.4	0.7	0.52	-0.29	19.00	15.02	24.78	28.88	20.95
Lower Pearl River - polar lipids														
PR-1-PL	82.8	3.9	2.8	1.7	0.9	7.4	0.6	0.57	-0.25	21.67	17.16	24.58	28.80	20.58
PR-2-PL	77.9	5.5	2.2	2.1	1.2	10.5	0.6	0.47	-0.32	16.40	12.94	24.63	28.76	20.50
PR-3-PL	76.3	5.8	4.3	2.3	1.2	9.4	0.7	0.56	-0.25	21.22	16.80	24.54	28.76	20.35
PR-4-PL	71.7	6.9	4.3	2.9	1.6	11.6	0.9	0.54	-0.27	20.41	16.15	24.68	28.76	20.50
PR-5-PL	86.1	4.1	2.3	1.5	0.8	4.9	0.4	0.51	-0.29	18.60	14.71	24.63	28.76	20.33
PR-6-PL	92.2	2.6	1.5	0.9	0.4	2.2	0.2	0.50	-0.30	18.14	14.34	24.68	28.76	20.50
PR-7-PL	94.6	1.3	1.1	0.7	0.4	1.7	0.1	0.60	-0.22	23.63	18.73	24.51	28.76	20.40
PR-8-PL	94.7	1.7	1.3	0.9	0.3	1.0	0.1	0.57	-0.24	21.99	17.41	24.53	28.73	20.43
PR-9-PL	95.6	1.7	0.6	0.7	0.3	1.0	0.2	0.46	-0.33	15.75	12.43	24.53	28.73	20.43
PR-10-PL	95.2	1.2	0.9	0.9	0.4	1.1	0.2	0.62	-0.21	24.31	19.27	24.51	28.76	20.40
Pearl River estuary - polar lipids														
PR-11-PL	51.2	7.3	7.4	3.9	2.8	26.1	1.2	0.63	-0.20	24.92	19.76	24.61	28.80	20.54
PR-12-PL	60.3	7.5	5.5	2.7	2.0	20.8	1.2	0.56	-0.25	21.22	16.80	24.64	28.84	20.36
PR-14-PL	36.9	7.5	7.3	3.1	3.1	40.9	1.2	0.61	-0.22	23.77	18.84	24.78	28.88	20.95

[a] PR, the Pearl River, which is followed by station numbers. CL, core lipid; PL, polar lipid. The sampling stations are shown in Fig. 2.
[b] Cren., Crenarchaeol; Cren.iso., Crenarchaeol regioisomer.
[c] The calibration is from Kim et al. (2010) or Kim et al. (2012).
[d] Sate-Ann, satellite-based annual mean surface water temperature; Sate-Jul, satellite-based July mean surface water temperature; Sate-Win, satellite-based winter mean surface water temperature.

Table A3

Table A3. Fractional abundance of arhcaeal isoprenoid GDGTs, TEX_{86}, and TEX_{86}-derived temperatures for soil samples collected within the catchment of the lower Pearl River and the Pearl River estuary.

Sample ID[a]	Fractional abundance of archaeal isoprenoid GDGTs (%)							TEX_{86}	TEX_{86}^{H}	SST-TEX_{86}^{H}
	GDGT-0	GDGT-1	GDGT-2	GDGT-3	GDGT-4	Cren.[b]	Cren.iso.[b]			(^{o}C, 2010[c])
Core lipids										
PR-Soil-1-CL	6.7	5.5	7.5	4.5	0.3	64.1	11.4	0.81	-0.09	32.30
PR-Soil-2-CL	15.0	6.0	8.3	4.3	4.1	59.8	2.5	0.72	-0.15	28.67
PR-Soil-3-CL	53.5	2.6	4.1	1.8	2.0	34.4	1.5	0.74	-0.13	29.50
PR-Soil-4-CL	21.7	4.9	7.5	2.7	3.1	58.7	1.6	0.70	-0.15	28.18
PR-Soil-5-CL	36.0	6.4	7.0	3.5	1.7	41.4	4.0	0.69	-0.16	27.75
PR-Soil-6-CL	27.9	7.7	9.5	7.2	3.4	42.5	1.8	0.71	-0.15	28.24
PR-Soil-7-CL	36.9	6.4	7.0	3.8	1.1	40.4	4.5	0.70	-0.15	28.18
PR-Soil-8-CL	23.8	7.9	9.9	8.6	5.3	41.3	2.9	0.73	-0.14	29.23
PR-Soil-9-CL	28.6	2.4	6.6	2.9	4.0	53.3	2.2	0.83	-0.08	33.05
PR-Soil-10-CL	51.3	8.0	8.7	3.9	1.5	25.9	0.6	0.62	-0.21	24.56
PR-Soil-11-CL	15.0	7.3	8.8	5.8	1.4	57.7	3.6	0.71	-0.15	28.59
PR-Soil-12-CL	44.2	6.7	8.7	3.0	1.2	35.4	0.9	0.65	-0.19	25.88
PR-Soil-13-CL	93.5	1.0	0.9	0.5	0.3	3.5	0.2	0.62	-0.21	24.17
PR-Soil-14-CL	37.1	6.7	7.7	4.7	2.4	38.3	3.1	0.70	-0.16	27.94
PR-Soil-15-CL	7.9	5.7	6.6	5.6	4.1	67.0	3.2	0.73	-0.14	29.21
PR-Soil-16-CL	9.9	4.6	9.0	4.0	4.0	64.2	4.4	0.79	-0.10	31.58
PR-Soil-17-CL	27.0	4.8	6.2	5.3	0.9	53.4	2.6	0.75	-0.13	29.94
PR-Soil-18-CL	7.9	7.5	13.0	10.6	4.8	49.6	6.6	0.80	-0.10	32.01
PR-Soil-19-CL	61.0	4.9	6.0	4.9	2.4	19.3	1.7	0.72	-0.14	28.84
PR-Soil-20-CL	11.9	7.3	12.9	7.5	4.5	49.8	6.0	0.78	-0.11	31.36
Polar lipids										
PR-Soil-1-PL	16.6	2.9	30.7	9.5	6.5	22.6	11.2	0.95	-0.02	36.99
PR-Soil-2-PL	44.0	9.6	25.4	7.7	9.8	1.9	1.1	0.78	-0.11	31.21
PR-Soil-3-PL	77.7	1.5	2.7	1.2	1.0	14.8	1.1	0.77	-0.11	30.78
PR-Soil-4-PL	57.0	6.8	3.5	12.4	16.9	3.1	0.3	0.70	-0.15	28.20
PR-Soil-5-PL	55.5	9.5	7.8	9.0	5.4	10.5	2.3	0.67	-0.18	26.58
PR-Soil-6-PL	43.5	12.3	12.6	9.2	0.1	17.9	4.4	0.68	-0.17	27.13
PR-Soil-7-PL	28.4	5.1	8.6	15.1	13.5	16.2	13.1	0.88	-0.06	34.72
PR-Soil-8-PL	35.0	8.8	14.3	11.7	0.0	27.7	2.5	0.76	-0.12	30.60
PR-Soil-9-PL	69.3	3.0	3.9	0.8	12.1	9.2	1.6	0.68	-0.17	26.95
PR-Soil-10-PL	60.5	6.4	9.4	6.6	2.5	11.2	3.2	0.75	-0.13	30.04
PR-Soil-11-PL	19.9	6.3	6.6	8.8	26.6	24.8	7.5	0.78	-0.11	31.40
PR-Soil-12-PL	57.8	8.7	10.7	5.3	5.5	11.3	1.2	0.66	-0.18	26.45
PR-Soil-13-PL	95.1	1.5	1.9	0.7	0.5	0.2	0.1	0.63	-0.20	25.08
PR-Soil-14-PL	46.0	12.0	13.1	10.1	0.2	15.7	2.7	0.68	-0.16	27.33
PR-Soil-15-PL	16.0	10.3	6.8	8.5	2.6	49.9	6.1	0.67	-0.17	26.91
PR-Soil-16-PL	25.5	12.8	12.4	16.0	19.9	8.2	5.5	0.73	-0.14	29.07
PR-Soil-17-PL	32.2	8.6	7.7	4.4	9.4	29.9	8.5	0.71	-0.15	28.25
PR-Soil-18-PL	11.9	7.7	13.5	10.7	3.7	43.3	9.5	0.81	-0.09	32.47
PR-Soil-19-PL	26.7	5.3	14.5	16.1	9.1	22.1	6.7	0.88	-0.06	34.66
PR-Soil-20-PL	14.3	15.3	16.9	7.1	1.9	33.8	11.0	0.70	-0.16	27.84

[a]PR, the Pearl
[b] Cren., Crenarchaeol; Cren.iso., Crenarchaeol regioisomer.
[c]The calibration is from Kim et al. (2010).

Table A4

Table A4. Archaeal diversity indices from filters in EPR.

Station	No. of clones	No. of OTUs	C%	*H*	1/*D*	*J*	S_{ACE}	S_{Chaol}
EPR4	42	23	59.52	2.91	19.13	85.63	71.95	69.33
EPR9	61	30	67.21	3.09	22.59	307.50	73.66	93.33
EPR12	85	10	94.11	1.08	1.84	15.00	19.47	15.00
EPR14	73	9	94.52	1.03	2.02	8.00	7.89	7.00

B. SUPPLEMENTAL FIGURES IN CHAPTER THREE

Fig. B1

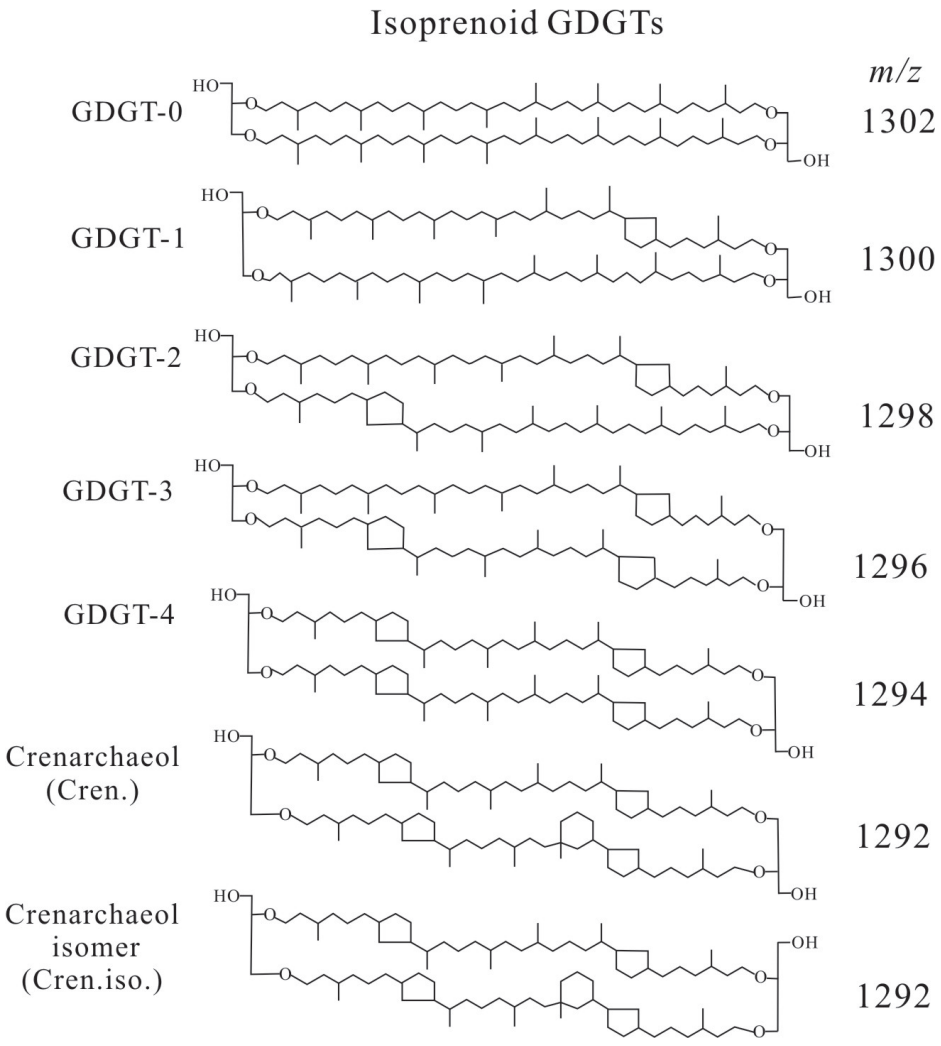

Fig. B1. Structures of archaeal core GDGTs described in the text.

Fig. B2

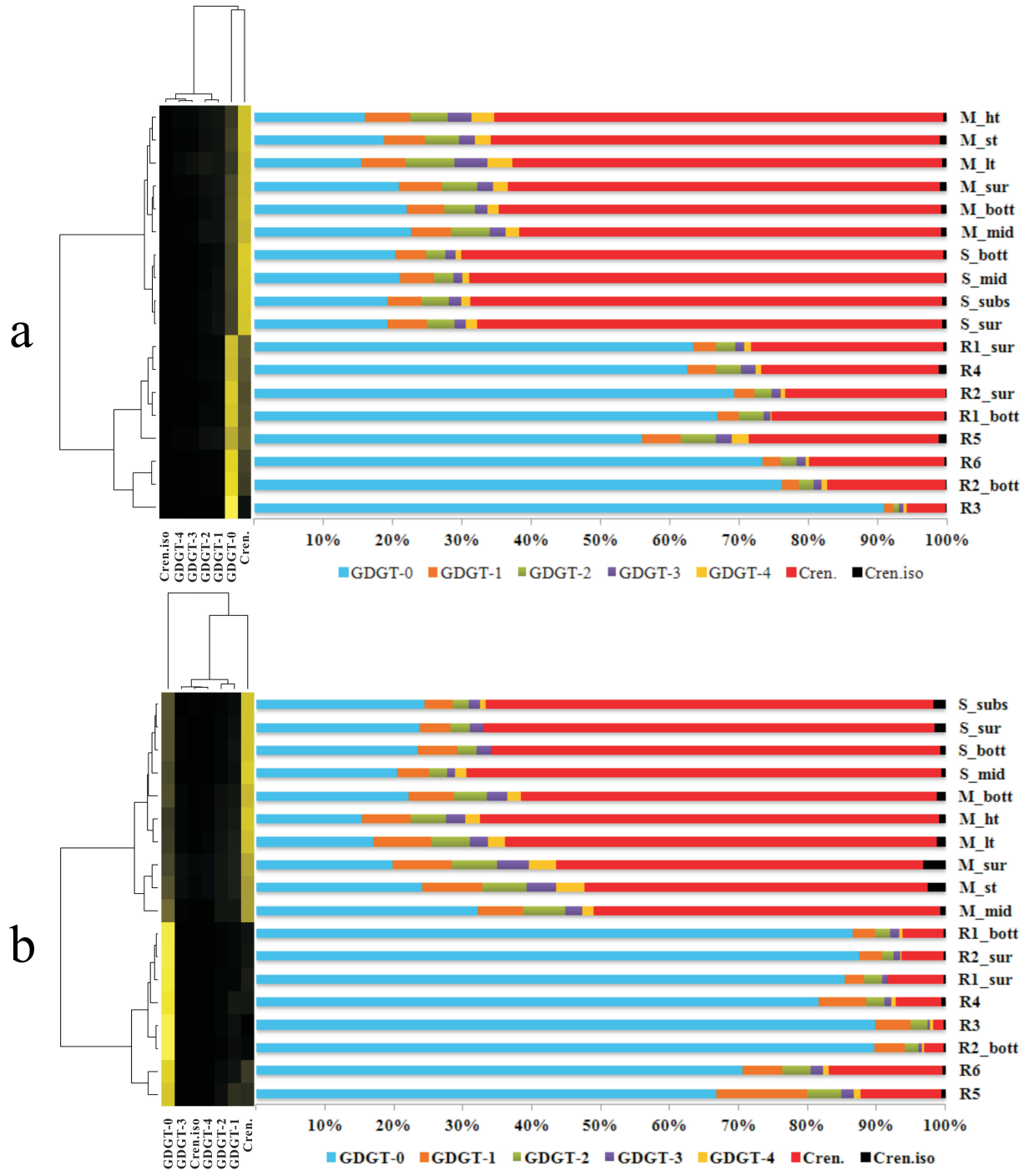

Fig. B2. Cluster analysis based on the relative abundance of CL- and phospho IPL-GDGTs.

Fig. B3

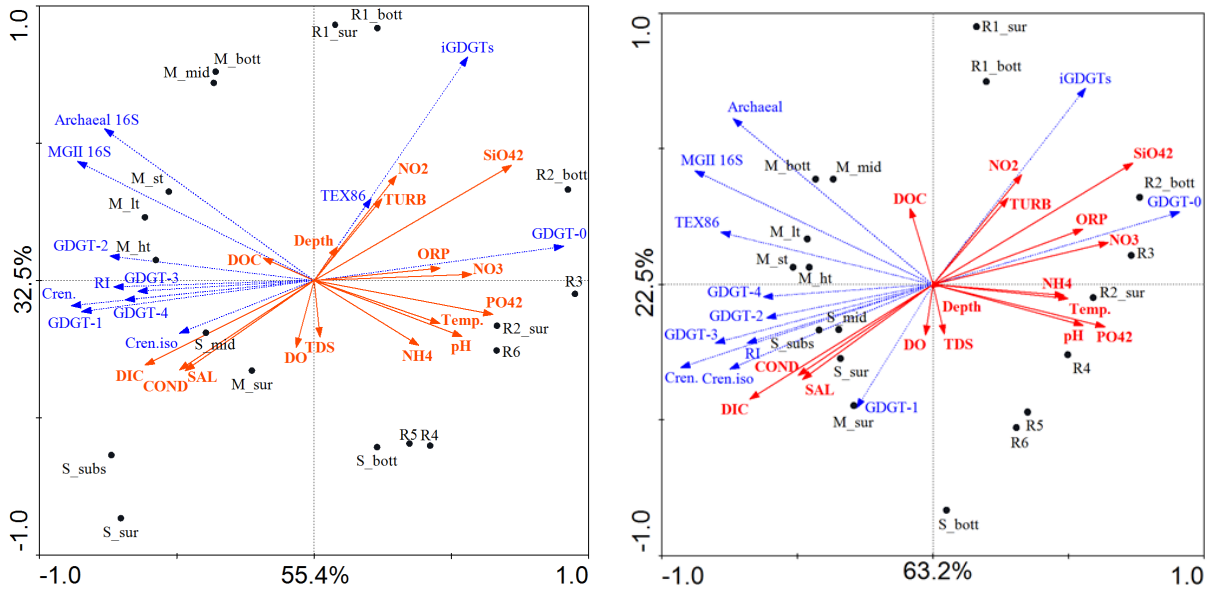

Fig. B3. RDA analysis based on the distribution of GDGTs and environmental parameters.